

Electronic Theses and Dissertations, 2004-2019

2007

Processing And Study Of Carbon Nanotube / Polymer Nanocomposites And Polymer Electrolyte Materials

Muthuraman Harish
University of Central Florida

 Part of the [Materials Science and Engineering Commons](#)
Find similar works at: <https://stars.library.ucf.edu/etd>
University of Central Florida Libraries <http://library.ucf.edu>

This Masters Thesis (Open Access) is brought to you for free and open access by STARS. It has been accepted for inclusion in Electronic Theses and Dissertations, 2004-2019 by an authorized administrator of STARS. For more information, please contact STARS@ucf.edu.

STARS Citation

Harish, Muthuraman, "Processing And Study Of Carbon Nanotube / Polymer Nanocomposites And Polymer Electrolyte Materials" (2007). *Electronic Theses and Dissertations, 2004-2019*. 3194.
<https://stars.library.ucf.edu/etd/3194>

PROCESSING AND STUDY OF CARBON NANOTUBE / POLYMER
NANOCOMPOSITES AND POLYMER ELECTROLYTE MATERIALS

by

MUTHURAMAN HARISH
B.Tech. Indian Institute of Technology Madras, 2005

A thesis submitted in partial fulfillment of the requirements
for the degree of Master of Science
in the Department of Mechanical, Materials and Aerospace Engineering
in the College of Engineering and Computer Science
at the University of Central Florida
Orlando, Florida

Fall Term
2007

© 2007 Muthuraman Harish

ABSTRACT

The first part of the study deals with the preparation of carbon nanotube/polymer nanocomposite materials. The dispersion of multi-walled carbon nanotubes (MWNTs) using trifluoroacetic acid (TFA) as a co-solvent and its subsequent use in polymer nanocomposite fabrication is reported. The use of carbon nanotube/ polymer nanocomposite system for the fabrication of organic solar cells is also studied.

TFA is a strong but volatile acid which is miscible with many commonly used organic solvents. Our study demonstrates that MWNTs can be effectively purified and readily dispersed in a range of organic solvents including dimethyl formamide (DMF), tetrahydrofuran (THF), and dichloromethane when mixed with 10 vol.% trifluoroacetic acid (TFA). X-ray photoelectron spectroscopic analysis revealed that the chemical structure of the TFA-treated MWNTs remained intact without oxidation. The dispersed carbon nanotubes in TFA/THF solution were mixed with poly(methyl methacrylate) (PMMA) to fabricate polymer nanocomposites. A good dispersion of nanotubes in solution and in polymer matrices was observed and confirmed by SEM and optical microscopy study. Low percolation thresholds of electrical conductivity were observed from the fabricated MWNT/PMMA composite films.

A carbon nanotube/ polymer nanocomposites system was also used for the fabrication of organic solar cells. A blend of single-wall carbon nanotubes (SWNTs) and poly3-hexylthiophene (P3HT) was used as the active layer in the device. The device

characteristics showed that the fabrication of the solar cells was successful without any shorts in the circuit.

The second part of the study deals with the preparation and characterization of electrode and electrolyte materials for lithium ion batteries. A system of lithium trifluoroacetate/PMMA was used for its study as the electrolyte in lithium battery. A variety of different processing conditions were used to prepare the polymer electrolyte system. The conductivity of the electrolyte plays a critical role in the high power output of a battery. A high power output requires fast transport of lithium ions for which the conductivity of the electrolyte must be at least 3×10^{-4} S/cm. Electrochemical Impedance Spectroscopy (EIS) was used to determine the conductivity of the polymer electrolyte films. Among the different processing conditions used to prepare the polymer electrolyte material, wet films of PMMA/salt system prepared by using 10vol% of TFA in THF showed the best results. At about 70wt% loading of the salt in the polymer, the conductivity obtained was about 1.1×10^{-2} S/cm.

Recently, the use of vanadium oxide material as intercalation host for lithium has gained widespread attention. Sol-gel derived vanadium oxide films were prepared and its use as a cathode material for lithium ion battery was studied. The application of carbon nanotubes in lithium ion battery was explored. A carbon nanotube /block copolymer (P3HT-b-PS) composite was prepared and its potential as an anode material was evaluated.

To my parents, who gave all I value, some debts are never repaid in full measure

ACKNOWLEDGMENTS

I wish to express my sincere thanks to my advisor, Dr. Qun (Treen) Huo, for her support, guidance, thoughtful discussions and patience. Without her motivation and guidance, this research work would not have been possible.

I am very grateful to Dr. Lei Zhai and Dr. Linan An for being on my thesis committee. I would like to thank Dr. Yong-ho Sohn and his student Prabhakar Mohan for his assistance with the electrochemical impedance spectroscopy study. I would also like to thank Paul Stokes for his help with the electrical measurements.

I thank the Materials Characterizations Facility (MCF) at UCF for offering the characterization facilities required for this research work. I would also like to acknowledge all the students in my group for their cooperation and support. I want to thank Himanshu Saxena for his assistance with the software used to draw the figures in the thesis. Special thanks to Md. Firoze Haque for all his help. He has stood by me, both at good and hard times. It is difficult to find people as great as him.

Above all, I would like to thank my family members, my father R. Muthuraman and mother Baby Muthuraman for their limitless sacrifices towards what I am today. I would like to give the fullest credit to my family members without whose support this thesis would never have been realized.

TABLE OF CONTENTS

LIST OF FIGURES	xi
LIST OF ACRONYMS	xv
CHAPTER 1 INTRODUCTION	1
1.1 Atomic Structure and Morphology of Carbon Nanotubes.....	3
1.2 Polymer/Carbon Nanotube Composites.....	6
1.2.1 Mechanical Properties.....	6
1.2.2 Electrical Conductivity	10
1.3 Polymer/Carbon Nanotube Nanocomposites: Processing Methods	14
1.3.1 Purification of Carbon Nanotubes	14
1.3.2 Solution Processing of Composites	16
1.3.3 Melt Processing.....	17
1.3.4 In-Situ Polymerization	19
1.3.5 Modification of Nanotubes	20
1.3.6 Dispersion by Conjugated Conducting Polymers	25
1.3.7 Third Component Assisted Carbon Nanotube Dispersion.....	28
1.3.8 Novel Methods of Composite Preparation.....	30
1.4 Carbon Nanotube/Polymer Composites in Organic Photovoltaic Devices.....	31
1.5 Overview of the Present Work.....	35
CHAPTER 2 EXPERIMENTAL.....	37
2.1 Purification, Dispersion of Carbon Nanotubes and Preparation of Nanocomposite Films	37

2.1.1 Chemicals.....	37
2.1.2 Characterization Instruments Used.....	37
2.1.3 Purification and Dispersion of Multi-Wall Nanotubes.....	38
2.1.4 Preparation of Nanocomposite Films.....	39
2.1.5 Carbon Nanotube Dispersion Study in Solution and in Nanocomposite Films.....	40
2.1.6 Electrical Conductivity Measurements.....	40
2.2 Fabrication of Carbon Nanotube/ Conducting Polymer Organic Solar Cells.....	41
2.2.1 Chemicals.....	41
2.2.2 Device Fabrication.....	41
CHAPTER 3 RESULTS AND DISCUSSION.....	45
3.1 Multi-Wall Nanotube Dispersion in Solution.....	45
3.2 Dynamic Light Scattering (DLS) Analysis.....	46
3.3 Scanning Electron Microscopy (SEM) Analysis.....	47
3.4 Transmission Electron Microscopy (TEM) Analysis.....	50
3.5 X-Ray Photoelectron Spectroscopy (XPS) Analysis.....	51
3.6 Nanocomposite Preparation and Carbon Nanotube Distribution in Composite Films.....	53
3.7 Electrical Conductivity Study of Nanocomposite Films.....	54
3.8 Fabrication and Characterization of Solar Cells.....	56
3.8.1 Contact Angle Measurements.....	56
3.8.2 Device Characteristics.....	58
CHAPTER 4 ELECTRODE AND ELECTROLYTE MATERIALS FOR LITHIUM-ION BATTERIES.....	60

4.1 The Development of Lithium Batteries	60
4.1.1 Lithium Metal Vs Lithium-Ion Batteries	60
4.2 Electrolytes for Lithium Batteries.....	61
4.2.1 The Requirements of Battery Electrolytes.....	62
4.2.2 Liquid Electrolytes.....	63
4.2.3 Solid Polymer Electrolytes	63
4.2.4 Polymer Gel Electrolytes	64
4.3 Cathode Material for Lithium Batteries.....	65
4.3.1 The Requirements of Cathode Materials	65
4.3.2 Vanadium Oxide as a Cathode Material for Lithium Batteries	66
4.4 Anode Material for Lithium Batteries.....	67
4.5 Overview of the Present Work.....	68
4.6 Electrochemical Impedance Spectroscopy (EIS).....	69
CHAPTER 5 SYNTHESIS AND CHARACTERIZATION OF ELECTRODE AND ELECTROLYTE MATERIALS	73
5.1 Synthesis of Electrode and Electrolyte Materials	73
5.1.1 Chemicals Used	73
5.1.2 Formulation of Electrolyte Films.....	73
5.1.3 Synthesis of Sol-Gel Derived Vanadium Oxide Films.....	74
5.1.4 Formulation of Carbon Nanotube/Block Copolymer Composites.....	74
5.2 Characterization of Electrode and Electrolyte Materials	75
5.2.1 Electrochemical Impedance Spectroscopy	75
5.2.2 Fourier Transform Infrared (FTIR) Spectroscopy	101

5.2.3 Scanning Electron Microscopy (SEM).....	105
CHAPTER 6 CONCLUSIONS AND FUTURE WORK.....	108
LIST OF REFERENCES.....	111

LIST OF FIGURES

Figure 1.1 Number of published articles and issued patents on carbon nanotubes as a function of year based on yearly publications catalogued in the CAPLUS and MEDLINE databases of the American Chemical Society.....	2
Figure 1.2 Schematic diagram that describes the “roll up” of the graphite sheet to make the nanotube.....	4
Figure 1.3 Illustrations of the atomic structure of (a) Arm-chair (b) Zigzag (c) Chiral nanotube.....	5
Figure 1.4 Schematic representation of the different kinds of dispersion of carbon nanotubes in a polymer matrix.....	8
Figure 1.5 Schematic representation of the electrical conductivity of carbon nanotube filled polymer composite with increasing filler loading fraction.....	10
Figure 1.6 Schematic device structure for solar cells in a) Bilayer configuration b) Bulk heterojunction configuration.....	33
Figure 2.1 Schematic of the etched ITO substrate.....	42
Figure 2.2 Top view of the device showing the Al back electrode.....	43
Figure 3.1 Photographs of the as-received MWNTs dispersed in (from left to right): N,N-dimethylformamide, dichloromethane, n-hexanol, toluene, tetrahydrofuran, acetonitrile. (a) Without the addition of TFA; (b) With addition of 10 vol% of TFA.....	46
Figure 3.2 Histogram showing the particle size distribution of MWNTs dispersed in THF for a) Without TFA b) 50µl/ml TFA c) 100 µl/ml TFA by dynamic light scattering measurements.....	47

Figure 3.3 SEM images of Type 1 MWNTs suspended or dispersed in THF and then deposited on graphite substrates: (a) MWNTs suspended in pure THF. (b) The as-obtained MWNTs dispersed in 10 vol% TFA in THF. (c) MWNTs after purification by multiple cycles of washing with 10 vol% TFA/DMF solvent and redispersed in 10 vol% TFA/THF solvent. (d) Magnified image of the top left region of (c).	49
Figure 3.4. TEM images of Type 1 MWNTs: (a) suspended in pure THF (b) after purification by multiple cycles of washing with 10 vol% TFA/DMF solvent and redispersed in 10 vol% TFA/THF solvent. Scale bar shown is 1 μm .	50
Figure 3.5 C1s X-ray photoelectron spectra of (a) untreated MWNTs; (b) MWNTs treated by TFA; (c) MWNTs treated by nitric acid.	52
Figure 3.6(a,b) Optical images revealing the distribution of MWNTs at different focus distances in the 0.25wt% MWNT/PMMA composite	53
Figure 3.7 Cross-section SEM images of the composite film containing 1 % of MWNTs at (a) low magnification (b) higher magnification	54
Figure 3.8 Room temperature electrical conductivity of MWNT/PMMA composites with MWNT aspect ratio of (a) 100 and (b) 1000	56
Figure 3.9 Contact angle on (a) ITO: 66.2° and (b) Glass: 49.8°, after standard cleaning.	57
Figure 3.10 Contact angle on (a) ITO: 18.2° and (b) Glass: 20.5°, after plasma cleaning.	57
Figure 3.11 Device characteristics of solar cells: a) With only P3HT as active layer b) With P3HT/0.3 wt% SWNT as active layer	58
Figure 4.1 Impedance network model (Randles circuit) for a metal in electrolyte.	71
Figure 4.2 Nyquist and Bode plots for a Randles circuit.	71

Figure 5.1 Nyquist plots for two samples of 50%salt and 10vol%TFA in THF as solvent in PMMA	77
Figure 5.2 Nyquist plots for two samples of 20%salt and 10vol%TFA in THF as solvent in PMMA	78
Figure 5.3 Nyquist plots for two samples of 10%salt and 10vol%TFA in THF as solvent in PMMA	79
Figure 5.4 Nyquist plots for two samples of 5%salt and 10vol%TFA in THF as solvent in PMMA	80
Figure 5.5 EIS of wet films of 20% Salt with 10vol% TFA inTHF as solvent, in PMMA.	81
Figure 5.6 EIS of wet films of 50% Salt with 10vol% TFA in THF as solvent, in PMMA.	82
Figure 5.7 EIS of wet films of 70% Salt with 10vol% TFA in THF as solvent, in PMMA.	83
Figure 5.8 EIS of wet films of 90% Salt with 10vol% TFA in THF as solvent, in PMMA	84
Figure 5.9 EIS of wet films of 20% Salt without TFA in THF, in PMMA.	85
Figure 5.10 EIS of wet films of 50% Salt without TFA in THF, in PMMA.	86
Figure 5.11 Nyquist plots for two samples of 20% TFA in PMMA.....	87
Figure 5.12 Nyquist plots for two samples of 10% TFA in PMMA.....	88
Figure 5.13 EIS of wet films of 20% Salt with 10vol% TFA in DMF as solvent, in PMMA.	89
Figure 5.14 EIS of wet films of 20% Salt without TFA, in DMF as solvent, in PMMA.	90

Figure 5.15 EIS of wet films of 50% Salt without TFA, in DMF as solvent, in PMMA.	91
Figure 5.16 Equivalent circuit model for a) type one b) type two nyquist plots.	93
Figure 5.17 SEM images to measure the film thickness from the cross section of (a) 5wt% (b) 10wt% (c) 20wt% (d) 50wt% salt and 10vol%TFA in THF as solvent in PMMA. The films were vacuum dried for a week.	94
Figure 5.18 Conductivity of various polymer electrolyte systems obtained by varying the processing conditions and the amount of salt	95
Figure 5.19 Nyquist Plots of the vanadium oxide cathode material by applying a DC potential of -0.25V.....	98
Figure 5.20 Nyquist Plots of the carbon nanotube composite material by applying a DC potential of 0.3V.	100
Figure 5.21 FTIR spectra of 30vol%TFA-PMMA (Blue curve), and 10 vol% TFA-PMMA (Red curve) and Pure PMMA (Black curve) film on a) day 4 b) day 12.	102
Figure 5.22 FTIR spectra of 10 vol% TFA-PMMA films a) vacuum-dried, on day 12 b) Oven-dried, on day 12.....	103
Figure 5.23 FTIR spectrum of Lithium trifluoroacetate/10vol%TFA/PMMA films.	104
Figure 5.24 SEM image of a) 0vol%TFA b)10vol%TFA c) 30vol%TFA in PMMA films	105
Figure 5.25 SEM images of the cross section of (a) 5wt% (b) 10wt% (c) 20wt% (d) 50wt% of salt in polymer electrolyte films.....	106
Figure 5.26 SEM image of the surface of the vanadium oxide films at high magnification.	107

LIST OF ACRONYMS

ABS	Acrylonitrile-Butadiene-Styrene
AIBN	Azobisisobutyronitrile
CNS	Carbon Nanospheres
CNTs	Carbon Nanotubes
CTAB	Cetyltrimethylammonium bromide
DLS	Dynamic Light Scattering
DMF	N,N-Dimethylformamide
DWNTs	Double-Wall Nanotubes
EIS	Electrochemical Impedance Spectroscopy
EMI	Electromagnetic Induction
FSS	Interfacial Shear Strength
HIPS	High Impact Polystyrene
HOMO	Highest Occupied Molecular Orbital
ITO	Indium Tin Oxide
LUMO	Lowest Unoccupied Molecular Orbital
PANI	Polyaniline
PANI-EB	Polyaniline-Emeraldine Base
PANI-LB	Polyaniline-Leucoemeraldine Base
PBO	Poly(p-phenylene benzobisoxazole)
PC	Polycarbonate
PEDOT	Poly(3,4-ethylenedioxythiophene)

PmPV	Poly(m-phenylenevinylene-co-2,5dioctyloxy-p-phenylenevinylene)
PP	Polypropylene
PPA	Polyphosphoric Acid
PPE	Poly(phenyleneethynylene)
PS	Polystyrene
PSS	Polystyrene Sulfonate
PVA	Polyvinyl Alcohol
P3HT-b-PS	Poly (3-hexylthiophene)-Polystyrene block copolymer
SDBS	Sodium Dodecyl Benzene Sulphate
SDS	Sodium Dodecylsulfate
SEM	Scanning Electron Microscopy
TEM	Transmission Electron Microscopy
TFA	Trifluoroacetic Acid
THF	Tetrahydrofuran
UHMWPE	Ultra High Molecular Weight Polyethylene
VGCF	Vapor Grown Carbon Fiber
XPS	X-Ray Photoelectron Spectroscopy

CHAPTER 1 INTRODUCTION

The first description of the unique and distinguishing features of Carbon Nanotubes is accredited to Iijima's *Nature* paper in 1991[1] which marked the birth of the nanotube revolution, garnering tremendous scientific and industrial attention since then. This third allotrope of carbon (diamond and graphite being the other two) has remarkable mechanical, thermal and electrical properties which in many cases exceeds the best of known materials. Single wall carbon nanotubes (SWNTs) show extremely high values of tensile modulus of 1TPA[2] and tensile strength (150-180 GPa)[3]. With a nearly one dimensional electronic structure, the metallic nanotubes exhibit a property known as "ballistic conduction". This means that they can transport electrons over long distances without scattering and enables them to carry high currents with essentially no heating. Similarly, easy propagation of phonons along the nanotube due to large mean free path lengths results in high thermal conductivity ($>3000\text{W/m.K}$)[4]. Due to these extraordinary properties of the carbon nanotubes, the zest among the researchers across the globe to tap their vast potential is still growing, even 15 years after their discovery. This can be better appreciated by noticing the astonishing growth trend in the number of published articles and issued patents every year (Fig 1.1).

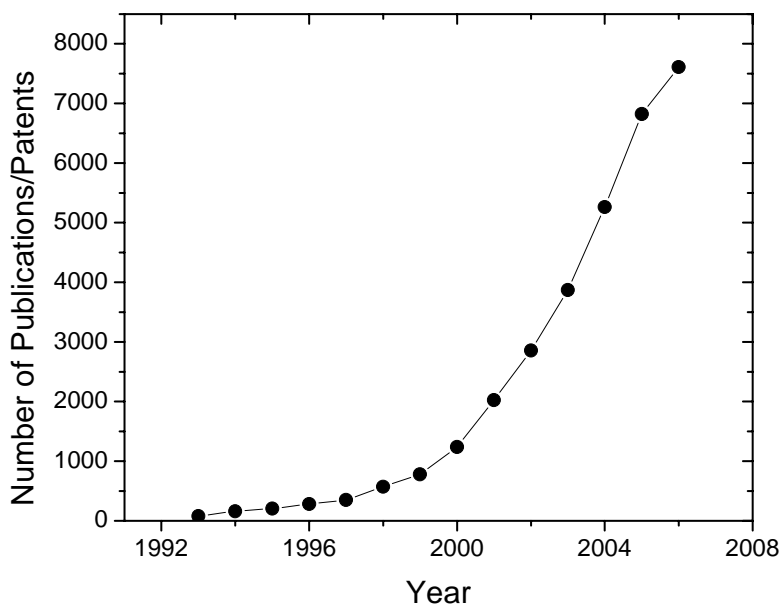


Figure 1.1 Number of published articles and issued patents on carbon nanotubes as a function of year based on yearly publications catalogued in the CAPLUS and MEDLINE databases of the American Chemical Society.

The widespread availability of carbon nanotubes since the late 1990s is a major contributing factor to this trend. A quick examination of the literature reveals the overwhelming diversity in scientific investigations, processing innovations and product development. They form the basis of new advanced materials with potential applications in various fields including nanotube reinforced materials, field-effect transistors, field emitters, molecular quantum wires, drug and gene delivery, tips for scanning probe microscopy, hydrogen storage, molecular diodes, electrochemical actuators, batteries, supercapacitors, photovoltaics and so forth [5-11].

1.1 Atomic Structure and Morphology of Carbon Nanotubes

Carbon nanotubes are long cylinders of covalently bonded carbon atoms, the end of which may or may not be capped by hemifullerenes. They are of different types: Single-wall carbon nanotubes (SWNTs), Multi-wall carbon nanotubes (MWNTs) and Double-wall carbon nanotubes (DWNTs). SWNT can be considered as a single sheet of graphite (a 2-D monolayer of sp^2 bonded carbon atoms arranged in a hexagonal array) rolled into a seamless cylinder. Most SWNTs have diameter typically close to 1nm. MWNT consist of concentric cylinders of graphite, coaxially arranged with interlayer separations of $\sim 0.34\text{nm}$, close to interplane spacing of graphite sheets [12]. The outer diameter of MWNTs ranges from as low as 2nm to sometimes more than 100 nm. DWNTs consist of two concentric graphite cylinders. The length of the nanotubes can be many thousands of times greater than the diameter.

It should be brought to the mind that the seamless rolling of the graphite sheet, by matching the dangling bonds at both the edges of the sheet, can be done in several ways. A translational shift along the edges before matching the dangling bonds would lead to a different orientation of the hexagonal array of carbon atoms forming the curved surface of the tube. This winding of the hexagonal arrays of carbon atoms in a helical fashion introduces *helicity* or *chirality* to the structure. The atomic structure of the nanotubes is described in terms of this helicity (or chirality) by defining the chiral vector C_h (Fig.1.2), by the equation

$$C_h = n a_1 + m a_2 \quad (1)$$

Where the integers (n, m) are the number of steps along the unit vectors (a_1 and a_2) of the hexagonal lattice.

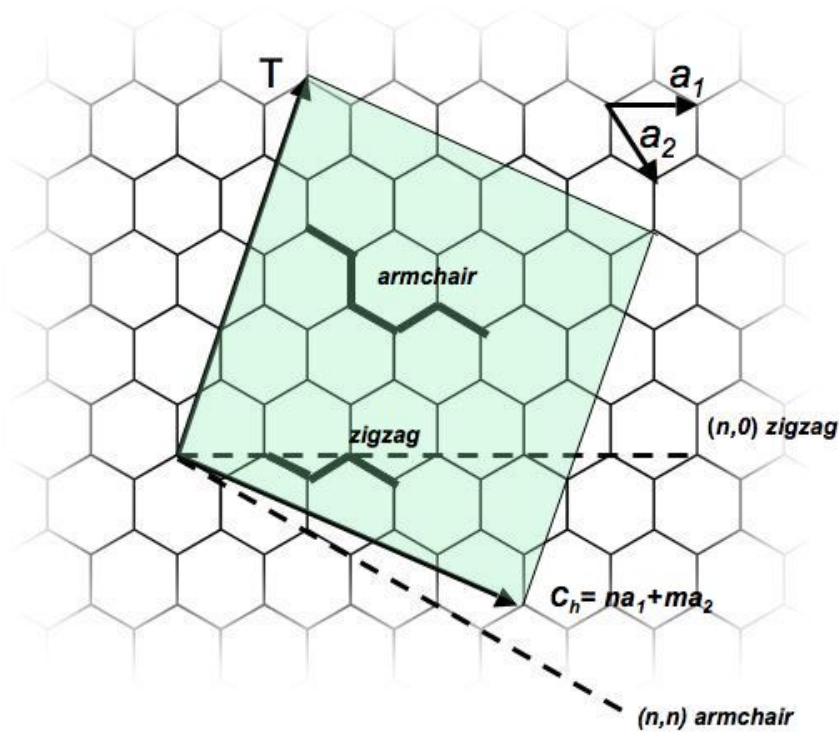
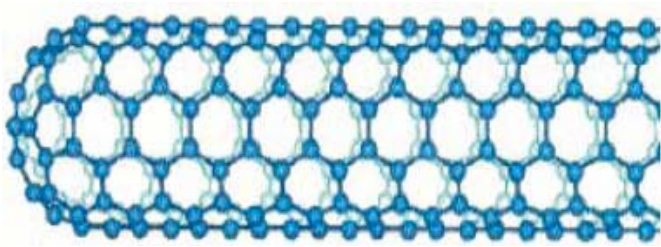


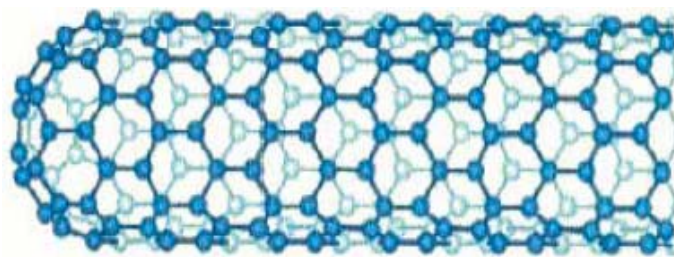
Figure 1.2 Schematic diagram that describes the “roll up” of the graphite sheet to make the nanotube.

By folding the graphite sheet into a cylinder such that the beginning and the end (n, m) of the chiral vector join together, we get the (n, m) nanotube. T is the direction of the axis of the tube. Based on the arrangement of the carbon bonds on the circumference of the nanotube, three types of carbon nanotube orientation can be specified. The nanotube can be armchair (n,n) (Fig.1.3), zigzag $(n,0)$ or chiral (all others). The structure of the nanotube strongly affects its electronic properties. For a given (n,m) SWNT, if $n-m$ is a multiple of 3 ($n-m=3i$, i being an integer $\neq 0$), then it is semi-metallic. All armchair SWNTs (i.e., $i=0$) are metallic, while SWNTs with $n-m \neq 0$ are semiconducting.

(a)



(b)



(c)

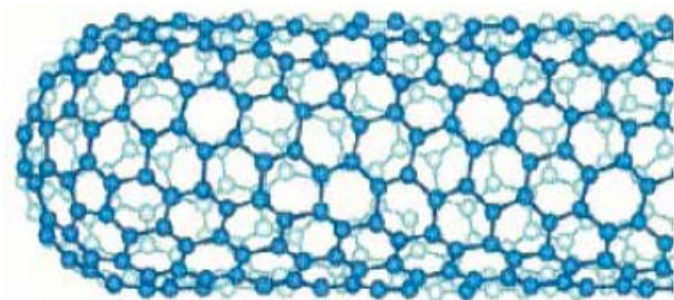


Figure 1.3 Illustrations of the atomic structure of (a) Arm-chair (b) Zigzag (c) Chiral nanotube.

The electronic properties of MWNTs are difficult to predict as each tube can have a variety of tube chiralities. This intriguing dependence of the electronic property on structural parameters further expands their range of applications.

1.2 Polymer/Carbon Nanotube Composites

Using pseudo one-dimensional fillers as a reinforcing agent has been a part of life since the beginning of the human civilization. Straw and mud in the form of bricks for building construction have been used since about 4000 B.C. The most visible application of composites is the use of steel reinforced concrete. Recently, there have been extensive research activities on the development of CNT/polymer nanocomposite materials [13-17]. Low volume additions (<5%) of the CNTs as fillers provide property enhancements that are comparable to conventional loading (10-40%) of traditional fillers (carbon black, carbon fiber, carbon graphite). Moreover, certain property enhancements are unique to carbon nanotubes, not normally possible with traditional fillers. . This combination of their small size and wonderful properties makes them special compared to other reinforcing fibers. CNT/polymer nanocomposites have shown promises in applications such as electromagnetic interference (EMI) shielding[18], photovoltaic devices[15] gas sensors[19], thermal management[20], corrosion protection[21] and transparent conductive coatings[22]. They are highly sought-after candidates to replace traditional metal and metal alloys for aircraft manufacturing.

1.2.1 Mechanical Properties

In general, the main requirements for the nanotubes to provide effective reinforcement in the composite are: good dispersion, interfacial stress transfer, large aspect ratio, and alignment. Fig 1.4 classifies different types of composites depending on the state of dispersion of the CNTs in the matrix. When the state of dispersion is poor, the polymer is unable to intercalate between the

sheets and a phase separated composite is obtained, the properties of which are similar to those obtained by using traditional fillers. When a polymer chain is able to penetrate between certain nanotubes, an intercalated nanocomposite is obtained, indicating a state of dispersion somewhere in-between that of the phase separated composite and the exfoliated nanocomposite. A complete and uniform dispersion to the level of isolated carbon nanotubes being individually coated with the polymer gives an exfoliated nanocomposite. The state of dispersion strongly influences the load transfer to the nanotube network. The effective moduli and strengths for the bundles are far lower than individual nanotubes. Thus the properties of the composite with bundles of nanotubes are dominated by shear slippage of individual nanotubes within the bundle. This intertube slippage then poses a serious limitation to their mechanical properties.

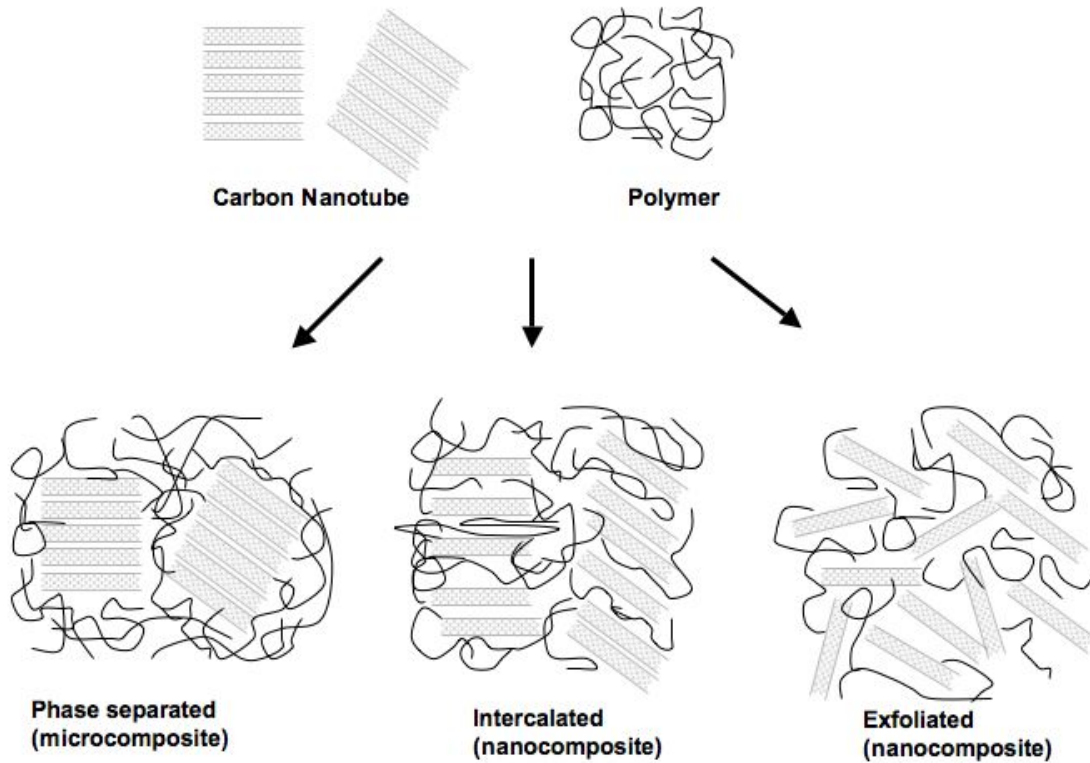


Figure 1.4 Schematic representation of the different kinds of dispersion of carbon nanotubes in a polymer matrix.

When an external stress, σ , is applied to the composite, the matrix experiences a greater strain, ϵ , than the composite which can be understood from the following relation.

$$\sigma = Y \cdot \epsilon \quad (2)$$

where Y can be Y_{NT} or Y_M , the modulus of the nanotube and the matrix respectively.

But we also know

$$Y_{NT} \gg Y_M \quad (3)$$

Therefore for a particular stress applied in the composite, the nanotube having a higher modulus experiences a smaller strain compared to the matrix. This results in a shear stress field in the matrix with the shear stress increasing along the direction of decreasing distance from the nanotube. This means that adjacent to the nanotube, the shear stress in the matrix can be very large. It is this interfacial shear stress, adjacent to the nanotube that controls the stress transfer to the nanotube. It can be shown that this stress also increases linearly with applied external stress. Hence it can be said that the stress on the nanotube increases linearly with external applied stress. However at some critical value of the interfacial shear stress either the matrix-nanotube interface or the matrix in the vicinity of the interface might fail and the load can no longer be efficiently transferred to the nanotube. This critical value of the shear stress is called the interfacial shear strength (IFSS) and controls the maximum stress transfer to the nanotube.

A large aspect ratio is required to maximize the load transfer from the matrix to the nanotubes. For effective load transfer, the fiber length has to exceed a critical length, l_c . This critical length for a nanotube, which resembles a hollow cylinder, is given by [23]

$$l_c = \frac{\sigma_f D}{2\tau} \left[1 - \frac{D_i^2}{D^2} \right] \quad (4)$$

where σ_f is the ultimate tensile strength of the fiber, D and D_i are the fiber external and internal diameters, and τ is the interfacial shear strength (IFSS). If the fiber length is less than l_c , the matrix cannot effectively grip the fibers and as a result they will slip.

Alignment is a less critical issue. Though alignment can maximize the strength and stiffness, aligned composites tend to have very anisotropic properties which may not be desirable for bulk samples. It is beneficial in the case of fibers where axial alignment helps maximize the reinforcement.

1.2.2 Electrical Conductivity

Carbon nanotubes have been demonstrated as by far one of the best nanofiller materials for transforming electrically nonconducting polymers into conductive materials. The electrical conductivity of insulating polymers filled with conductive filler is discussed in terms of the percolation phenomena.

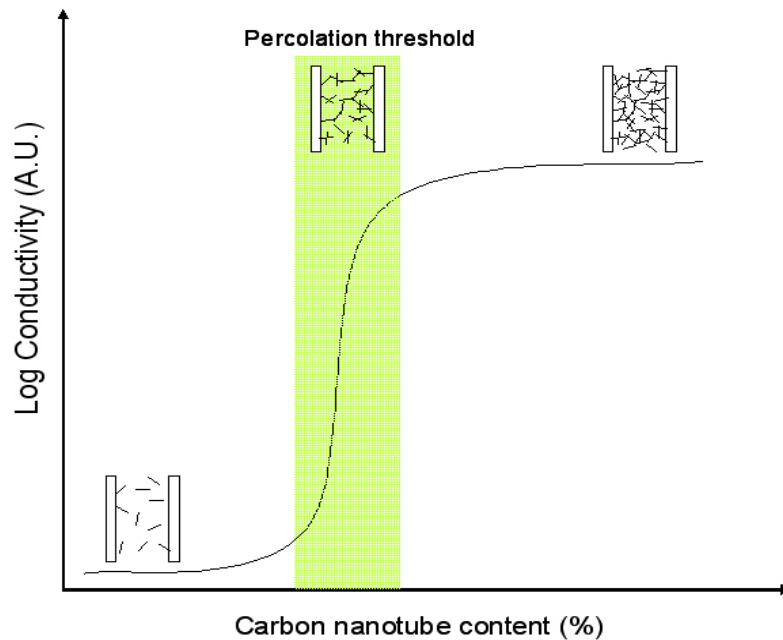


Figure 1.5 Schematic representation of the electrical conductivity of carbon nanotube filled polymer composite with increasing filler loading fraction.

At low concentrations, below the percolation threshold, the conductivity remains very close to that of the insulating polymer matrix as the electrons still have to travel through the insulating matrix between the conductive filler particles. When a critical volume fraction of the filler, called the percolation threshold, is reached, the conductivity drastically increases by many orders of magnitude (Fig 1.5). This coincides with the formation of conductive pathways of the filler material forming a three dimensional network, which span the macroscopic sample. The electrons can now predominantly travel along the filler and move directly from one filler to another. Increasing the amount of filler material further, levels off the conductivity, the maximum conductivity of the composite.

There is a considerable variability in the percolation threshold values reported for polymer/carbon nanotube composites as it is strongly influenced by several factors such as dispersion, aspect ratio, purity and alignment. Dispersion is probably the more fundamental issue. The strong van der Waals interactions between the nanotubes bundles them together. Due to the absence of hydrogen atoms in the CNTs, these interactions are notably larger than the polymer-polymer interactions and have been found to be $\sim 0.5\text{eV/nm}$ [24]. This bundling of the nanotubes reduces their aspect ratio and decreases the number of entities in the spatial distribution of the nanotubes in the polymer matrix, thereby increasing the percolation threshold. It is expected that the percolation threshold for the electrical conductivity of carbon nanotube/polymer composites decreases by increasing the aspect ratio of the nanotubes. This has been shown both experimentally and theoretically. Munson-McGee[25]used statistical arguments to determine the critical volume fraction in a percolating network of an anisotropic, three-dimensional cylinder distribution by estimating the probability of a cylinder intersecting any

number of other cylinders in the distribution. This can be directly compared to the percolating network of CNTs in polymer matrix. The statistical estimations showed a strong dependence of the percolation threshold on the aspect ratio. The critical volume fraction varied from about 12% for an aspect ratio of 10 to less than 1% when the aspect ratio was 1000 for the 3D random distribution. Bai and Allaoui [26] performed experimental investigation on the effect of length of MWNTs on the electrical properties of the composite and found more than an eightfold decrease in the percolation threshold of MWNT/ epoxy composites when the MWNT length was increased from 1 to 50 μ m. Whereas the traditional filler materials such as carbon black or graphite have very low aspect ratios (<500) and therefore, large filler concentrations are required to achieve the desired level of conductivity. The lower loadings of the higher aspect ratio fillers also offer the advantage of minimally increasing the melt viscosity, which facilitates processing and reduces component weight. However, it should also be stressed that the higher aspect ratio nanotubes are also more difficult to disperse. This is clear from a quick examination of the van der Waals interaction energies for two parallel cylinders (radii R_1 and R_2) separated by a distance D and of length L [27]

$$W = - \frac{AL}{12\sqrt{2}D^{3/2}} \left(\frac{R_1 R_2}{R_1 + R_2} \right)^{1/2} \quad (5)$$

where A (Hamaker constant) = $\pi^2 C\rho_1\rho_2$. C is the coefficient in the atom-atom pair potential, and ρ_1 and ρ_2 , are the number of atoms per unit volume. Also, the SWNTs are more difficult to disperse than the MWNTs due to a greater surface area per unit volume (MWNTs are essentially concentric single walled tubes and therefore tend to have larger sizes compared to SWNTs).

The carbon nanotube alignment in a polymer matrix can be brought about by different ways. In the case of melt fiber spinning[28] or shear deformation[29] wherein the polymer matrix flows, the shear and extension forces in these processes compel the polymer chains to an extended conformation along the flow direction as opposed to the previous random conformations, thereby aligning the nanotubes. When the flows stops, the polymer chains quickly revert back to the original random conformations due to the entropic considerations, whereas, in contrast, the nanotubes remain in the aligned configuration and can do so indefinitely upon cooling of the polymer matrix. Pre-aligned arrays of carbon nanotubes have been incorporated into polymers by infiltrating a polymer or monomer into the arrays, followed by in situ polymerization. Raravikar et al. found that the infiltration of the monomers into the aligned MWNTs was largely driven by the wetting action of the liquid against the nanotube walls and the low viscosity of the liquid [30]. Du et al.[31] studied the effect of nanotube orientation on the electrical conductivity using SWNT/ PMMA composites. The SWNT concentration was fixed (2wt%) and the orientation of the nanotubes was controlled by the processing conditions (extrusion rate, wind up speed) during the extensional flow. The extent of the nanotube alignment was given by a full width at half maximum (FWHM) from scattering measurements, where 0° and 180° correspond to perfect alignment and isotropic distribution (i.e., random positioning) of SWNTs, respectively. It was found that the electrical conductivity of the composite, measured parallel to the alignment direction, shot up with increasing FWHM (i.e., decreasing alignment) and at intermediate levels of nanotube alignment (FWHM~ 100° to 140°) the composite had the maximum conductivity, higher than that of the isotropic condition (FWHM of 180°). The effect of nanotube alignment is more pronounced at low loadings. At near perfect alignment conditions the nanotubes do not touch each other, thereby destroying the percolating pathways. Intermediate levels of nanotube

alignment leads to the formation of a much more efficient network having fewer redundancies than that occur by random positioning of the nanotubes.

1.3 Polymer/Carbon Nanotube Nanocomposites: Processing Methods

In the fabrication of nanocomposite materials, a good dispersion and adhesion of the CNTs with polymer matrices play a critical role in translating the excellent properties of the CNTs in the nanoscale to structural and multifunctional properties on the macroscale and obtaining nanocomposite materials with expectant and reproducible properties and performances. Another issue is the inconsistent quality of nanotube supply, as different synthesis methods yield CNTs of different characteristics, type and amount of impurities. Without purification, the impurities persist throughout the processing and are incorporated with the CNTs into the polymer matrix, affecting the performances of the final composite. Also, many other technological applications require that the carbon nanotubes be pure. But these problems have been a major challenge to date. Numerous processing methods and chemical modification strategies have been developed to address these challenges. While significant insights have been achieved in addressing these issues, there are still problems that need to be resolved.

1.3.1 Purification of Carbon Nanotubes

Several strategies have been developed over the past decade in achieving this goal. Most purification methods remove the contaminants (which are mainly amorphous carbon and catalyst

particles) by treatment with oxidizing acids. In a reported method[32], SWNTs were treated with concentrated nitric acid (HNO_3 , 70 vol%) under sonication for a few minutes and the suspension was then refluxed at 120-130°C for 4h, under magnetic stirring. Dense yellow vapours of nitrogen dioxide evolved, indicating the oxidation of hydrocarbons into alcohols, carboxylic acids, ketones or aldehydes and of the cobalt and nickel catalysts into their corresponding ions. Subsequent cycles of centrifugation and washing were carried out to give the final product. Yields between 30 and 50% could be obtained. Other treatments include acids such as hydrochloric acid (HCl)[33], or a mixture of nitric (HNO_3) and sulphuric (H_2SO_4) acid[34]. A two-step process of thermal annealing in air and acid treatment has also been used[35]. The nanotube powder was first thermally annealed in air at 470°C which burnt out the carbonaceous impurities. This was followed by an acid treatment with HCl for 24 h which etched away the catalytic particles. It should be noted that purification methods based on the use of these acids lead to a significant oxidation of nanotube walls which results in the damage of their intrinsic structure also cause cutting of nanotubes, reducing their aspect ratio.

In a different technique, carbon nanotubes prepared by pulsed laser ablation were purified by microfiltration[36]. No oxidative or heat treatments were required. The purification involved the suspension of carbon nanotubes in an aqueous solution using a cationic surfactant which was then forced through a microfiltration cell using an overpressure of N_2 . Most of the impurities, carbon nanospheres (CNS) and metal nanoparticles, passed through the filter while SWNTs were trapped. Duesberg et al.[37] used chromatographic procedures on a surfactant dispersed nanotube solution to give impurity free and size separated MWNTs. Georgakilas et al.[38] reported a 3 step process for the purification of SWNTs starting with the functionalization of the

CNTs, based on the 1,3 dipolar cycloaddition of azomethine ylides in DMF suspension. This led to the improved solubilization of the CNTs while leaving the catalyst nanoparticles insoluble. Consequently, a product free of catalyst particles but with the carbon impurities still present, could be obtained at this stage. This was followed by the separation of soluble adducts and recovery by the use of a solvent/non solvent technique. This step removed the remaining amorphous carbon impurity from the material. The final step was the annealing of the CNTs at high temperature leading to a thermal removal of the functional groups attached to the nanotubes giving pristine nanotubes.

1.3.2 Solution Processing of Composites

All the solution processing methods of preparing composites are variations of a general scheme which follows. The nanotubes are first dispersed in a suitable solvent by energetic agitation. The second step comprises of *directly mixing* the nanotubes and the polymer in solution by energetic agitation. The solvent is then left to evaporate under controlled conditions, leaving behind the polymer composite. The energetic agitation can be brought about by shear intensive mechanical stirring, magnetic stirring or ultrasonication. Ultrasonication can be provided in different forms: Mild ultrasonication is provided by a bath while a tip or a horn can be used for high power sonication. The forces in energetic agitation promote the exfoliation of nanotubes from the bundles. However, it should be noted that prolonged use of high-power sonication can introduce defects on the nanotube walls and shorten the nanotube length (i.e., reduce the aspect ratio), which is detrimental to the nanotube properties.

In a solution processing technique, pre-aligned MWNTs have been incorporated into an epoxy resin with a relatively low viscosity by shear intensive mechanical stirring, using a dissolver disk [39]. A very low percolation threshold of 0.0025 wt% of CNTs was achieved by favoring the formation of aggregates by controlling stirring time and speed while curing. The formation of the conducting networks was not induced by a truly statistical percolation based on a random distribution of individual high aspect ratio fillers, but was facilitated by the pre-alignment procedure, which led to the formation of a more efficient network than that occurs by random positioning of the fillers.

In another technique, MWNTs were first dispersed in ethanol in an ultrasonic bath. This solution was then mixed with an epoxy resin under stirring. A low viscosity of the resin solution was maintained by a choice of proper experimental conditions to ensure a good dispersion of the nanotubes. The solvent was then allowed to evaporate and the mixture was then cured by the addition of hardener. It was not possible to break up all the entanglements of the nanotubes by the dispersion process used and the percolation was found to be below 0.04 wt%.

Solution-processing technique has been used to obtain homogeneous nanotube dispersions in MWNT/ PS[40], MWNT/ PVA[41], SWNT/PVA[42], MWNT/ UHMWPE[43], MWNT/ PP[44] composites.

1.3.3 Melt Processing

The use of the solution processing technique at an industrial scale would require large volumes of toxic solvents such as chloroform, tetrahydrofuran (THF) etc., for the solubilization of the

polymer and the nanotubes, which is undesirable. Solution processing can be unsuitable for polymers that are insoluble. In such cases, the melt processing technique is a common alternative and is also most compatible with the current industrial practices such as injection molding, blow molding, extrusion and internal mixing. In particular, this technique is very useful in dealing with thermoplastic polymers which soften when heated. The process involves heating the polymer above its melting point if the polymer is semi-crystalline or its glass-transition temperature if the polymer is amorphous, to form a viscous fluid. Carbon nanotubes can then be mixed into the melt by high shear mixing. However, melt blending is generally less effective as compared to solution blending in dispersing polymers. It is also limited to low concentrations (< ~5 wt %), as high viscosities at higher loadings cause subsequent processing difficulties. There can be an unexpected degradation of the polymer at high shear rates. Therefore, the processing conditions have to be optimized for different polymer-nanotube combinations and different nanotube types and weight fractions.

Composites of polycarbonate (PC)/ MWNT[45] were prepared by diluting a PC based masterbatch containing 15 wt% MWNTs using melt mixing in a micro compounder at 260° C. After mixing, the sample was extruded through a heated cylindrical die. It was observed that the small scale extruder had a comparable mixing efficiency to that of a larger scale extruder and the percolation was achieved between 1 and 1.5 wt% MWNT. Due to the enhanced shear forces and increased viscosity at higher loading of nanotubes, there was some polymer degradation, experimentally observed by a decrease in T_g and the molecular weight of the polymer.

Andrews et al.[46] dispersed MWNTs in a range of commercial polymers such as high-impact polystyrene (HIPS), acrylonitrile-butadiene-styrene (ABS), and polypropylene (PP). Variables such as temperature, mixing time, rotor speed and MWNT concentration were investigated in the study. It was found that at any given temperature, the nanotube dispersion showed a significant improvement as the mechanical energy input into the mix was increased. The increase in energy input was achieved by increasing the residence time and/or the rotor speed. However it was found that the high shear mixing results in tube breakage. The mean tube length fell with increasing energy input with the aspect ratio falling to one-fourth of its initial value for samples showing good dispersion of nanotubes. A percolation threshold around 0.05 vol% was found for the MWNT-PP films. Similar result was obtained when HIPS was used as the matrix but not with ABS, suggesting a segregation of MWNTs in this case.

Melt processing technique has been used to prepare carbon nanotube / PP[47], polyimide [48], and nylon-6[49] composites with homogeneous nanotube dispersions.

1.3.4 In-Situ Polymerization

This technique first starts with the dispersion of CNTs in the monomer solution followed by polymerization of the monomer to give polymer/CNT composite. Depending on the molecular weight and the molecular weight distribution required, chain transfer, radical, anionic and ring opening metathesis polymerizations can be used for in-situ polymerization processing. This strategy is particularly important for the preparation of polymers which are insoluble or thermally unstable and hence cannot be prepared by solution or melt processing. Carbon

nanotubes dispersed in epoxy matrix form the majority of composites made by in-situ polymerization processing. In this case, the nanotubes are first dispersed in the resin, followed by curing of the resin with the hardener. Zhu et al. employed this technique to fabricate epoxy nanocomposites by an esterification reaction using end-cap functionalized SWNTs. The nanocomposites had a 30% higher tensile modulus after the addition of 1% SWNT. Jia et al.[50] reported the the synthesis of PMMA/ MWNT composites by in-situ radical polymerization using 2,2'-azobisisobutyronitrile (AIBN) as the initiator. Kumar et al.[51] reported preparation of ultra-strong poly(p-phenylene benzobisoxazole) (PBO) composites with SWNTs in polyphosphoric acid (PPA) by in-situ PBO polymerization. Note that as the polymerization progresses the viscosity of the reaction mixture increases, limiting the extent of in-situ polymerization.

In general, In-situ polymerization can be used to prepare composites containing carbon nanotubes that can be covalently or non-covalently bound to the nanotubes. Non-covalent binding involves physical adsorption of the polymer molecules on the carbon nanotubes through van der Waals and π - π interactions. Covalent functionalization enables grafting of polymer macromolecules onto the walls of carbon nanotubes. The role of covalent and non-covalent functionalization is considered in more detail in the subsequent sections.

1.3.5 Modification of Nanotubes

The inefficient dispersion of the nanotubes weakens the mechanical strength of the composite materials. Another problem is the poor interfacial bonding (CNTs to the matrix), which leads to fiber pullouts during stress, causing failure of the composite. The following approach implies a

strategy of either functionalizing the walls or the defect sites of the nanotubes or the modification of the polymer matrix which renders better dispersion of the NTs, increased interfacial interactions and also expands the utility of the nanotube structure.

1.3.5.1 End and Defect Site Functionalization

The end caps of the nanotubes are composed of fullerene-hemispheres (when not closed by the catalyst particle). The high curvature of the end caps make them more reactive compared to the sidewalls. Some defects of the six-membered carbon structures of the nanotubes, such as the pentagon-heptagon pairs called Stone-Wales defects, stem from the initial formation of the tubes. Treatment of the nanotubes with strong acids generates oxygenated functional groups on these end and defect sites that serve as anchor groups for further functionalization. A main advantage of solubilizing the nanotubes by this method is that the electronic structure of the CNTs is essentially preserved.

SWNTs have been functionalized with esters at defect sites leading to improved dispersion in solvents like tetrahydrofuran (THF) and chloroform (CHCl_3)[52]. Amidation and esterification reactions are also reported to have attached derivatized lipophilic and hydrophilic dendrons to the SWNTs and increased solubility in hexane and chloroform has been observed[53]. SWNTs functionalized with zwitterions[54], have rendered the separation of the tubes according to their lengths using gel permeation chromatography.

CdSe quantum dots[55], Au and Ag nanoparticles[56], peptide nucleic acid (PNA) strands[57] have been attached to ends and defect sites of the SWNTs. The attachment of the nanoparticles

to the tubes by functionalization provides a novel strategy of altering the optical and electronic properties of the tubes which have potential applications in photovoltaic cells and optoelectronic devices[58]. Bio-inspired moieties like PNA have been hybridized with complementary DNA sequences, leading to its potential use as biological sensors[57]. The functionalization of the coordination compounds to the ends and sidewalls of SWNTs, like SWNT-RhCl(PPh₃)₃ adduct[59], further broadens the range of SWNT applications by including their usage as catalyst supports.

1.3.5.2 Functionalization of Nanotube Walls

In CNTs, the π -orbital misalignment between adjacent carbon atoms is the major factor that results in the addition reactions to CNTs being energetically favorable[60]. The misalignment is associated with the bonds of the hexagonal carbon network which are neither parallel nor perpendicular to the tube axis but at an angle to the tube circumference. It turns out that this misalignment is the origin of torsional strain in the nanotubes and the relief of this strain controls the extent to which the addition reactions occur on the walls of the nanotube. It should be noted that since the π -orbital misalignment scale inversely with the tube diameter[61], smaller diameter tubes are expected to be more reactive than the larger diameter ones.

Many researchers have tried to solubilize NTs through various sidewall-functionalization routes and most of them need a highly reactive intermediate to attack the carbon nanotube. Though a high degree of solubilization is achieved there is a loss of the intrinsic electronic structure. The covalent bond formation at the nanotube walls has a profound impact on the metallic properties of the SWNTs. The metallic tubes change to a semiconductor, as the covalent bonding opens up a gap at the Fermi level[62]. It was also shown that the covalent sidewall attachments can

decrease the maximum buckling force of the nanotubes by about 15% and thereby reduce the final mechanical properties of the composite[63]. The various sidewall-functionalization routes include fluorination, ozonolysis, grafting polymer chains on nanotube walls, organic functionalization and so forth. Purified nanotubes were treated with fluorine gas in a reactor to provide fluorinated nanotubes with increased solubility in organic solvents[64]. The fluorine on the walls can be displaced with various nucleophiles such as organolithium and Grignard reagents to give nanotubes functionalized with different organic moieties[65]. Ozone was added to the walls of the NTs by a treatment of dispersion of the CNTs in methanol with ozone at -78°C[66]. The primary ozonide that is initially formed is cleaved to give oxygenated functional groups on the sidewalls. This method also led to the purification of the CNTs along with the sidewall-functionalization. Functionalization was achieved with substituted benzenediazonium salts in several ways including electrochemical reduction of the salt[67] and treating the surfactant wrapped nanotubes with the salt in aqueous solution[68]. A methodology involving functionalization of SWNTs with pyrrolidine by the 1,3-dipolar cycloaddition of azomethine ylides[69] results in exceedingly high solubility of CNTs in organic solvents (50mg/ml).

Recently, many efforts on polymer composites have focused on engineering the nanotube/polymer interface for optimal composite properties. Polymer grafted nanotubes provide a remarkable route to disperse the nanotubes and improve the interfacial stress transfer between the nanotube and the polymer. The two main strategies for the covalent attachment of the polymer to the nanotubes are defined as the “grafting to” and “grafting from” methods. The former method relies on the attachment of the already preformed polymer chains with functionalized end groups to the functional groups on the nanotube surface via different chemical

reactions. The “grafting from” method is based on the covalent immobilization of the polymer initiators on the nanotube surface and subsequent in-situ polymerization of the monomeric species with the formation of polymer chains bound to the nanotube. The advantage of the “grafting from” technique is that a high grafting density can be achieved whereas in the “grafting to” technique, the initial polymer chains bound to the nanotube sterically hinder the addition of more macromolecules to the surface leading to a low grafting density. On the other hand, the advantage of the “grafting to” technique is that preformed commercial polymers of specific mass and distribution can be used whereas the other method requires a strict control of the amount of the initiator, substrate and the conditions for polymerization reaction.

Using the “grafting from” approach, Qin et al.[70] reported the grafting of polystyrene sulfonate (PSS) by in-situ radical polymerization. The composite could be dispersed in aqueous media due to the negative charges of the polymer chain and the impurities could be separated by centrifugation. Vishwanathan et al.[71] treated SWNTs with sec-butyllithium which exfoliated the bundles and generated carbanions on the nanotube surface. When styrene was added, these carbanions initiated anionic polymerization, resulting in polystyrene-grafted nanotubes. Recently Tong et al.[72] modified SWNTs via in-situ Ziegler-Natta polymerization of polyethylene. The surface of the SWNTs was initially functionalized with the catalyst ($MgCl_2/TiCl_4$) and then ethylene was polymerized to give polyethylene grafted nanotubes. Although the exact mechanism is unclear, the authors suggest a possible cross linking between the two components. The PE grafted nanotubes were then mixed with commercial PE by melt blending. Xia et al.[73] used an ultrasonic initiated in-situ emulsion polymerization of acrylates to fabricate composites. The MWNTs were covalently functionalized with poly (butylacrylate) (PBA) and PMMA

polymers. These polymer-encapsulated nanotubes were then well dispersed in a Nylon 6 matrix. The interfacial- adhesion improved and with the addition of 1wt% of the filler the yield strength improved ~30% and Young's modulus increased ~35%.

The “grafting to” approach was first demonstrated by Fu et al.[74] in 2001. The carboxylic acid groups on the surface of the nanotubes were converted to acyl chlorides by refluxing with thionyl chloride. These acyl chloride moieties were then used in esterification reactions with the hydroxyl groups of the dendritic PEG polymers. An organometallic modification strategy was introduced by Blake et al.[75] in which the MWNTs were initially functionalized with n-butyllithium and subsequently coupled with chlorinated polypropylene leading to elimination of LiCl. Bhattacharya et al.[76] have developed fully integrated nanotube composite materials through functionalization of MWNTs by covalently attaching ferritin protein molecules onto the surface of the nanotubes. A dramatic increase in the modulus (100-110%) of PVA was observed with the addition of 1.5 wt% ferritin functionalized nanotubes.

1.3.6 Dispersion by Conjugated Conducting Polymers

Another approach consists of using a polymer having a structure tailored for interaction with the NTs. It is realized by non covalent functionalization of the NTs with conjugated polymers which involves the physical adsorption of the polymer chains on the nanotube surfaces via interactions of the π -delocalized structure of the conjugated polymer with the delocalized π -electronic structure of the CNTs. This non-covalent modification of the CNTs disrupts the van der Waals interactions that cause the CNTs to aggregate into bundles. With the interaction between the

polymer and the CNT walls, the conformation of the polymer is modified, leading to a helical wrapping of the polymer around the CNT [77]. Short and rigid polymers have also been used[78], which interact with the CNTs via π -stacking without polymer wrapping. These short and rigid polymers are particularly suitable for small diameter CNTs. In these cases, the polymer wrapping approach works poorly, as the polymer conformation may be unfavourable to cause a satisfactory dispersion. The conjugated polymer solution is also reported to purify the CNTs effectively and non-destructively[79], as the amorphous graphite particles settle out while the suspension of the CNTs is still stable.

There are two general methods of preparation of composites comprising of CNTs and conducting polymer. The first one involves the direct mixing of the two components and the other consists of a chemical synthesis. The former method aims for intimate mixing of the two components and in most of the cases involves an undoped conducting polymer to mix with the CNTs. This procedure can lead to a doping process as observed generally by mixing a polymer and a doping agent. The latter involves a chemical or an electrochemical polymerization of the monomer with the addition of CNTs as a supplementary agent. The interaction between the conducting polymer and the CNT can be that either the conducting polymers are doped with the nanotubes (i.e., a charge transfer occurs between them) or the conducting polymer functionalizes the CNTs. Baibarac et al.[80], prepared two types of composites based on polyaniline (PANI) and single-walled carbon nanotubes (SWNT). The first one obtained by direct mixing of SWNTs powder to the polyaniline-emeraldine base (PANI-EB) solution. This led to composites containing PANI in leucoemeraldine-base (PANI-LB) and emeraldine-salt (PANI-ES) form, covalently functionalized and doped with the CNTs, respectively. The second type prepared by

chemical polymerization of the monomer in the presence of SWNTs followed by the deprotonation of the obtained PANI-ES to give PANI-EB. This led to composites of PANI salt doped with carbon nanotubes. The reaction conditions had also transformed SWNTs to fragments of shorter length. The system consisting of NTs and conjugated polymers form the basis for composite materials with device applications. A better understanding of the interactions between the polymer and the CNT will allow the optimization of the properties of the prepared nanocomposites would help in deciding the conditions for making composites for desired applications, with improved performances. For example, composites made with polypyrrole and aligned NTs have shown exceptional charge storage capacities, which may lead to potential applications in supercapacitors and secondary batteries.

For nanocomposites made of CNTs and conjugated polymer, a mixed conduction process exists, as both the filler and polymer matrix are conductive. The conductivity of most conjugated polymers is dependent on molecular weight distribution, degree of purity, defect concentration, and conformation. Therefore it is not possible to describe the conductivity behaviour of such composites on the basis of percolation theory. Below the true percolation threshold, which corresponds to the formation of a network of CNTs in the polymer matrix, the conductivity still increases due to the introduction of charge carriers into the polymer, even if there is no network of conducting paths in the system. Hence, it is important to be able to determine if the conductivity increase is due to the increase in number of complete conductive paths (above the true percolation threshold) or if it is due to a combination of increased carrier donation by the CNTs and increase in partial conductive paths formed by conjugated polymers (still below the percolation threshold), to determine the true percolation threshold. Coleman et al.[81] reported

the preparation of SWNT-PmPV composites by mixing SWNT with PmPV in toluene. The true percolation threshold of the composite was between 8 and 9% of CNTs.

1.3.7 Third Component Assisted Carbon Nanotube Dispersion

A third component in the polymer-CNT composite preparation is also used, which assists the incorporation of exfoliated CNTs in the polymer matrix, preferably without altering the intrinsic properties of the CNTs. In most studies, a surfactant is used as the third component. During sonication of the solution containing the bundles of surfactant dispersed nanotubes, the compression and the rarefaction waves induced in the medium by the ultrasound, has the energy required to overcome the van der Waals interactions in the CNT bundles and leads to CNT exfoliation. At the same time, the surfactant molecules adsorb onto the surface of the exfoliated nanotube walls. The colloidal dispersion of the CNTs with the adsorbed surfactant molecules is stable due to the electrostatic and/or steric repulsion. Anionic surfactants such as sodium dodecylsulfate (SDS) or sodium dodecyl benzene sulphate (SDBS); Cationic surfactant such as cetyltrimethylammonium bromide (CTAB) and polysaccharide (gum Arabic, GA) have been extensively used to disperse, exfoliate and stabilize the CNTs. Barraza et al.[82] reported the preparation of SWNT-PS and SWNT-styrene-isoprene copolymer nanocomposites using mini-emulsion technology. SWNTs were first purified with HNO₃ and then dispersed under sonication, with the help of CTAB. The initiator AIBN dissolved in ethanol was then added to the SWNT suspension. The resulting mixture was then added under stirring to a mixture of solvent (hexadecane), catalyst (PS-AlCl₃ acid complex) and monomer (styrene/ styrene-isoprene). An emulsion was obtained by an additional sonication step and then polymerization

was carried out. The conductivity increased ten orders of magnitude from 10^{-14} S/m for unmodified PS to 10^{-4} S/m for the final SWNT-PS composite and the percolation threshold was between 4 to 8 wt% of the NTs.

Although a layer of polymer adsorbed onto the surface of the NTs can give a better dispersion of the NTs in the matrix, its addition can decrease the maximum conductivity value reached by increasing the inter-tube resistance. Usually, the addition of a surfactant also influences the wetting behaviour, which in turn could affect the mechanical properties of the composite significantly. Regev et al.[83] showed the significant influence of the surfactant on the final conductivity of the composite. A contribution of several factors like the ability of the surfactants to exfoliate the nanotubes, coupling-interaction between the adsorbed surfactants and the nanotubes, and its capability to desorb from the CNT surface and migrate into the polymer matrix during and/or after processing of the nanocomposite influenced the final conductivity of the composite.

Ramasubramaniam et al.[84] reported the dispersion of CNTs in chloroform under sonication by using a conjugated polymer, poly(phenyleneethynylene) (PPE), as the third component. The PPE coated SWNTs were then incorporated in a matrix of PC or PS. The percolation thresholds were 0.045 wt% and 0.11 wt% SWNTs for the SWNT-PS and SWNT-PC composites respectively. The maximum conductivity of the SWNT-PS composite reached 6.89S/m at 7 wt% SWNTs, 14 orders of magnitude higher conductivity of pure PS and the conductivity increased from 10^{-13} S/m, the typical conductivity of pure PC, to 4.81×10^2 S/m for SWNT-PC composites at 7wt% of CNTs. A third component assisted dispersion of CNTs has also been reported by our

group[85]. MWNT-P3HT-PMMA ternary composites were prepared by first dissolving 0.5wt% (based on PMMA) of P3HT in THF. 10 vol% of TFA was then added to the P3HT solution and sonicated briefly. Appropriate amounts of MWNTs and PMMA powder were added to the prepared solution and after the polymer dissolved, films were cast. An exceptionally low percolation of 0.006 wt% MWNTs was found for the ternary composites.

Besides surfactant and conjugated polymers, polyelectrolytes [86], surfactant-like block copolymers[87], proteins and DNAs[88, 89] have been used as a third component to facilitate the dispersion of NTs.

1.3.8 Novel Methods of Composite Preparation

A number of innovative nanocomposite fabrication methods that are distinct from the traditional methods as described above have been reported. A simple method of infiltration of polymer from solution into a pre-existing network of nanotubes was first demonstrated by Coleman et al.[90]. Thin sheets of SWNT films (Buckypaper) were made by Buchner filtration. These porous sheets were then dipped in polymer solutions for various times before rinsing and it was found the polymer mass fractions of up to 30 wt% could be incorporated. Vigolo et al[91] developed an elegant “coagulation spinning” method for producing composite fibers. SWNTs dispersed in a surfactant solution and then injected into a rotating bath of PVA dissolved in water. The nanotubes coagulated to mesh as the nanotube dispersion destabilised as the polymer molecules replaced the surfactant molecules on the nanotube surface. The mesh was converted to fiber by a slow draw process, which had a significantly enhanced alignment. Another interesting technique

was developed by Mamedov et al[92] which involved the layer by layer (LBL) assembly of composite film by alternating the substrate between the chemically modified SWNTs and polyelectrolyte solutions. The advantage with this fabrication method was that the film thickness could be controlled easily and nanotube loading up to 50wt% could be obtained.

1.4 Carbon Nanotube/Polymer Composites in Organic Photovoltaic Devices

Research on organic solar cells is based on conjugated polymers. These polymers comprise a backbone chain of sp^2 hybridized carbon atoms and the π electrons of these chains are delocalized in nature due to isomeric effect. The optical and electronic properties of these materials are essentially determined by the molecular orbitals that are made from the summation of the individual atomic orbitals in the molecule. The highest occupied molecular orbital (HOMO) and the lowest unoccupied molecular orbital (LUMO), largely determine the properties of the molecule. Depending on the placement of the orbitals, the conjugated polymers can exhibit a wide range of band gaps, showing insulating to metallic-like properties. If the band gap of the organic semiconductor is large only a small portion of the incident solar energy is absorbed. A lower band gap enables a higher harvesting of solar photons. Another point to be observed is that the absorption coefficients of the organic semiconductors can be as high as 10^5cm^{-1} which means a thickness of around 100 nm is enough to absorb most of the photons. This leads to the conclusion that the band gap of the conjugated polymer is the limiting factor in the absorption of solar light and lower band gap polymers should be used for higher solar absorption. The absorption of a photon in organic semiconductors results in the formation of excitons (electron-hole pairs bound together by coulombic attraction). The absorption of a photon induces excitons

with binding energies ranging from 0.05 to $> 1\text{eV}$ [93]. Unlike inorganic semiconductors wherein the absorption of a photon results in the production of free electron-hole pairs, the photoexcited electrons in organic semiconductors are coulombically bound because of the following reasons. First, as the dielectric constant of the organic phases is usually low, the attractive coulomb potential well around the electron-hole pair extends over a large volume. The electron's wave function is spatially restricted, localizing in the potential well of its conjugate hole due to the narrow bandwidth resulting from the non-covalent electronic interactions between the organic molecules being weak.

For free carriers to be generated, the excitons must be dissociated. This can happen in the presence of strong electric fields, at a defect site in the material or at an interface between two materials. At the interface, where an abrupt change in potential energy can occur (band offset), strong localized electric fields are possible. The dissociation at the interface can lead to either electron transfer from the donor material to the acceptor material or hole transfer from the acceptor to the donor. But this photoinduced charge transfer only occurs when the exciton reaches such an interface within its lifetime. Typically the excitons can diffuse over a length of approximately 5-15 nm[94]. Therefore, if the exciton diffusion length is less than the donor-acceptor phase separation distance, the excitons would decay via radiative or nonradiative pathways leading to a loss in power conversion. In the other case, when the diffusion length is more than the distance from the interface such as that between a conjugated polymer (donor) and fullerenes or carbon nanotubes (electron acceptor materials), there is release of an electron from the LUMO of the "donor" to the LUMO of the acceptor material at a lower energy. This leaves a hole on the HOMO of the donor. The electrons and holes are now separated and are transported

in their respective materials to the electrodes. Using asymmetrical contacts (a low work-function electrode for the collection of electrons and a high work function electrode for the collection of holes), leads to an external electric field which acts as a driving force for the charge carriers to reach the electrodes. Another driving force can be the concentration gradients of the respective charges, which lead to a diffusion current. The transport of the charges is also governed by the diffusion lifetime of the charges, after which recombination may take place during the journey to the electrodes.

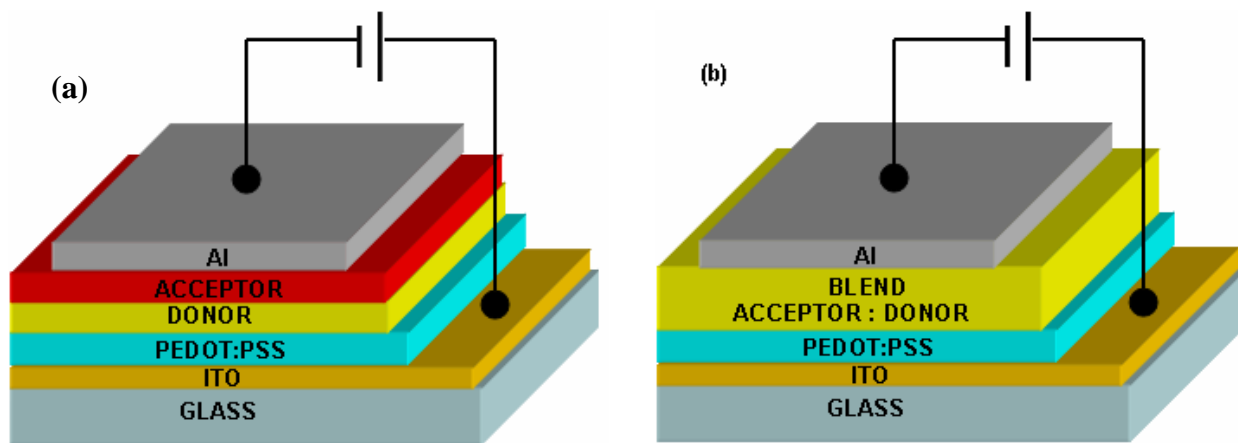


Figure 1.6 Schematic device structure for solar cells in a) Bilayer configuration b) Bulk heterojunction configuration

The general device structure of the solar cells is shown in Fig 1.6. The devices are fabricated in sandwich geometry. Glass or plastic like PET with a coating of ITO is used as the substrate for the fabrication of the solar cells. ITO is used as the electrode as it is transparent and conducting. The coating of ITO is further structured by chemical etching. On this transparent conducting substrate which forms one of the electrodes of the solar cell, a coating of PEDOT:PSS is given.

The purpose of the PEDOT:PSS layer is to improve the surface quality of the ITO electrode as the large variations of the ITO morphology on glass results in local areas with high electric fields during operation which can cause rapid polymer degradation. The layer of ITO also facilitates the hole injection/extraction. The active layer is then coated on top of this layer which can be the sequential stacking of the donor and acceptor materials on top of each other as shown in fig 1.6a. or the donor and acceptor material can be blend into a single layer as shown in fig 1.6b. In the bilayer heterojunction device, only the excitons that are created within 5-15nm distance from the interface, can dissociate to give free charges. Therefore, there is a loss of photons which are absorbed further away from the interface and this drastically limits the photocurrent and the overall efficiency of the bilayer solar cells. The bulk heterojunction device as shown in fig 1.6b is a blend of the donor-acceptor components which dramatically increases the surface area of the donor-acceptor interface. Such a phase separation in the nanometer length scale results in an interface being present within the exciton diffusion length at any point in the volume of the active layer. Both the phases need to form percolated pathways (continuous interpenetrating network) for the holes and electrons in their respective phases to be transported to their contact electrodes. This results in an improved efficiency of the solar cells. In the last step, the charge carriers are extracted from the device through ITO which forms the hole contact on one side and the Al electrode which forms the electron contact on the other side.

1.5 Overview of the Present Work

As discussed previously, the purification and dispersion of carbon nanotubes become a relevant and important issue in obtaining expectant and reproducible properties and performances for its technological applications. We herein report for the first time on the use of trifluoroacetic acid as a co-solvent for purification and dispersion of MWNTs, and the development of binary nanocomposites using the dispersed MWNTs, and PMMA through an all-solution process. TFA is a strong acid (100 000 times more acidic than acetic acid) but much less oxidative than nitric acid[95]. It is volatile (boiling point 72 °C) and highly miscible with water and many common organic solvents. The hydrophobic moiety of TFA, trifluorocarbon, along with a polar carboxyl group, provides a good solvation effect to organic compounds and materials. From our past research experience, it was noticed that co-solvents of TFA with other organic solvents can efficiently dissolve many organic compounds that tend to aggregate together through van der Waals interactions, hydrogen bonding, and other noncovalent interactions. We surmised that TFA may help dispersing carbon nanotubes as well. From the present study, it was found that TFA is indeed a good co-solvent to assist dispersion of CNTs in organic solvents and polymer matrices. Another advantage provided by TFA-assisted CNT dispersion is that, after the nanofillers and other components are dispersed into the polymer matrices, TFA will be evaporated off from the nanocomposite, avoiding a substantial plasticizing effect as caused by the addition of surfactants and other third components used to assist CNT dispersion. Apart from the dispersion of the nanotubes, a mixture of TFA with DMF was also used for the purification of the nanotubes. The use of conventional oxidizing acids also leads to the oxidation of the walls of the nanotube along with its purification which is undesirable. By using the mixture of TFA

with DMF, purification was achieved without the oxidation of nanotube walls. This was confirmed by X-Ray photoelectron spectroscopy (XPS) study. All the nanocomposite materials prepared from TFA-dispersed carbon nanotubes showed significantly low percolation thresholds of electrical conductivity. At about 0.12wt% of the CNT loading ratio, the conductivity has already risen to 10^{-3} S/cm.

Organic solar cells using a blend of SWNTs and conjugated polymer for the active layer were fabricated. The nanotube acts as an electron acceptor material and also allows the transport of electrons by providing percolation paths. The thickness of the active layer of the organic solar cells is extremely small. This makes the fabrication of organic solar cells a delicate process as the chances of shorts or bad contacts are high. The solar cells were successfully fabricated without any of these problems by adopting a proper structuring of the electrode surface by chemical etching and careful cleaning of the ITO surface.

CHAPTER 2 EXPERIMENTAL

2.1 Purification, Dispersion of Carbon Nanotubes and Preparation of Nanocomposite Films

2.1.1 Chemicals

During this study, two types of MWNTs were used. The first one was obtained from Aldrich (length: 5-9 μm , dia: 110-170 nm, aspect ratio ~ 100) designated as Type 1 and the second (length: 5-20 μm , dia: 15 ± 5 nm, aspect ratio ~ 1000) (Type 2) was purchased from Nano-Lab. PMMA with a weight average molecular weight of $120\,000\text{ g mol}^{-1}$, and all solvents used in this study were purchased from Aldrich. All solvents were reagent grade and used as received.

2.1.2 Characterization Instruments Used

2.1.2.1 Scanning Electron Microscopy (SEM)

The specimens were coated with a Pd-Au film by an Emitech Magnetron Sputter Coater before imaging in order to avoid electric charge build-up. The specimens then were observed by a JEOL 6400 SEM at an accelerating voltage of 5 kV.

2.1.2.2 Transmission Electron Microscopy (TEM)

MWNT samples in appropriate solutions were dropcast onto an untreated holey carbon coated TEM grid and the dried thin film sample was examined by a FEI Tecnai F30 TEM.

2.1.2.3 Dynamic Light Scattering (DLS)

The samples were taken in a quartz cuvette and DLS measurements were done using Malvern Zetasizer Nano Series (Nano-ZS) instrument. The data was analysed by Malvern DTS software.

2.1.2.4 X-Ray Photoelectron Spectroscopy (XPS)

The XPS spectrum of the samples was measured using ESCALab 220_XL instrument using a monochromatic K_{α} source.

2.1.2.5 Electrical Conductivity Measurements

The resistance of the film was measured by two probe method with a Keithley 6517A Electrometer/High-Resistance meter for samples with a high resistance and Keithley 2400 was used for samples with a lower resistance. The conductivity was calculated from the resistance values as discussed in the subsequent sections.

2.1.3 Purification and Dispersion of Multi-Wall Nanotubes

It has been reported that some impurities from the as-produced CNTs may be washed off by suspending the nanotubes in DMF[96]. We used a co-solvent of DMF and TFA to purify type 1 MWNTs. 8 mg of CNTs were ultrasonically dispersed in 18 ml DMF and 2 ml TFA and subsequently centrifuged at 6000 rpm for 6 min. The supernatant liquid was decanted and the solid was then redispersed for a further cycle of dispersion/centrifugation/decantation. Overall, five purification cycles were performed. After purification and drying in vacuum, MWNTs were

dispersed in various solvents for further studies. The type 2 MWNTs were used for dispersion study and nanocomposite preparation without further purification.

For dispersion study, 3 mg MWNTs were suspended in 5 mL of the following solvents: DMF, dichloromethane, n-hexanol, toluene, THF, and acetonitrile, with and without the addition of 10 vol% of TFA. The suspensions were sonicated in a water bath for 30 min (for solvents with TFA) or 1 hr (for solvents without TFA) with temperature maintained at 5 °C. The dispersion was examined both visually and by SEM studies.

2.1.4 Preparation of Nanocomposite Films

MWCNT/PMMA nanocomposite films with different CNT loading ratios were prepared using identical processing conditions by varying the filler type and content. The appropriate amount of MWCNTs was first dispersed in a solution of 10 % TFA in THF (total volume 3 ml) by ultrasonication for 1 hr in an ice water bath. PMMA powder was then added to the resulting dispersion and the mixture was sonicated further until the entire polymer was dissolved. The temperature of the water bath was maintained at 5 °C. The solution was then cast onto a clean glass substrate using a draw-down bar at 50 mil and the solvent was allowed to evaporate in a fume hood for at least 72 hrs.

2.1.5 Carbon Nanotube Dispersion Study in Solution and in Nanocomposite Films

For CNT dispersion study in a PMMA-free solution, a drop of CNT dispersion was cast on a graphite surface and the dried films were visually examined by a JEOL 6400 Scanning Electron Microscope (SEM) at an accelerating voltage of 5 kV. For CNT dispersion study in nanocomposite films, two techniques were used. First, optical microscope was used to examine the nanotube distribution visually. This study was conducted only on low aspect ratio Type 1 MWCNT using an Olympus BX51 microscope with a ColorView soft imaging system. Because the nanotube diameter of Type 1 MWCNT is in the range of 110-170 nm, the nanotubes can be visually seen through the optical microscope. Images were taken at different focus distances to reveal the distribution of the CNTs inside the composite film. The second method is through SEM of the cross section of the composite films.

2.1.6 Electrical Conductivity Measurements

The room temperature dc electrical conductivity of the composite films was measured using a standard two-probe technique. The nanocomposite films were first sand-polished slightly to expose the inner surface of the films. Then conductive silver paint strips were applied on the film surface as source and drain electrodes. The silver paint coating provides a good contact with the filler network within the specimen. The electrodes were spaced approximately $L = 5$ to 10 mm apart with a length of $w = 20$ mm. Data was collected by means of LabView interfaced with the Keithley 2400 for samples with lower resistance and the Keithley 6517A was used for samples with higher resistance. The resistance R was extracted from the linear I-V curves that were taken

from -2 to 2 V, which was reproducible over several sweeps. The conductivity was determined by the equation $\sigma=L/(R*w*t)$, where t is the thickness of the film. The thicknesses of the films were obtained from SEM study of the cross section of the broken films. For some samples, the conductivity was also measured with four probe technique and the results were in good agreement with the two-probe method.

2.2 Fabrication of Carbon Nanotube/ Conducting Polymer Organic Solar Cells

2.2.1 Chemicals

Regioregular-polythiophene was purchased from Aldrich. The purified SWNTs were bought from Carbon Nanotechnologies Inc, with an average length of 800nm. The ITO coated glass was purchased from Metavac, Inc. All the solvents were reagent grade and purchased from Aldrich.

2.2.2 Device Fabrication

For the fabrication of solar cells, the substrate used is a transparent electrode made of Indium tin oxide (ITO) coated glass. These glass plates are conductive on only one side where the ITO is coated. These substrates were then cut into appropriate sizes of about 1cm x 2cm. To avoid shorts in the device some of the ITO must be removed from the surface. This is done by etching ITO in an acidic bath. To avoid etching away all the ITO we have to cover part of the glass slide with a mask. This is done by a black adhesive tape which covers only the part of the glass where the ITO coating should stay. Half of the ITO layer coated on the glass was etched by dipping it

into a solution of 80vol% concentrated hydrochloric acid and 20 vol% DI water for 45 min. Following etching, the substrate was rinsed thoroughly with DI water to remove the acid. Under the adhesive tape, the ITO is not etched and covers the area of intended shape and size. Fig 2.1 shows the illustration of the etched substrate. Because of the extremely small thickness of the active layers in the organic solar cells, a very thorough cleaning is necessary to avoid shorts or bad contacts between the layers. The cleaning is done by adopting a standard procedure comprising sequential sonication for 10mins in each of the following solvents: acetone, ethanol and isopropyl alcohol. The substrate was dried with a blow of nitrogen after each sonication step. The substrate is then spin coated with a layer of PEDOT:PSS. This is a transparent conductive polymer which is coated to enhance the contact between the ITO electrode and the active layer.

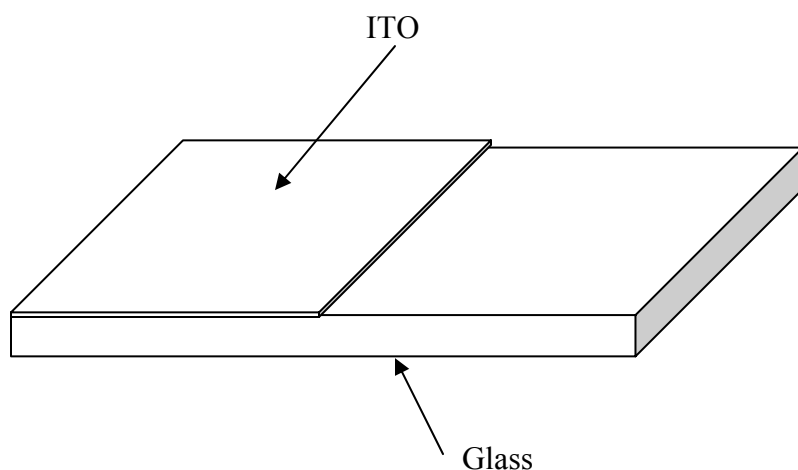


Figure 2.1 Schematic of the etched ITO substrate.

The optimum film thickness of this layer is between 50 and 100nm. This was achieved by trial and error. The 0.3 wt% of PEDOT:PSS solution was distributed evenly on the glass substrate which was subsequently rotated at of 1300 rpm for 40s. Due to the centrifugal forces, a very thin

and homogenous film is coated on the surface of the substrate. The substrate coated with PEDOT was then annealed at 110 °C for 45 mins. The thickness of the layer was 50nm as measured by alpha step profilometer. The active layer was prepared by the following procedure. First regioregular-polythiophene (a p-type semiconducting polymer) was weighed and dissolved in chloroform to a concentration of 5mg/ml. Either this solution was used as it is or calculated amounts of SWNTs were dispersed in the solution by sonication for 45min. The active layer was then coated to the PEDOT layer by spin coating at a speed of 2000rpm for 40s which gave a film thickness of about 200nm as measured by the alpha step profilometer. The fabrication of the solar cell is finished after the coating of the back electrode. An Aluminum foil mask is prepared and aligned to the substrate so that the metal electrode is deposited only on the area as shown in the fig 2.2.

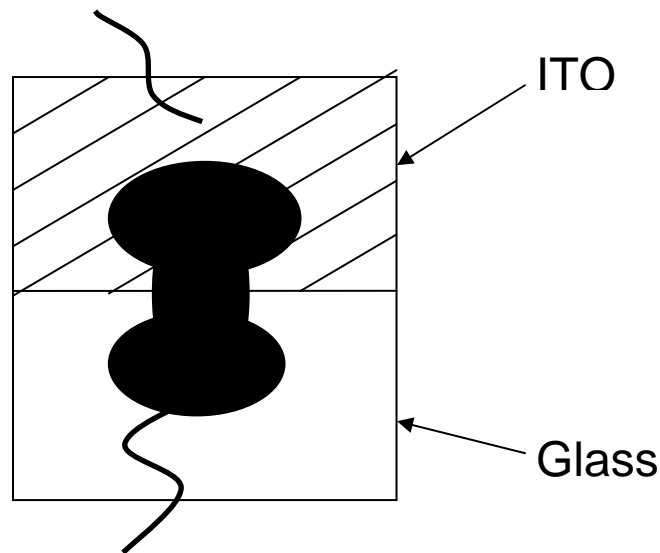


Figure 2.2 Top view of the device showing the Al back electrode

Al metal was thermally evaporated for this purpose. The film thickness was monitored and final thickness of the Al back electrode was 45nm. The design avoids the problem of a short circuit especially when giving a wired connection to the two electrodes of the solar cell namely the ITO

and the top Al layer. A wired connection for the top Al layer is given at the black circular region which does not have the ITO layer below it. To draw a connection from the ITO a small region of the coating is scraped to expose the ITO surface. All the wires are joined by applying a silver paste and allowing it to dry.

CHAPTER 3 RESULTS AND DISCUSSION

3.1 Multi-Wall Nanotube Dispersion in Solution

We first tested the dispersion of Type 1 MWNTs in a range of organic solvents including DMF, dichloromethane, n-hexanol, toluene, THF, and acetonitrile without TFA. After mixing the as-received MWNTs with the solvents, the mixtures were sonicated for 1 hr. Although the MWNTs showed a certain degree of dispersion during the sonication, they precipitated out in a few minutes in most solvents after the sonication was stopped, except in DMF and n-hexanol (Fig 3.1a). The good dispersion of MWNTs in these two solvents is believed to be associated with the high viscosity of the solvents. After the MWCNT bundles are mechanically broken apart, the high viscosity of these two solvents prevents the fast re-bundling of the nanotubes. However, these two solvents are not good solvents for polymer processing due to their high boiling points and high viscosity. After the addition of TFA (10 vol %) and sonication for 30 min, the dispersion of the MWNTs in all of the above organic solvents increased significantly, as seen from Fig 3.1b. After the sonication was stopped, all the dispersions were stable for at least 45 mins, a time sufficiently long for further wet processing of polymer nanocomposites. The best dispersion was observed from TFA/THF solvent. Moreover, after the addition of polymers, the dispersions are metastable for a much longer period owing to the increased viscosity of concentrated polymer solution.

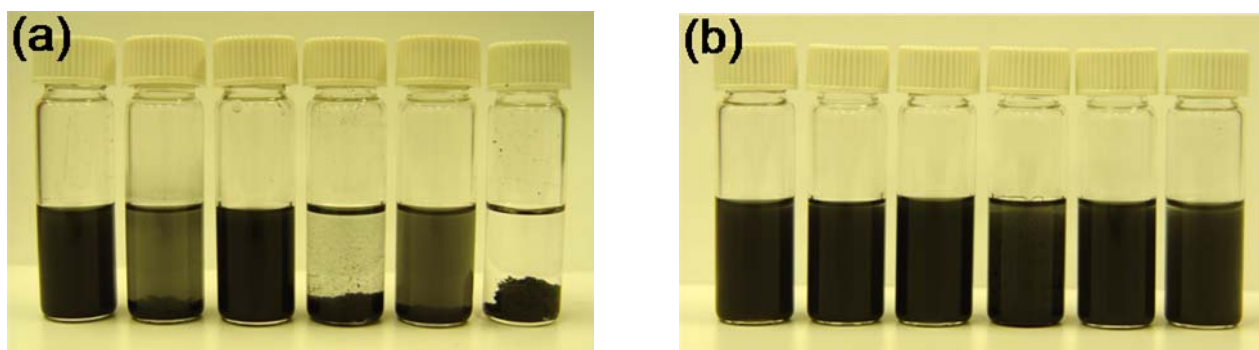


Figure 3.1 Photographs of the as-received MWNTs dispersed in (from left to right): N,N-dimethylformamide, dichloromethane, n-hexanol, toluene, tetrahydrofuran, acetonitrile. (a) Without the addition of TFA; (b) With addition of 10 vol% of TFA.

3.2 Dynamic Light Scattering (DLS) Analysis

Due to the anisotropic nature of the carbon nanotubes, DLS analysis cannot reveal accurate size information of the carbon nanotubes. Nevertheless, the DLS experiments can give a qualitative indication on the relative dispersion of MWNTs as a function of the concentration of TFA. Fig 3.2a shows the statistics of the particle size distribution for MWNT dispersed in THF without TFA. In this case, only minimum amount of MWNTs can be dispersed in solvent, with the majority of the sample quickly precipitated to the bottom of the sample tube after sonication is stopped. For nanotubes that went into the solution, an average size of 500 nm was observed from the nanotubes. Fig 3.2b and Fig 3.2c show the dispersion of MWNTs in THF with TFA concentration of 5vol% and 10vol%, respectively. The average of the size distribution was found to be about 360 nm and 280 nm for the samples with TFA concentration of 5 and 10vol%,

respectively. A clear trend of the peak shifting towards lower size of the nanotubes and therefore a better dispersion of nanotubes can be observed with an increase in the concentration of TFA.

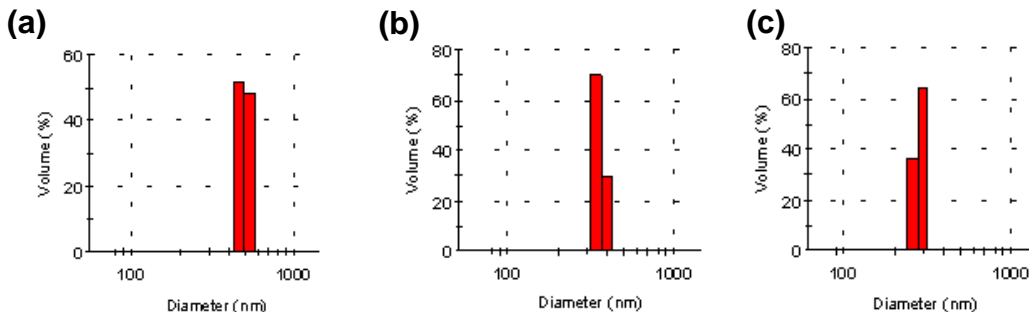


Figure 3.2 Histogram showing the particle size distribution of MWNTs dispersed in THF for a) Without TFA b) 50µl/ml TFA c) 100 µl/ml TFA by dynamic light scattering measurements.

3.3 Scanning Electron Microscopy (SEM) Analysis

The degree of dispersion of the Type 1 MWNTs was examined by SEM. The samples for SEM study were prepared by allowing a drop of MWNT dispersion in THF or 10% TFA/THF to dry on a graphite substrate. Fig 3.3a shows a typical image of the MWNTs dispersed in pure THF. Most MWNTs in this case are still severely aggregated together. Dispersion is remarkably improved for the MWNTs dispersed in 10 vol% TFA/THF solvent (Fig 3.3b). However, one can also notice the presence of a large amount of spherical particles which are carbonaceous impurities and metal catalysts. Using a mixed 10% TFA/DMF solvent, we purified the MWNTs as described in the experimental section. Fig 3.3c shows the image of purified MWNTs re-dispersed in 10 vol% TFA/THF. Fig 3.3d is a magnified image of the top left region of Fig 3.3c. There is a drastic decrease of impurity particles in the MWNT dispersion. As a strong acid, TFA helped dissolve some small carbonaceous particles, metal catalysts and other impurities that were

eliminated from the sample after a few repeated washing cycles. Also noticed from the SEM image (Fig 3.3c), the average length of the TFA-treated MWNTs remained about the same as original untreated nanotube sample. Unlike dispersion prepared from mechanical force or strong oxidation acids, TFA treatment did not cause nanotube shortening.

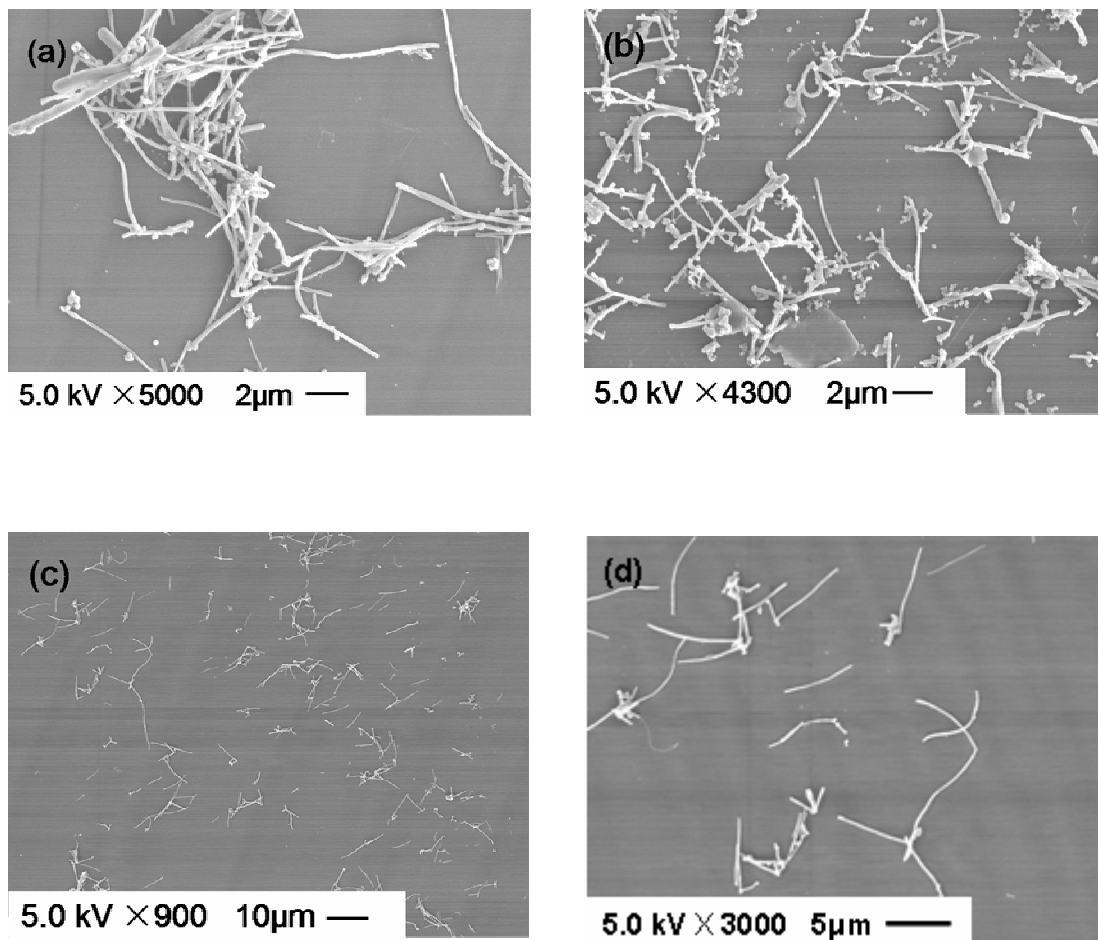


Figure 3.3 SEM images of Type 1 MWNTs suspended or dispersed in THF and then deposited on graphite substrates: (a) MWNTs suspended in pure THF. (b) The as-obtained MWNTs dispersed in 10 vol% TFA in THF. (c) MWNTs after purification by multiple cycles of washing with 10 vol% TFA/DMF solvent and redispersed in 10 vol% TFA/THF solvent. (d) Magnified image of the top left region of (c).

3.4 Transmission Electron Microscopy (TEM) Analysis

For the TEM analysis, the samples were prepared in a similar way, by allowing a small volume of MWNT dispersion to deposit onto the copper grid and the excess amount of liquid was carefully removed. The samples were then examined by a FEI Tecnai F30 transmission electron microscope. Fig 3.4a shows the typical image of as received MWNTs dispersed in pure THF. The catalyst impurities and the aggregation of MWNTs can be clearly seen. Fig. 3.4b shows the TEM image of purified MWNTs re-dispersed in 10 vol% TFA/THF. The number of impurity particles has significantly reduced and there is visible improvement in the dispersion.

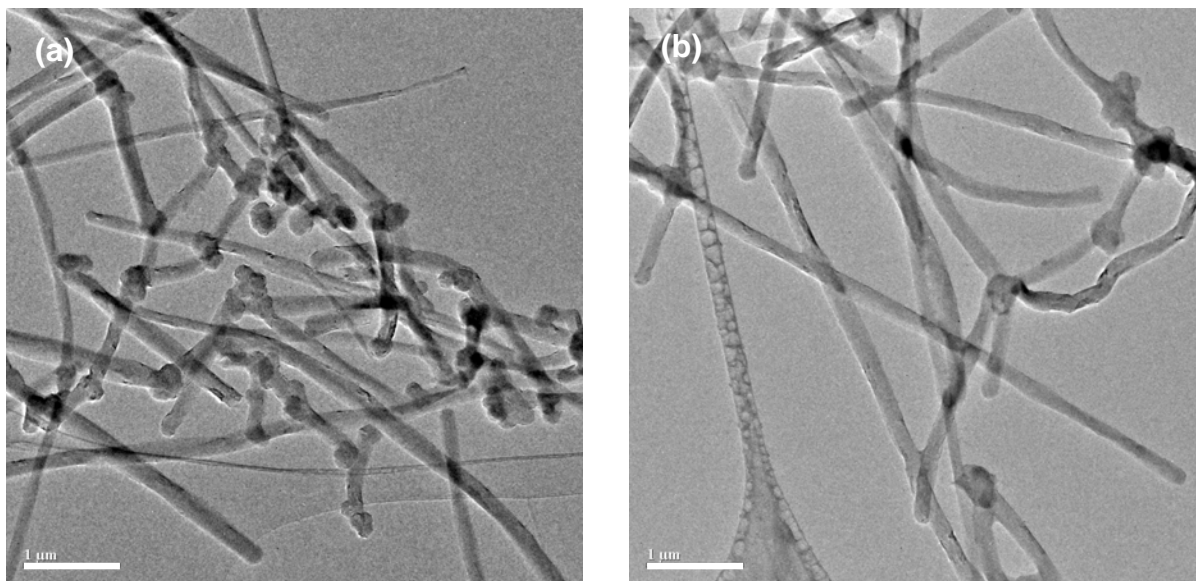


Figure 3.4. TEM images of Type 1 MWNTs: (a) suspended in pure THF (b) after purification by multiple cycles of washing with 10 vol% TFA/DMF solvent and redispersed in 10 vol% TFA/THF solvent. Scale bar shown is 1 μm .

3.5 X-Ray Photoelectron Spectroscopy (XPS) Analysis

As mentioned earlier, because TFA is a much less oxidative acid than nitric or sulfuric acid, it is expected that the treatment of CNTs with mixed TFA/organic solvents will not lead to the oxidation of nanotube walls. X-ray photoelectron spectroscopy (XPS) was used to examine the types of carbon that exist in the treated and untreated Type1 MWNT samples. Shown in Fig 3.5a is the C 1s XPS spectrum of the as-received MWNTs. Two peaks were identified, one is a major peak at 284.7 eV, which is assigned to the conjugated C in CNTs, and a minor peak at 287.7 eV, which is attributed to impurity carbon in the form of C-OH[97, 98]. After purification of the MWNTs by mixed TFA/DMF solvent, the major peak at 284.7 eV remains the same, but the minor peak at 287.73 eV diminished almost completely (Fig 3.5b). This result suggests that indeed MWNTs can be effectively purified by multiple washing cycles using TFA/DMF mixed solvent. As a comparison, the C 1s XPS spectrum of nitric acid-treated[32] MWNTs is shown in Fig 3.5c. A peak corresponding to oxidized carbon at 289.1 eV in the form of COOH groups[66, 99] can be clearly seen. In contrast, no oxidized carbon peak can be seen in TFA-treated MWNTs (Fig 3.5a and b).

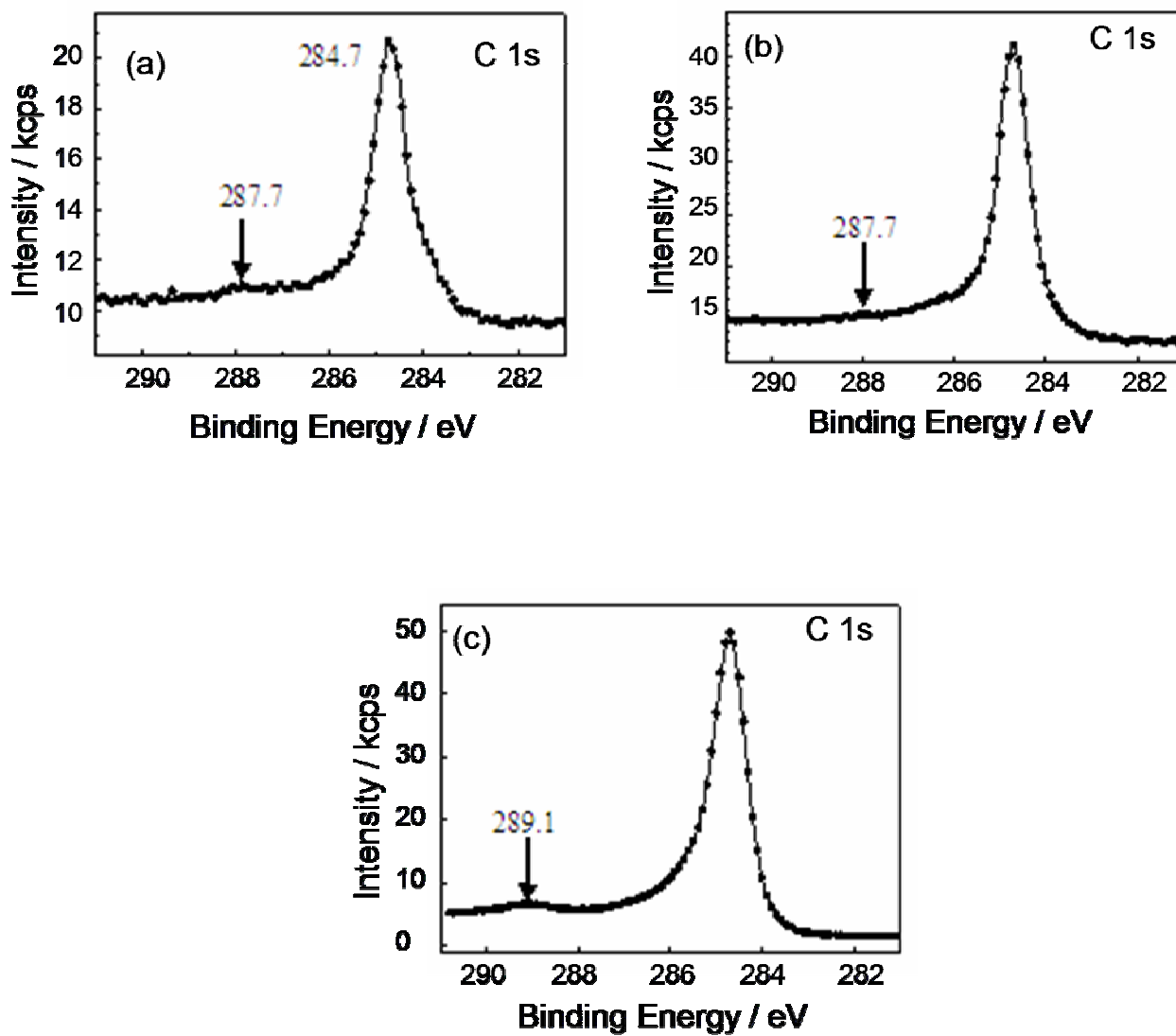


Figure 3.5 C1s X-ray photoelectron spectra of (a) untreated MWNTs; (b) MWNTs treated by TFA; (c) MWNTs treated by nitric acid.

3.6 Nanocomposite Preparation and Carbon Nanotube Distribution in Composite Films

Nanocomposite thin films with a thickness around 100 μm were prepared by simply casting the dispersed carbon nanotube/polymer solution on glass substrates using a drawdown bar. The films were dried by leaving them in a fume hood for a few days. The dispersion of CNTs in nanocomposite films was first examined by optical microscope. For each film, multiple images were taken at different focus distances to reveal the distribution of the CNTs inside the composite film. Fig 3.6. shows a few representative images of the MWNT/PMMA composite at different focus distances. A small amount of CNT aggregates are observed in the composite film.

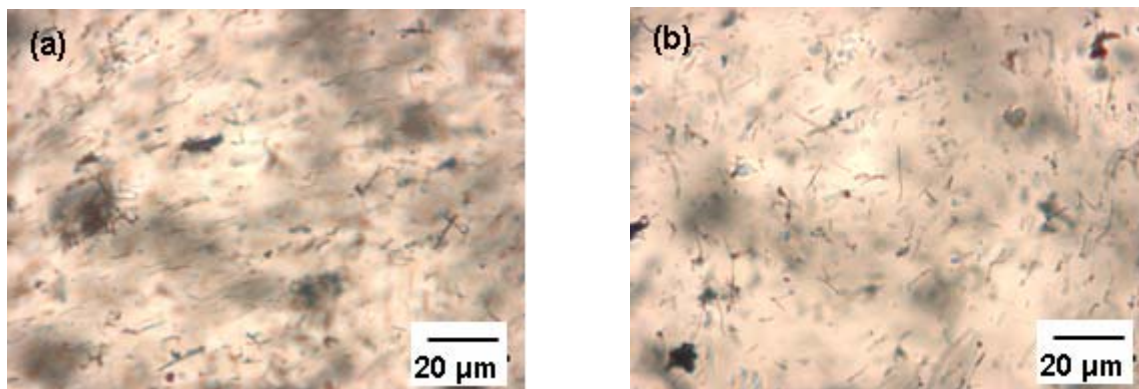


Figure 3.6(a,b) Optical images revealing the distribution of MWNTs at different focus distances in the 0.25wt% MWNT/PMMA composite

The dispersion of CNTs was further examined by SEM analysis of the cross section of the broken films. Fig 3.7a. shows the typical thickness of the films that were prepared in this study. Fig 3.7b is a magnified view of the cross section of the broken film which shows individual MWNTs distributed through the cross section.

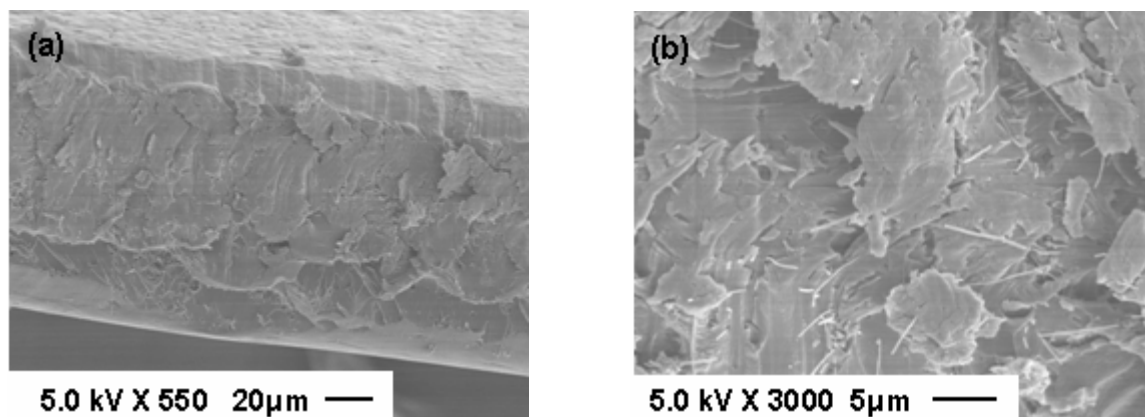


Figure 3.7 Cross-section SEM images of the composite film containing 1 % of MWNTs at (a) low magnification (b) higher magnification

3.7 Electrical Conductivity Study of Nanocomposite Films

Carbon nanotubes have been demonstrated as by far one of the best nanofiller materials for transforming electrically nonconducting polymers into conductive materials. The electrical conductivity was measured on nanocomposites with different loading ratios of MWNTs. The electrical conductivity of Type 1 and 2 MWNT/PMMA composite films were plotted against the loading ratio of MWNTs (Fig 3.8. a,b). For the nanocomposites prepared in this study, the conductivity follows a typical percolation scaling law. A percolation threshold is a particular nanofiller loading ratio where dramatic conductivity increase may be observed. For a system

comprising of a random distribution of the filler material in a matrix, this value is closely related to the dispersity of nanofillers in the polymer matrix and also the aspect ratio of carbon nanotubes. For Type 1 composites (Fig 3.8a) at a filler concentration below 0.5 %, the conductivity of the film remains very low. One can notice that around 0.65% the conductivity of all three sets of films increases drastically. At an approximate loading ratio of 1.25%, the conductivity of the nanocomposite stabilized at about 10^{-3} S/cm. For the high aspect ratio MWNTs (Fig. 4.8b), the conductivity of the nanocomposite reached to 10^{-3} S/cm at 0.2 wt% nanotube loading ratio. The percolation thresholds are 0.65 wt% and 0.12 wt% for Type 1 (aspect ratio 100) and Type 2 (aspect ratio 1000) MWCNT/PMMA composites, respectively. It should be noted here that in most reported nanocomposites using a similar aspect ratio (~ 100) of MWNTs as in our study [100-102], percolation thresholds fall in the range of 1.44-7.5 wt%. The decreased percolation threshold of our composites is a strong evidence of a better dispersion of CNTs in the polymer matrix.

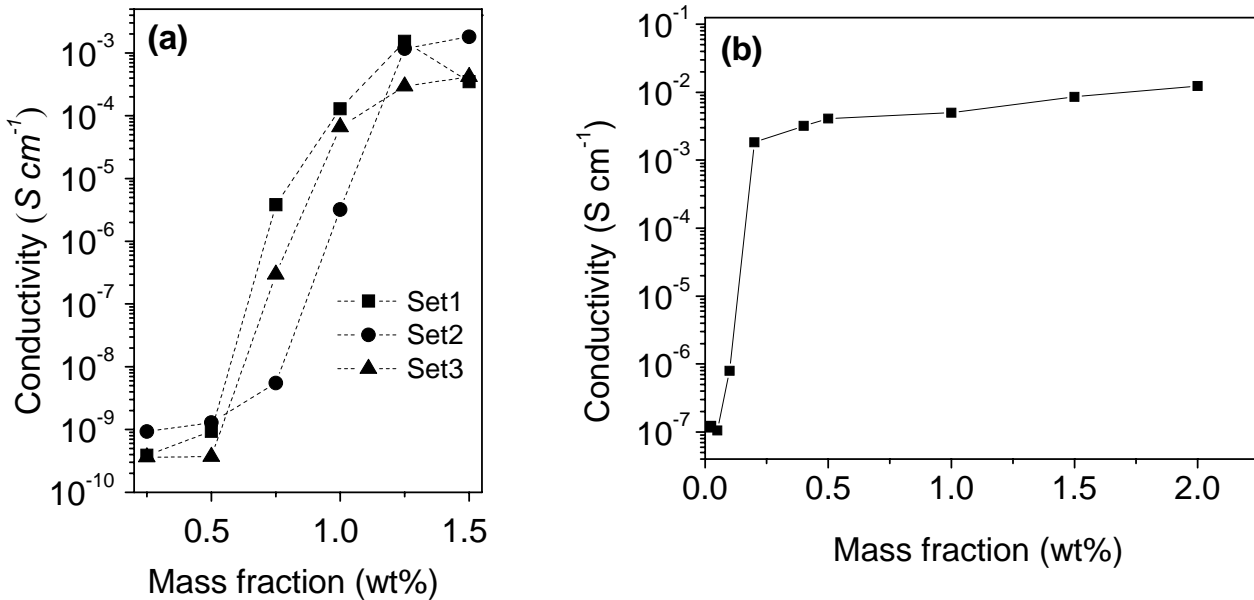


Figure 3.8 Room temperature electrical conductivity of MWNT/PMMA composites with MWNT aspect ratio of (a) 100 and (b) 1000

3.8 Fabrication and Characterization of Solar Cells

3.8.1 Contact Angle Measurements

While coating a layer of PEDOT:PSS onto the substrate, it was noticed that the coating was not uniform over the entire substrate due to the different surface properties of the glass and ITO. This was studied by contact angle measurements on the glass and ITO surface. The as-received ITO coated glass had a contact angle of 77.1° and the glass had a contact angle of 48.4° . The non uniform coating of the PEDOT layer is due to the large difference in the contact angles on the

ITO and glass. The contact angles obtained after the standard cleaning procedure is shown in fig 3.9.

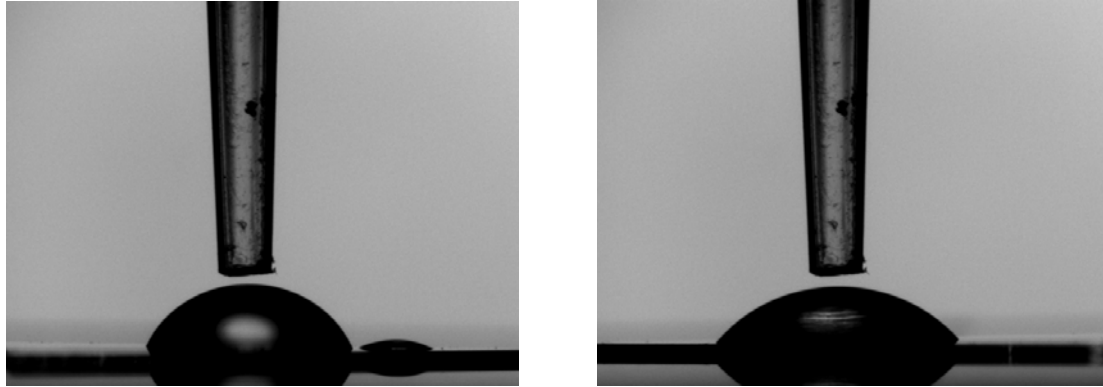


Figure 3.9 Contact angle on (a) ITO: 66.2° and (b) Glass: 49.8° , after standard cleaning.

Though the contact angle improved, with it being 66.2° on ITO and 49.8° on glass after the standard cleaning procedure, the difference was still large enough and gave non uniform coating properties. To make the substrate more hydrophilic, it was then treated with oxygen plasma for fifteen minutes and the contact angles were measured. The results are shown in fig 3.10.

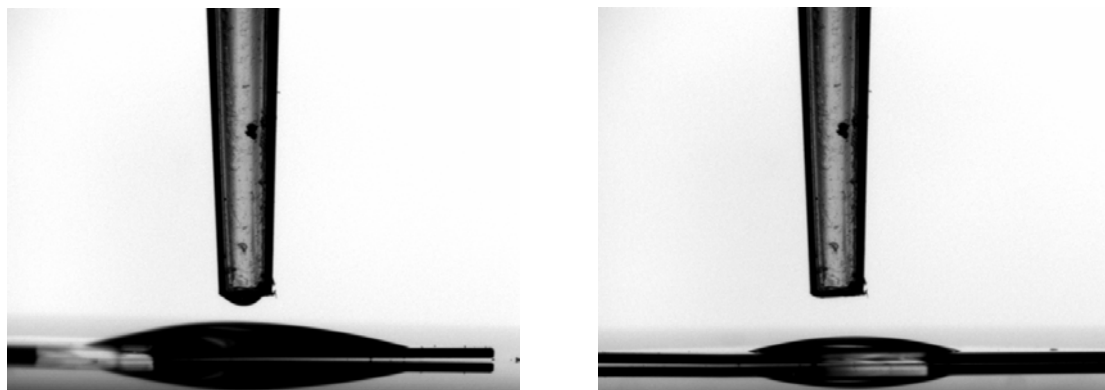


Figure 3.10 Contact angle on (a) ITO: 18.2° and (b) Glass: 20.5° , after plasma cleaning.

The contact angle measurements showed superior results after plasma cleaning. It was found to be 18.2° on the ITO surface and 20.5° on the glass surface. The decrease in contact angles shows an increase in the hydrophilic character of the substrate, favorable to the coating of PEDOT:PSS solution. Due to a small difference in the contact angles, a uniform substrate coating was also obtained.

3.8.2 Device Characteristics

The current-voltage (I-V) characteristics of the solar cells are shown in Fig 3.11. The data was collected by means of LabView interfaced with a keithley instrument. The dark circles show the I-V taken in the absence of light while the open circles show the I-V characteristics in the presence of light. A small illumination bulb was used as a light source. From the fig 3.11, it is clearly visible that the device fabrication was successful without shorts in the circuit.

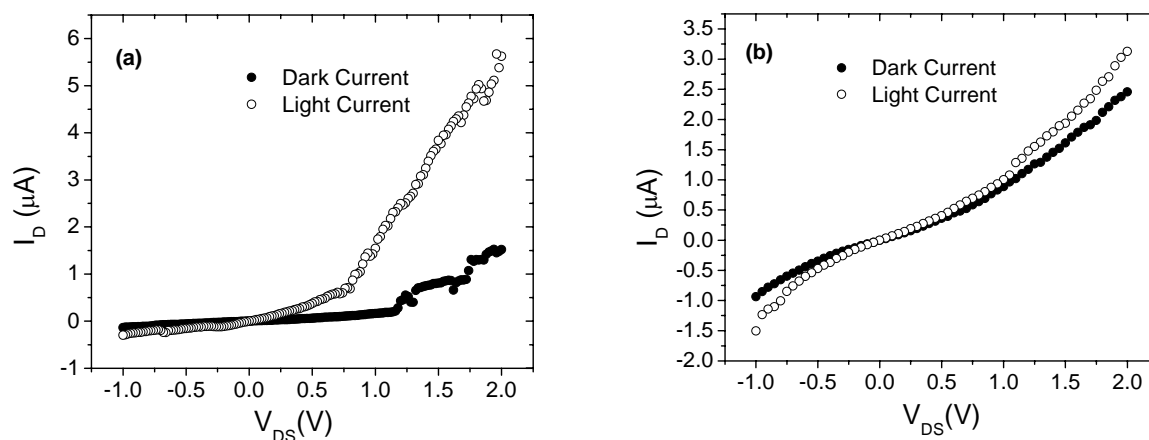


Figure 3.11 Device characteristics of solar cells: a) With only P3HT as active layer b) With P3HT/0.3 wt% SWNT as active layer

A high dark current is observed in the case when the SWNTs/conducting polymer blend is used as the active layer. One reason could be that the dimension of the nanotube (~800nm) is much higher than the thickness of the active layer (~200nm.). Also the active layer is sensitive to atmospheric oxygen and water and can quickly deteriorate in the presence of these factors. As the fabrication was not performed in controlled atmospheric conditions such as a glove box, it can be expected that the efficiencies are very low.

CHAPTER 4 ELECTRODE AND ELECTROLYTE MATERIALS FOR LITHIUM-ION BATTERIES

4.1 The Development of Lithium Batteries

With a growing demand for smaller, lighter, and more powerful energy sources for modern mobile technologies such as cellular phones, laptops, camcorders etc., lithium batteries have rapidly replaced the nickel-cadmium (Ni-Cd) and nickel metal hydride (Ni-Mh) batteries as a dominant force in the rechargeable battery market. Lithium has the highest electrochemical potential (-3.04V versus the standard hydrogen electrode) and is the lightest metal which makes it an ideal material for batteries to produce high energy per unit weight. The output voltage of its unit cell is in the range of 3 to 4.2 volts as compared to 1.5V for Ni-Cd and Ni-MH cells.

4.1.1 Lithium Metal Vs Lithium-Ion Batteries

The two kinds of technologies developed for lithium batteries are the lithium metal technology and lithium ion technology. The first one uses lithium metal as the anode while the second one uses the intercalation compounds as the anode. Though the lithium batteries have a high capacity and variable discharge rate, it has its own shortcomings. During the charging process of the battery, the lithium metal tends to deposit on the electrode in the form of needle-like crystals, called dendrites. This phenomenon can prove to be dangerous during charging, as the needle-shaped crystals can grow to such an extent that they penetrate the separator and create a short circuit between the electrodes, which leads to explosion hazards. To rectify this problem, the

lithium metal was later substituted by its alloy with Al[103] solved the dendrite problem but the system did not possess sufficient cyclability due to significant changes in volume during operation. Because of the inherent instability of the lithium metal, a second type of lithium cell, the lithium ion or rocking-chair cell was developed which is designed to operate on the mechanism of intercalation. No lithium metal is necessary in this type of cell as lithium is always held as a guest in one of the insertion electrodes depending on the state of charge.

4.2 Electrolytes for Lithium Batteries

There are two different approaches to assemble the cells, one is by using a liquid electrolyte and the other is by using a solid polymer electrolyte. There are significant differences between the two approaches which are reflected in the areas of cost, size and safety as would be discussed further.

The cost of manufacturing Li-ion batteries with liquid electrolyte is higher as the winding, canning and hermetic sealing processes associated with it are complex and expensive. For the Li-ion polymer cells, all the components of the cell-the electrodes, the solid polymer electrolyte and the packaging are on continuous feed rolls and can be sandwiched together into finished batteries in one smooth process. This allows for lowering the cost and increasing the speed and volume of battery production.

The liquid Li-ion cells cannot be made too large due to safety considerations stemming from the presence of the liquid electrolyte. On the other hand, the widths and the lengths of the solid

polymer electrolytes are very flexible allowing the Li-ion cells to be designed for the space available in the product instead of the product being designed to accommodate the size and shape of the battery. Also, the electrolyte of a solid polymer Li-ion cell cannot leak, making it intrinsically safer than a liquid Li-ion cell.

4.2.1 The Requirements of Battery Electrolytes

The role of electrolytes is crucial to achieve the high performance of lithium batteries for which the electrolytes need to fulfill the following requirements.

- A typical conductivity above 0.1mS/cm are needed at room temperatures to allow a reasonable current density.
- The electrolyte must be electrochemically stable in the voltage window defined by the electrode reactions. Preferably it should be stable in a wider voltage range (>4V) to accommodate for overcharge and discharge reactions.
- They should be chemically compatible with the other components of the battery like the electrodes and other material that may be in contact with it in the whole temperature range of operation.
- A good thermal stability in the operating temperature range is required especially if in contact with a lithium electrode.
- A solid polymer electrolyte should have a good mechanical strength to afford the lamination process and for liquid electrolytes reducing the flammability is a concern.

4.2.2 Liquid Electrolytes

Aqueous liquid electrolytes cannot be used for lithium batteries. Even though some inorganic electrolytes like lithium iodide have been used as an electrolyte for lithium cells, organic non-aqueous electrolytes are the most commonly used.

The organic electrolytes which are used for lithium batteries are a mixture of conductive lithium salts and organic solvents which are liquid at room temperature. Most of the organic solvents are required to work well outside their window of thermodynamic stability against lithium metal but fortunately this electrolyte stability is kinetically controlled

In addition to stability, a high conductivity of the electrolyte is desirable for which the organic electrolyte should be able to dissociate the lithium salts effectively. A high dielectric constant of the solvent aids the separation of ion pairs. A low viscosity of the solvent and a high degree of salt dissociation are also required for high conductivity.

4.2.3 Solid Polymer Electrolytes

Armand[104] reported an elegant method to combine the elastomeric and electrolytic properties by using polymer electrolytes for applications in solid state electrochemical devices, especially lithium batteries. Poly(ethylene oxide) was found to solvate many metal salts such as LiBr, LiCl, LiSCN, LiClO₄, LiSO₃CF₃, LiBF₄, LiPF₆, and LiAsF₆ [105]. However the conductivity of the complexes reached only 10⁻⁸-10⁻⁷S/cm at room temperature. The transport of Li ion in the

electrolyte is favored when the PEO is in the amorphous phase. This was the reason for low conductivity of the electrolyte at ambient temperatures due to the higher crystallization ratios of the polymer host. The ionic conduction in most lithium-salt based polymer electrolytes is dominated by anions[106]. This is detrimental to the battery as it leads to concentration polarization which can ultimately cause the failure of the battery. Armand et al[107] synthesized a new lithium salt, lithium bis(trifluoromethanesulfonyl)imide (abbreviated as LiTFSI) in which the big anion caused an extensive charge delocalization and had a plasticizing effect on the electrolyte making the PEO chain more flexible. Many related imide salts have been synthesized and studied in a search to find the most satisfactory electrolyte [108-111].

Other polymers like polydimethylsiloxane $[-(\text{CH}_3)_2\text{SiO}-]_n$ and poly(dichlorophosphazene) $[-\text{Cl}_2\text{P}=\text{N}-]_n$ have been used as polymer backbones with different lengths of oligo-oxyethylenes attached as side chains have also been used as polymer hosts to form the polymer-salt complex.

4.2.4 Polymer Gel Electrolytes

The advantage of solid polymer electrolytes is that they are not subject to leakage, but the lithium ion conductivities in most cases is in the range of 10^{-8} to 10^{-5} S/cm, which is not sufficient for most battery applications. By using a liquid electrolyte, an ionic conductivity of the order of 10^{-3} S/cm or above can be achieved but the disadvantage is that the battery is prone to electrolyte leakage. Polymer gel electrolytes offer the advantage of both without the drawbacks. These electrolytes in addition to the salt and the polymer have an additional plasticizer, which act as chain lubricants, added to them. The suitable plasticizers are most often the same as the suitable

liquid electrolytes. A lightly plasticized material (10 to 25% additive) can increase the ionic conductivity by an order of magnitude[112]. Polymer gel electrolytes which contain 60 -95% of the liquid electrolyte, are only 2-5 times less conductive than their liquid electrolyte counterparts[112]. The commonly used plasticizers are usually the less volatile solvents such as ethylene carbonate (EC), propylene carbonate (PC), dimethyl formamide (DMF), methylethyl carbonate (MEC), diethyl carbonate (DEC), γ -butyrolactone or polyethylene glycol ethers.

4.3 Cathode Material for Lithium Batteries

Research and development has been targeted towards the development of lithium metal free batteries which have the advantages of dimensional stability and improved chemical stability. These batteries were originally termed as “Rocking Chair” batteries, the concept of which was demonstrated by using transition metal compound anode and cathode. The commonly studied intercalation compounds for lithium rocking chair batteries come under the following types: Li_xMO_2 (M refers to Co or Ni) type compounds, manganese oxide type compounds ($\text{Li}_x\text{Mn}_2\text{O}_4$), vanadium oxide ($\text{Li}_x\text{V}_2\text{O}_5$) type compounds.

4.3.1 The Requirements of Cathode Materials

- The free energy of the reaction of Li ion with the cathode should be high so that its electrochemical potential with respect to the anode is high. Also its electrochemical potential should preferably remain constant while discharging.

- It should show high charge per mass values by being able to react with several moles of lithium for every mole of the active material which would enable a high charge capacity.
- It should have a good electronic conductivity as required for high power applications and also to minimize energy losses due to resistive heating. Good ionic conductivity is also required to minimize polarization losses and allow fast ion migration during charging and discharging reactions.
- The reaction with lithium ions should be thermodynamically reversible and also allow many charge-discharge cycles.

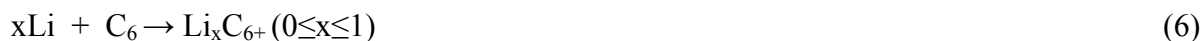
4.3.2 Vanadium Oxide as a Cathode Material for Lithium Batteries

Vanadium oxide is a promising material for cathode in lithium ion battery as they tend to form layered structures and these layered structures can incorporate lithium into their lattice space. In fact it has been shown that the V_2O_5 can intercalate upto 3.3 moles of lithium per mole of the oxide which substantially exceeds other intercalation host materials such as CoO_2 , Mn_2O_4 , NiO_2 . Also, the insertion process associated with the cathode is thermodynamically reversible which means that all the lithium that is intercalated during discharge is removed upon anodic charging. This reversibility is maintained over multiple charge discharge cycles and the cathode has acceptable charge and discharge current density. No degradation of the cathode electrolyte interface occurs during battery cycling. Different synthesis techniques yield different varieties of V_2O_5 like glasses[113, 114], xerogels[115] and aerogels[116] which further creates possibilities for improvement in the lithium ion transport and other parameters. In addition to crystalline V_2O_5 , amorphous and low crystalline materials have also yielded promising results. Mesoporous

V₂O₅ aerogels having nanometer sized domains connected together to give porous materials have been synthesized. These porous materials had a superior capacity as compared to V₂O₅ powder cathodes[117].

4.4 Anode Material for Lithium Batteries

Carbon based materials have been the material of choice for use as anode materials of lithium-ion batteries. The lithium intercalation into carbonaceous materials such as coke[118], natural graphite[119-121], highly oriented pyrolytic graphite (HOPG)[122], vapor grown carbon fiber (VGCF)[123] have been extensively studied. These carbon anode materials have a graphitic or disordered structure. By “graphitic” it does not mean that the material has a perfectly layered structure but it rather means that these layers are incorporated in the structure. The Li ion intercalates into these layered structures in a specific manner. Certain specific layers are first occupied till the repulsive interactions of the Li ions drive the intercalation reactions to another layer. The intercalation of Li ion into carbon follows the reaction



The lithium insertion capabilities strongly depend on the species of carbon materials as the capacity is affected by the physical characteristics such as crystal structure and/or alignment of crystallites. The discovery of new crystalline forms of carbon such as single and multi-walled carbon nanotubes opens the opportunity to further increase the lithium doping capability. SWNTs with their high aspect ratios provide high accessibility to the entire carbon structure for Li interaction when compared to the regular carbon lamellas which are circumferentially oriented and block much of the particle interior. Though the accessibility of the SWNTs is mitigated

somewhat by the bundling effects due to the van der Waals forces, these materials should still provide higher accessibility than the conventional graphitic anode materials.

4.5 Overview of the Present Work

The operating voltages of the lithium-ion batteries rule out the use of aqueous electrolyte systems. Moreover, even with the selection of organic solvents, the operating voltages for Li-ion batteries are still outside the thermodynamic stability window of these solvent systems. Fortunately, the electrolyte decomposition of the solvents is kinetically controlled permitting extended use in the operating potentials of lithium ion batteries. The choice of the solvent has to be made considering the viscosity and the dielectric constant. High dielectric constant solvents facilitate the dissociation of the salt but these solvents are also highly viscous due to the molecular interactions which alter the charge on the molecules. A low viscosity of the solvent is required for a high conductivity of the electrolyte films and easier polymer electrolyte processing. With this in mind, two solvents, THF and DMF were chosen for the purpose of preparing the polymer electrolyte films. PMMA was chosen for the study as it readily combined with lithium trifluoroacetate in solution to produce a stable electrolyte. It is also supposed to have a superior chemical stability when in contact with highly oxidizing cathode materials. The objective is to find the processing conditions which give the most favorable results as desired for the polymer electrolyte materials. Vanadium oxide is a material known to have a large capacity for lithium insertion. Also, other factors discussed in the previous section make it the most suitable cathode material. Similar reasoning goes with carbon nanotube/block copolymer composite which was chosen as the material for the anode. A lot of research has been done and is

still being done as there still remains room for improvement in these major areas of lithium ion battery technology. The purpose of the present work is to synthesize, characterize and evaluate the performance of these materials.

4.6 Electrochemical Impedance Spectroscopy (EIS)

Impedance spectroscopy is a powerful tool to characterize many of the electrical properties of electrochemical systems and their interfaces. The Ohms law for a DC signal is given by

$$R = \frac{V}{I} \quad (7)$$

where R is the resistance which impedes the flow of the current I when a potential V is applied across the circuit. When an AC signal is applied

$$Z = \frac{V}{I} \quad (8)$$

where Z is defined as the impedance

In an EIS measurement, a small AC excitation signal is applied over a range of frequencies that span from a few milli-Hertz to many kilo-Hertz and the electrochemical impedance response is measured. In order to characterize the ac waveform, vector analysis is used. It can be described in terms of its amplitude and phase characteristics or in terms of a real part and an imaginary part of a complex number. When the current and voltage are expressed in terms of a complex number, the resulting expression for the ac impedance Z is also defined in terms of the same coordinate axis as the current and voltage vectors as follows.

$$\bar{Z} = \bar{Z}^* + j\bar{Z}^{**} \quad (9)$$

The superscripts * and ** correspond to the real and imaginary component of the vector.

The magnitude of the ac impedance is given by

$$|Z| = \sqrt{(Z^*)^2 + (Z^{**})^2} \quad (10)$$

and the phase angle (ϕ) is defined as

$$\phi = \arctan\left(\frac{Z^{**}}{Z^*}\right) \quad (11)$$

To make use of the complex numbers that are obtained from the EIS measurement, the system under test is modeled as a collection of electronic components such as resistors and capacitors in series or parallel combinations. A model with a proper combination and values of the circuit elements will give a frequency response that is similar to that measured by the EIS experiment. Each of the elements have a physical significance (e.g., microstructure, properties, degradation, grain growth etc). Fig 4.1 shows a Randles circuit which models the electrochemical impedance of many simple electrochemical systems. A double layer is established at the interface between the electrode and the electrolyte in which the positive and negative ions are separated due to a sheath of hydration. This double layer acts as a capacitor C_d which is in parallel with polarization resistance R_p due to the charge transfer reaction. The ionically conducting electrolyte impedes the transfer of charge and acts as a resistor R_s in series with C_d and R_p .

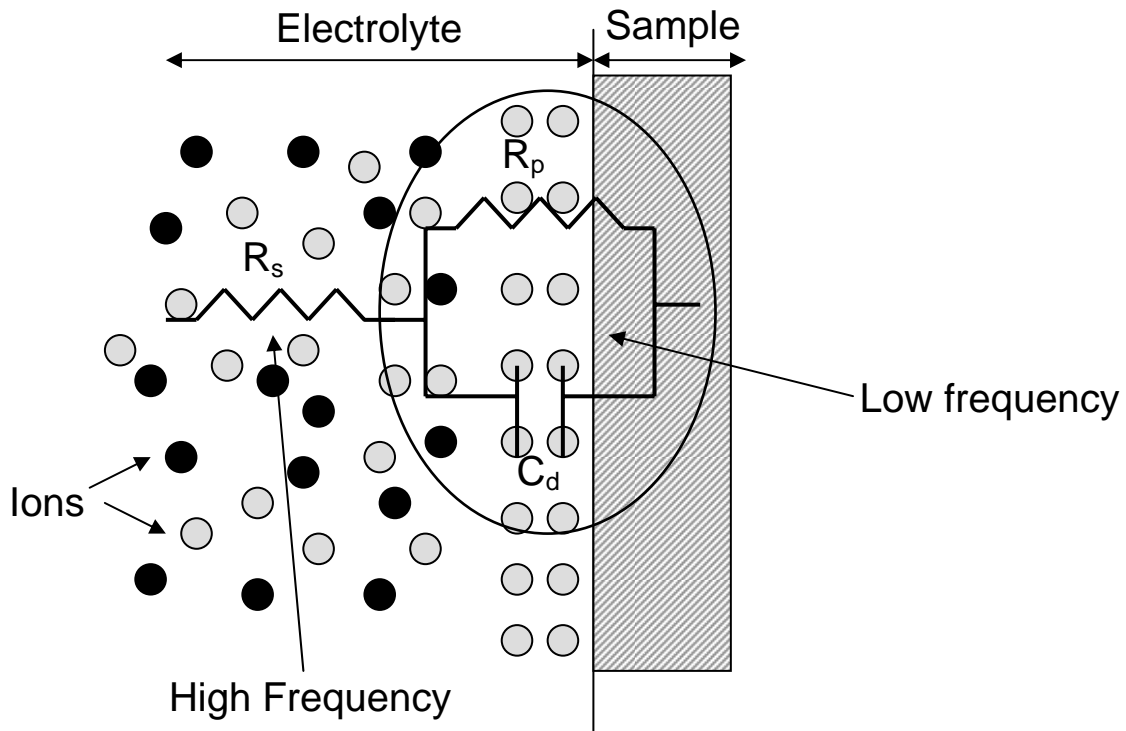


Figure 4.1 Impedance network model (Randles circuit) for a metal in electrolyte.

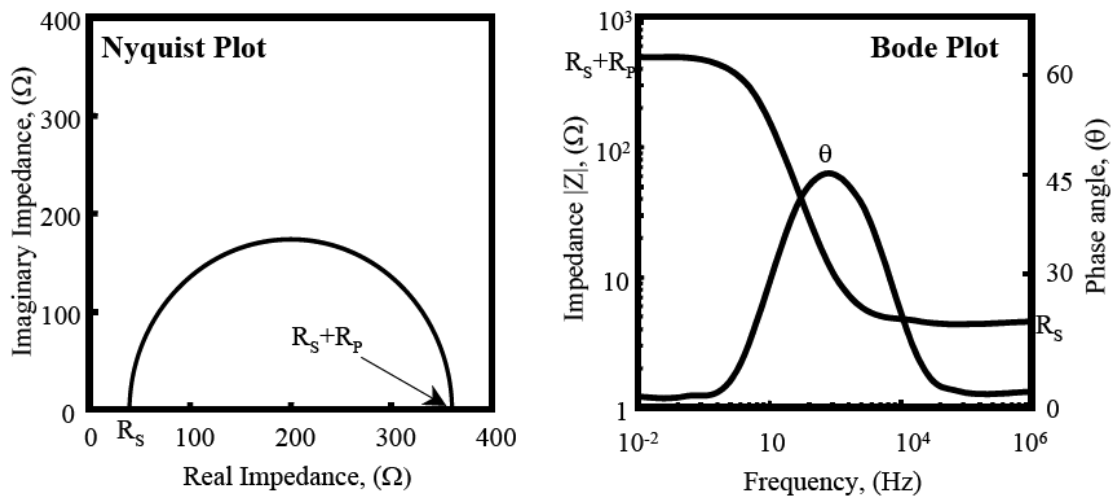


Figure 4.2 Nyquist and Bode plots for a Randles circuit.

The Nyquist and Bode plot for the Randles circuit is shown in Fig 4.2. The left of the semicircle in the Nyquist plot shows the high frequency response and the low frequency response lies on the right. The real axis value of the resistance closer to the origin gives the solution resistance and the other intercept gives the sum of solution and polarization resistance. For the Bode plot, the solution resistance and the sum of solution and polarization resistance can be found by looking at the values of the intercept along the y-axis.

CHAPTER 5 SYNTHESIS AND CHARACTERIZATION OF ELECTRODE AND ELECTROLYTE MATERIALS

5.1 Synthesis of Electrode and Electrolyte Materials

5.1.1 Chemicals Used

PMMA with a weight average molecular weight of 120 000 g mol⁻¹, V₂O₅, lithium trifluoroacetate and all solvents used in this study were purchased from Aldrich. P3HT-b-PS block copolymer (one of the component of lithium battery anode material) was synthesized by McCullough group by a previously reported procedure with above 98% head-to-tail regioregularity.[124, 125]. SWNT was purchased from Carbon Nanotechnologies with a diameter of 0.8-1.2 nm and a length of 100-1000 nm. The purity was above 65%. All solvents were reagent grade and used as received.

5.1.2 Formulation of Electrolyte Films

PMMA was the polymer material and lithium trifluoroacetate was the salt chosen for the polymer-electrolyte system. The electrolyte films were made under different processing conditions. Two different solvents, THF and DMF were used to prepare the films. The solvent was either allowed to evaporate by keeping the samples in vacuum for a week or the solvent was allowed to remain in the films. The films were also prepared with and without the addition of TFA as a cosolvent in the films. Designated amounts of lithium trifluoroacetate was first

dissolved in THF/DMF with/without 10vol%TFA made upto 3ml. Calculated amount of PMMA powder was then added to the solution and was then dissolved in an ultrasonic bath. Samples with various percentages of the salt in the polymer were prepared this way. The solutions were then drawn on stainless steel electrodes and then sandwiched with another electrode on top of it.

5.1.3 Synthesis of Sol-Gel Derived Vanadium Oxide Films

Vanadium oxide films were prepared by a Sol-gel route according to a reported procedure[126]. 500mg of V_2O_5 powder was dissolved in 30ml of 15% H_2O_2 solution under magnetic stirring. The reddish brown solution thus formed was then heated in a water bath at 80°C for 30mins, transforming it into a viscous solution. This solution was then dip-coated on polished stainless steel substrates and was then heat treated in an oven at 150°C for 1h to give homogeneous films. The thickness of the films as measured by alpha-step profilometer was found to be 5 μ m.

5.1.4 Formulation of Carbon Nanotube/Block Copolymer Composites

The use of carbon nanotube /block copolymer (P3HT-b-PS) as an anode material for the Li- ion batteries was studied. The block copolymer (P3HT-b-PS) contains two structural segments, a conjugated poly (3-hexylthiophene) (P3HT) moiety and a polystyrene (PS) segment. It is expected that the conjugated polymer block will form π - π interactions with carbon nanotubes, therefore, break the strong Van der Waals interactions between nanotube bundles, while the polystyrene block will be dangling on the outer surface of the CNTs and provide the de-bundled CNTs with good solubility and stability in organic solvents. A good dispersion of the SWNTs is

necessary to provide a high accessibility to Li ions for intercalation. SWNTs were dispersed in chloroform by mixing with P3HT-b-PS and then sonicated for 1 hr with the water bath temperature maintained at 18-20°C. A 2:1 weight ratio of the block copolymer and the SWNTs was used to prepare the solution. Nanocomposite thin films were then cast on polished stainless steel electrodes.

5.2 Characterization of Electrode and Electrolyte Materials

5.2.1 Electrochemical Impedance Spectroscopy

EIS measurements were conducted using IM6e BAS ZAHNER™ frequency response analyzer. For the polymer electrolyte films, stainless steel panels which sandwiched the polymer films formed the two electrodes for the impedance measurements. The typical dimensions of the films between the electrodes were 200µm x 25mm x 40mm. For the anode and cathode materials, a standard three-electrode arrangement was adapted with Pt as counter electrode, and saturated calomel electrode as the reference electrode. The electrolyte used was 1M lithium perchlorate (LiClO₄) in propylene carbonate solution. A scan range of 0.1Hz to 1MHz was used and the perturbation voltage was 10mV. All the measurements were done at room temperature. Once the specimen was connected, a hold-time was allowed till the DC potential stabilized. All the impedance measurements were repeated for a statistically confident data.

5.2.1.1 Electrolyte Material

All the electrolyte materials made under different processing conditions were tested by electrochemical impedance spectroscopy. Fig 5.1-5.4 shows the nyquist plots for polymer electrolyte material with different percentages of salt and in the presence of 10vol %TFA in THF. All the samples were dried in vacuum for atleast a week before testing. In another set of experiment similar films were prepared with various percentages of salt and 10vol%TFA in THF as solvent but this time the films were kept wet. Fig 5.5-5.8 shows the Nyquist plot of these polymer electrolyte films for various percentages of salt in the electrolyte system. To study the effect of TFA in the polymer electrolyte system, two different processing conditions were used. For the first system, wet films of Salt in PMMA with THF as solvent were prepared, but this time without the addition of 10 vol% TFA. Fig 5.9-5.10 shows the nyquist plot of the films. The second system was the addition of 10vol% of TFA in THF and the film was vacuum dried. As no salt was added, the second system primarily aimed to study the effect of only TFA on the conductivity of the polymer films. The nyquist plot of the films are shown in Fig .5.11-5.12.

To compare the effect of the solvent on the conductivity of the polymer electrolyte DMF was also used instead of THF. Wet polymer films were prepared using 10vol%TFA in DMF but it was found that a loading ratio greater than 20% of the salt could not be achieved for the films processed using DMF as a higher loading caused its precipitation from the solvent system. The nyquist plot of this polymer electrolyte system is shown in Fig 5.13. Polymer electrolyte processing was then carried out without the use of TFA as a cosolvent with DMF but again it was noticed that loading of the salt could not be increased more than 50% due to the same

reasons as mentioned above. Fig 5.14-5.15 show the nyquist plots of the aforementioned polymer electrolyte system.

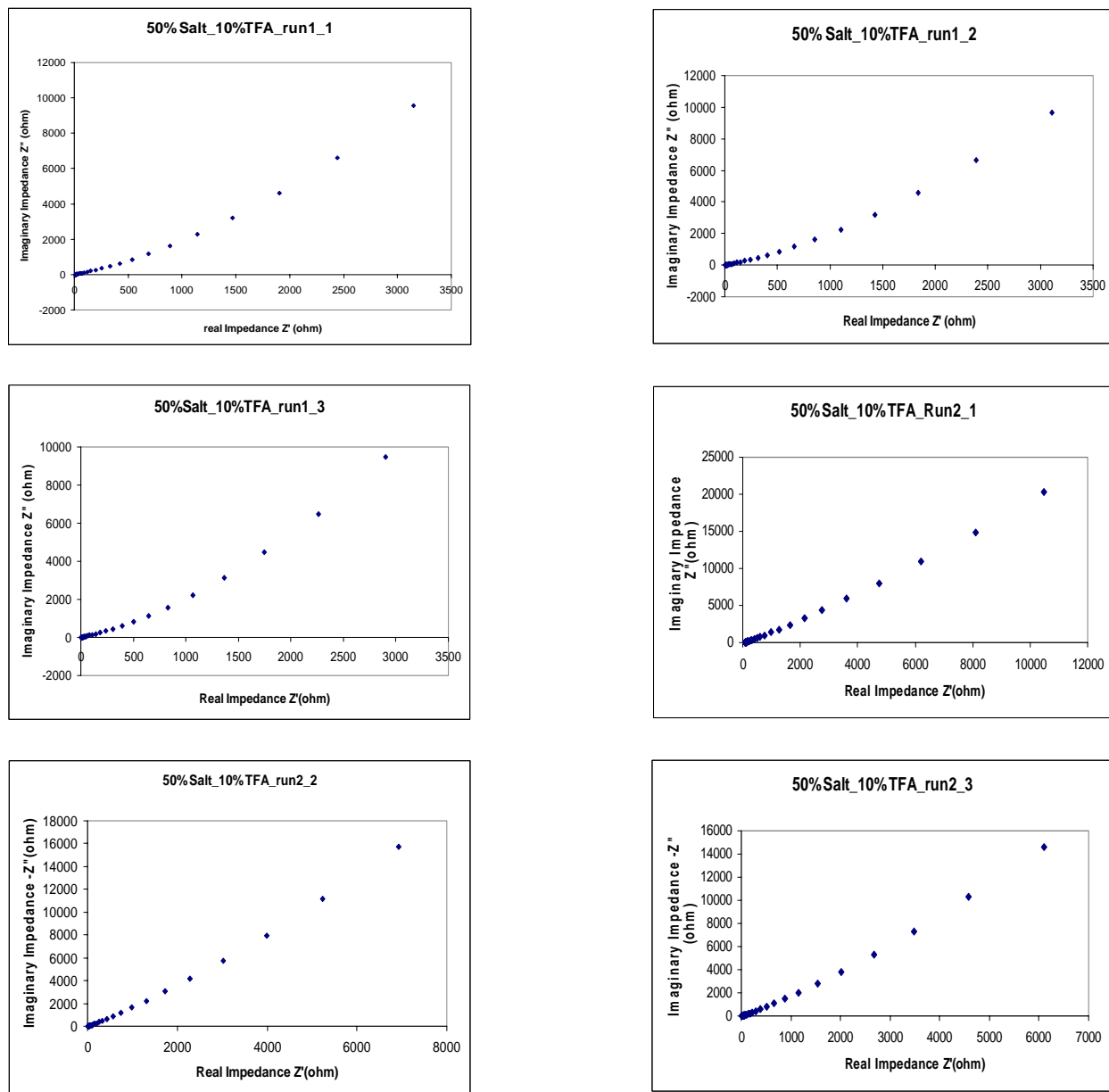


Figure 5.1 Nyquist plots for two samples of 50%salt and 10vol%TFA in THF as solvent in PMMA

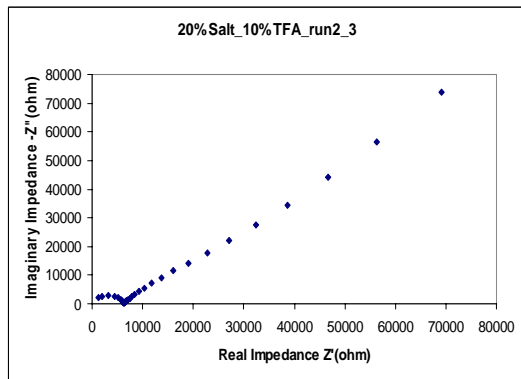
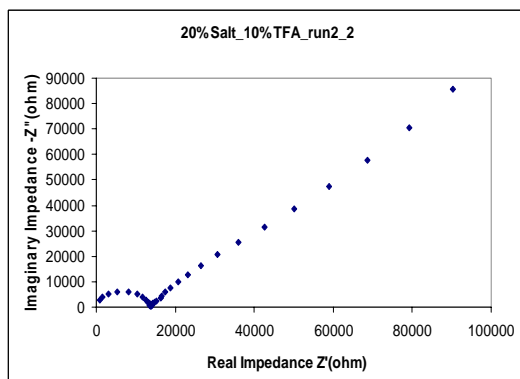
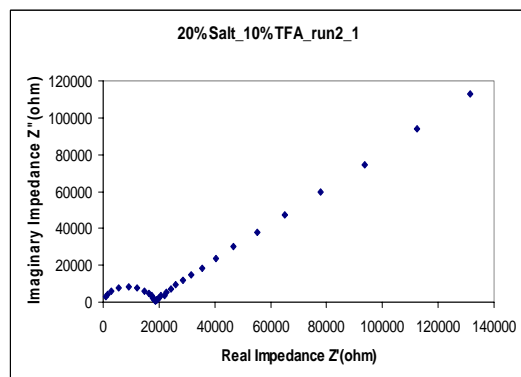
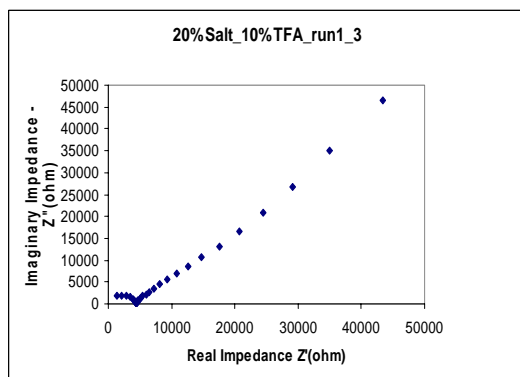
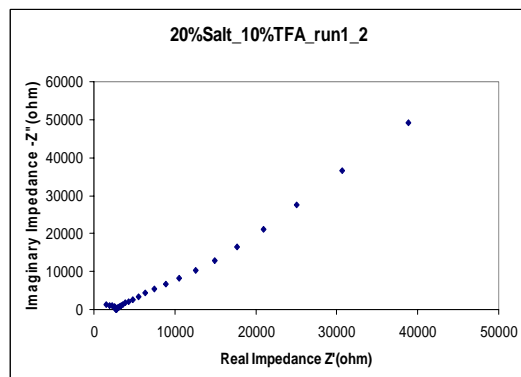
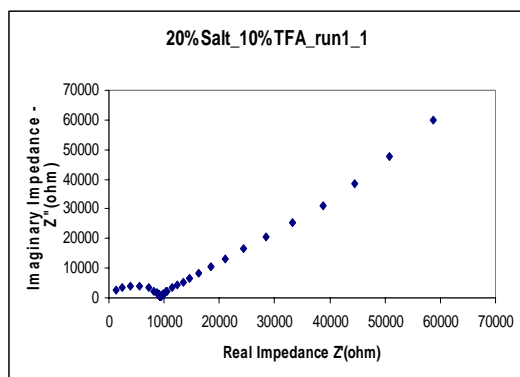


Figure 5.2 Nyquist plots for two samples of 20%salt and 10vol%TFA in THF as solvent in PMMA

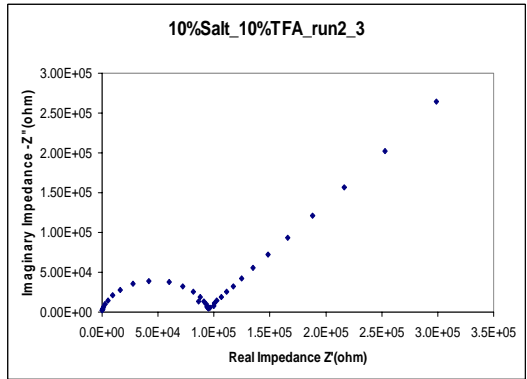
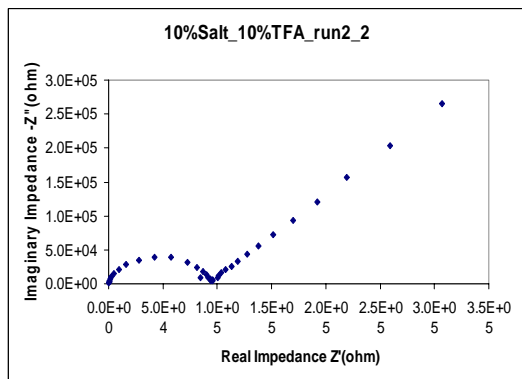
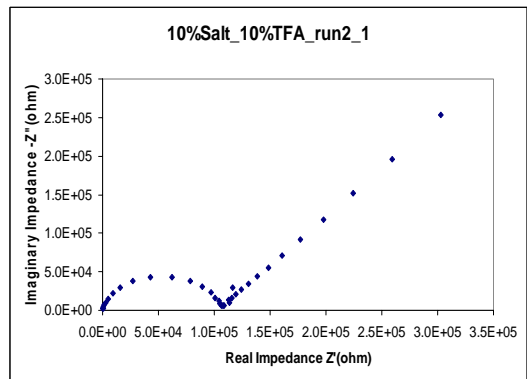
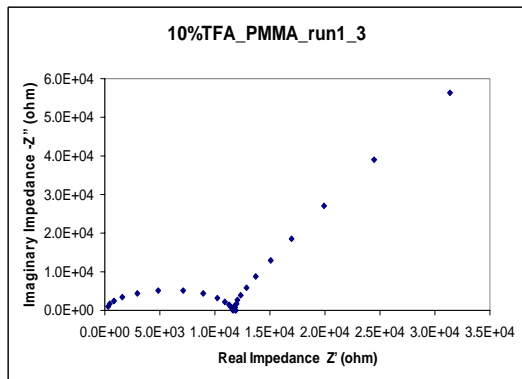
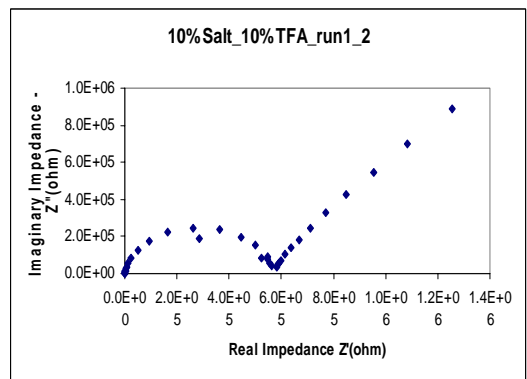
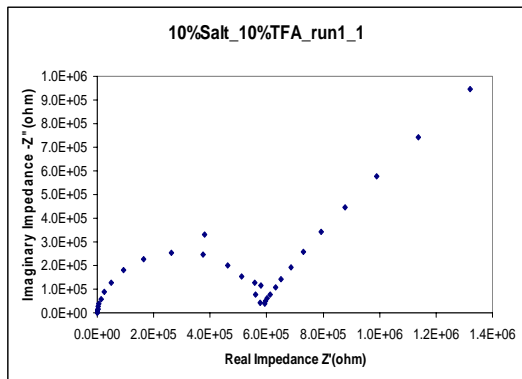


Figure 5.3 Nyquist plots for two samples of 10%salt and 10vol%TFA in THF as solvent in PMMA

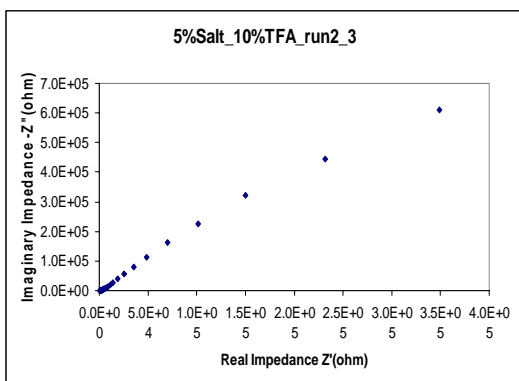
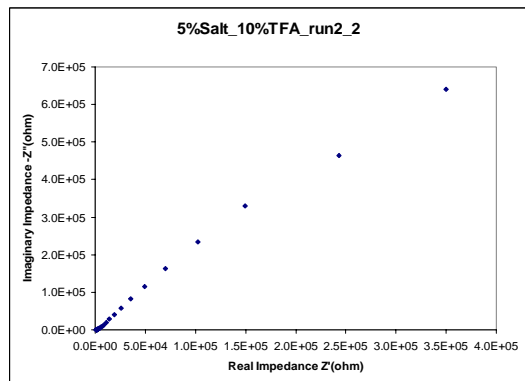
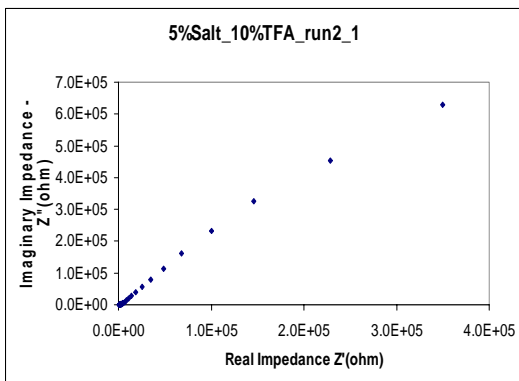
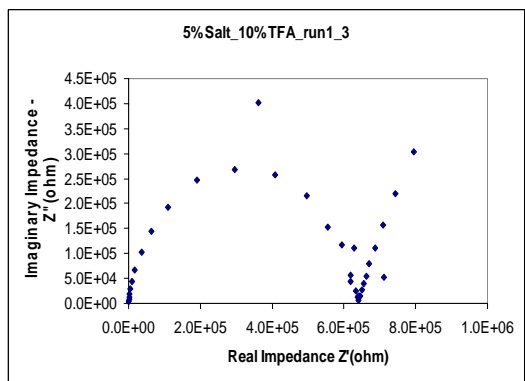
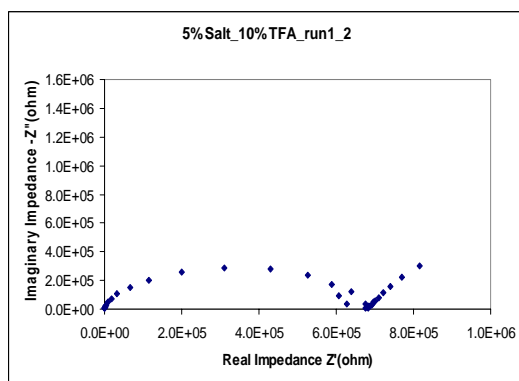
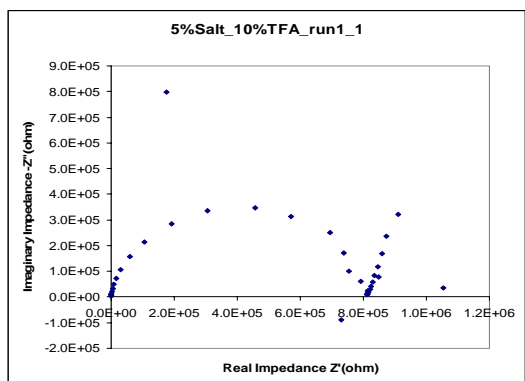


Figure 5.4 Nyquist plots for two samples of 5%salt and 10vol%TFA in THF as solvent in PMMA

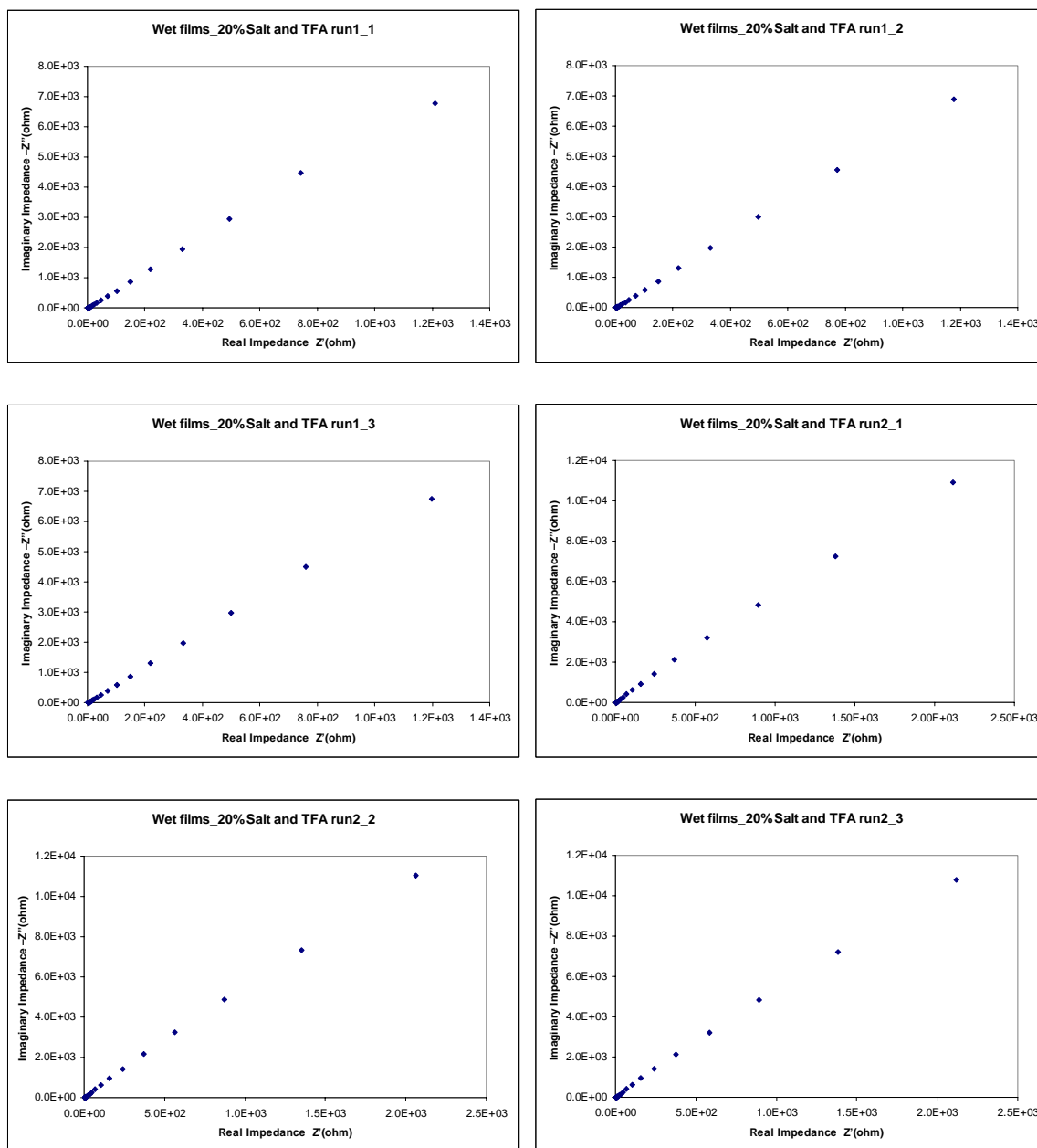


Figure 5.5 EIS of wet films of 20% Salt with 10vol% TFA in THF as solvent, in PMMA.

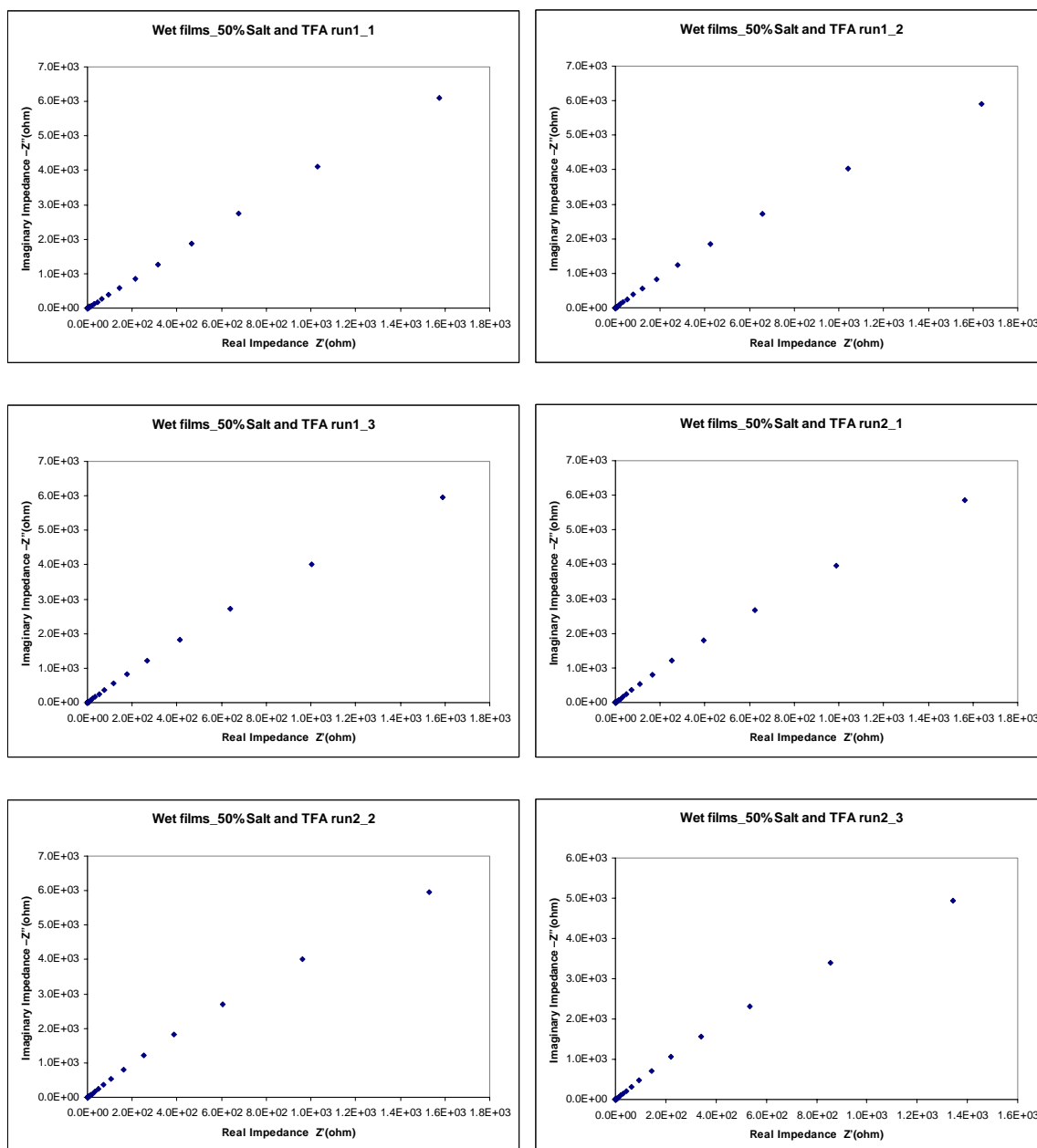


Figure 5.6 EIS of wet films of 50% Salt with 10vol% TFA in THF as solvent, in PMMA.

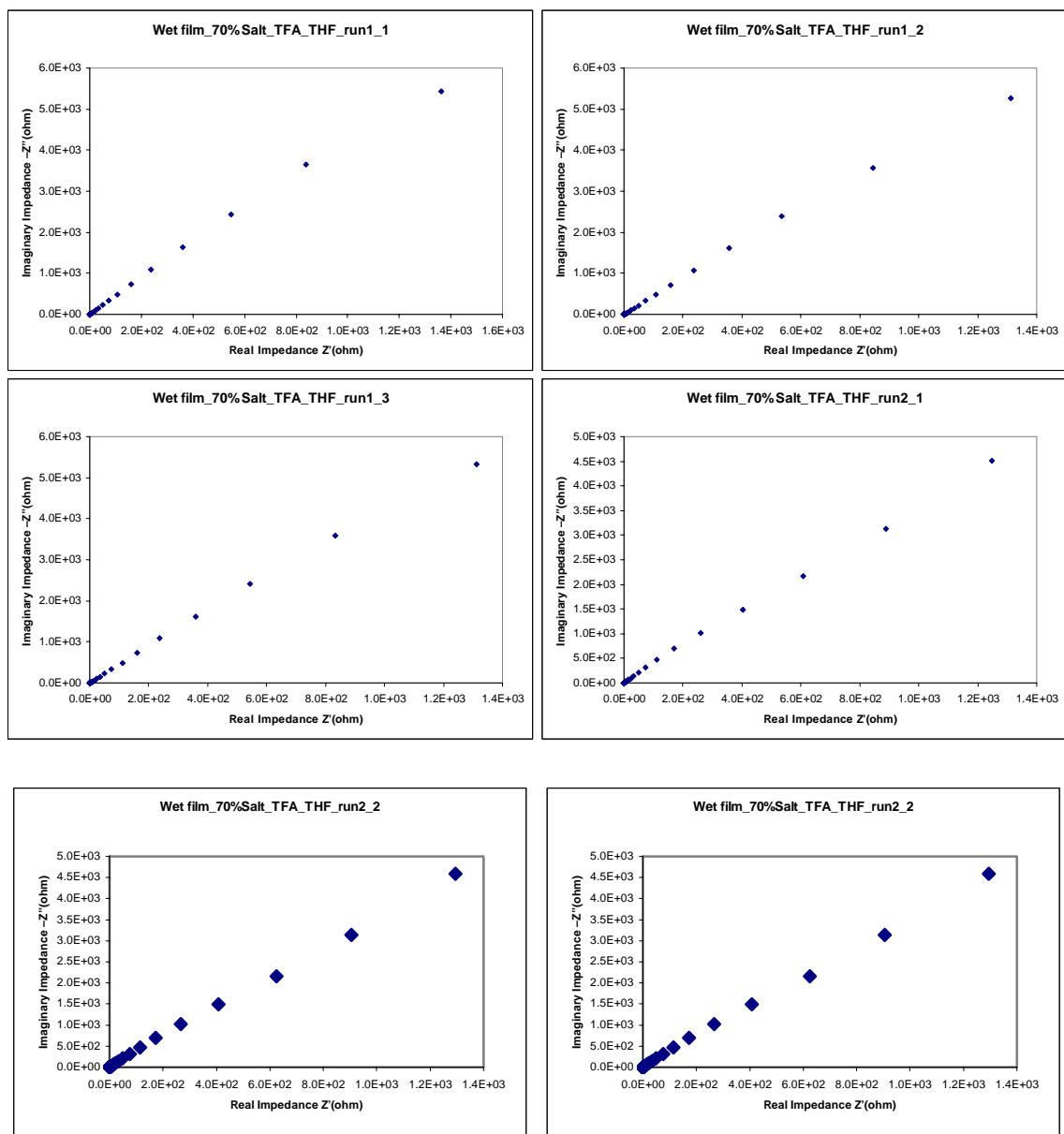


Figure 5.7 EIS of wet films of 70% Salt with 10vol% TFA in THF as solvent, in PMMA.

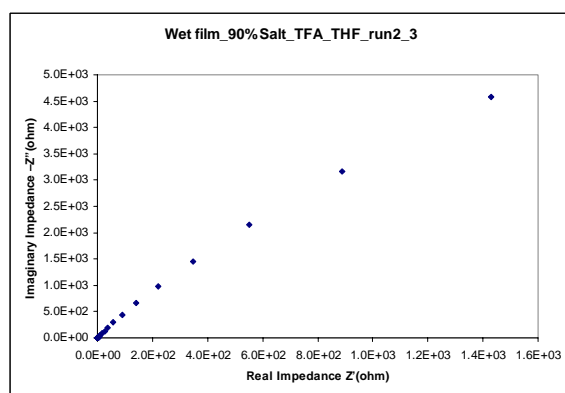
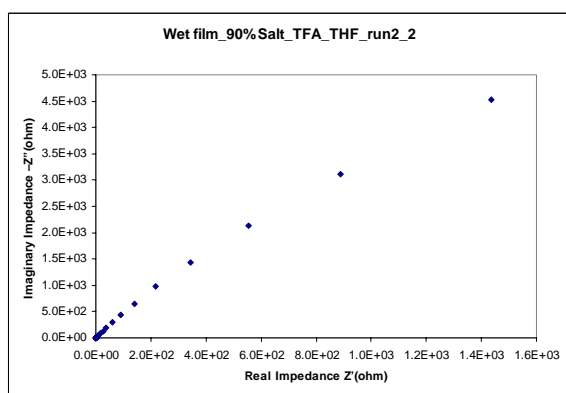
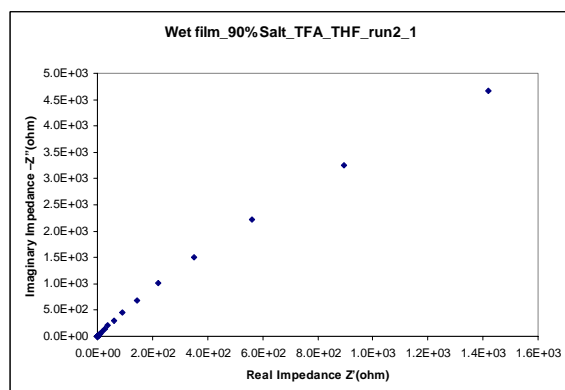
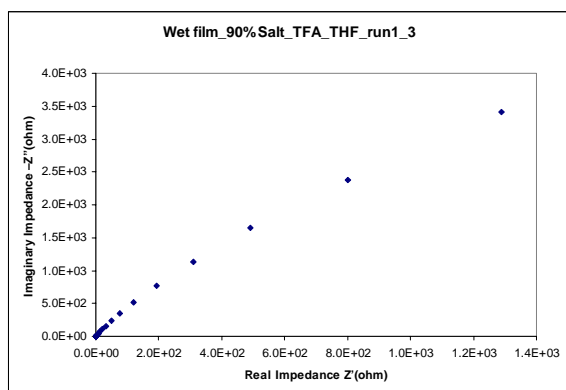
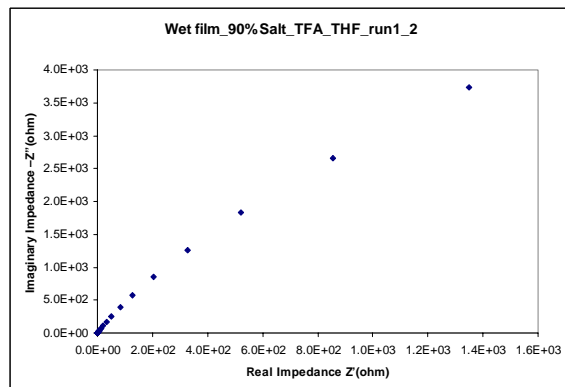
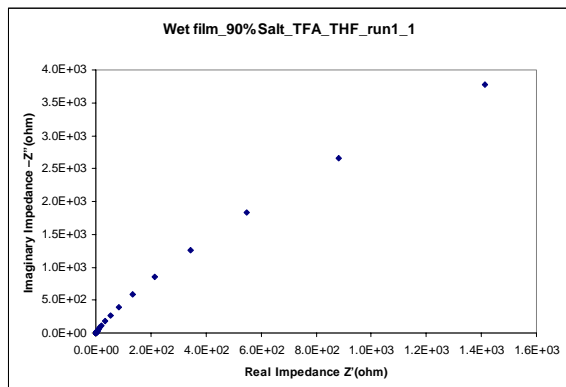


Figure 5.8 EIS of wet films of 90% Salt with 10vol% TFA in THF as solvent, in PMMA

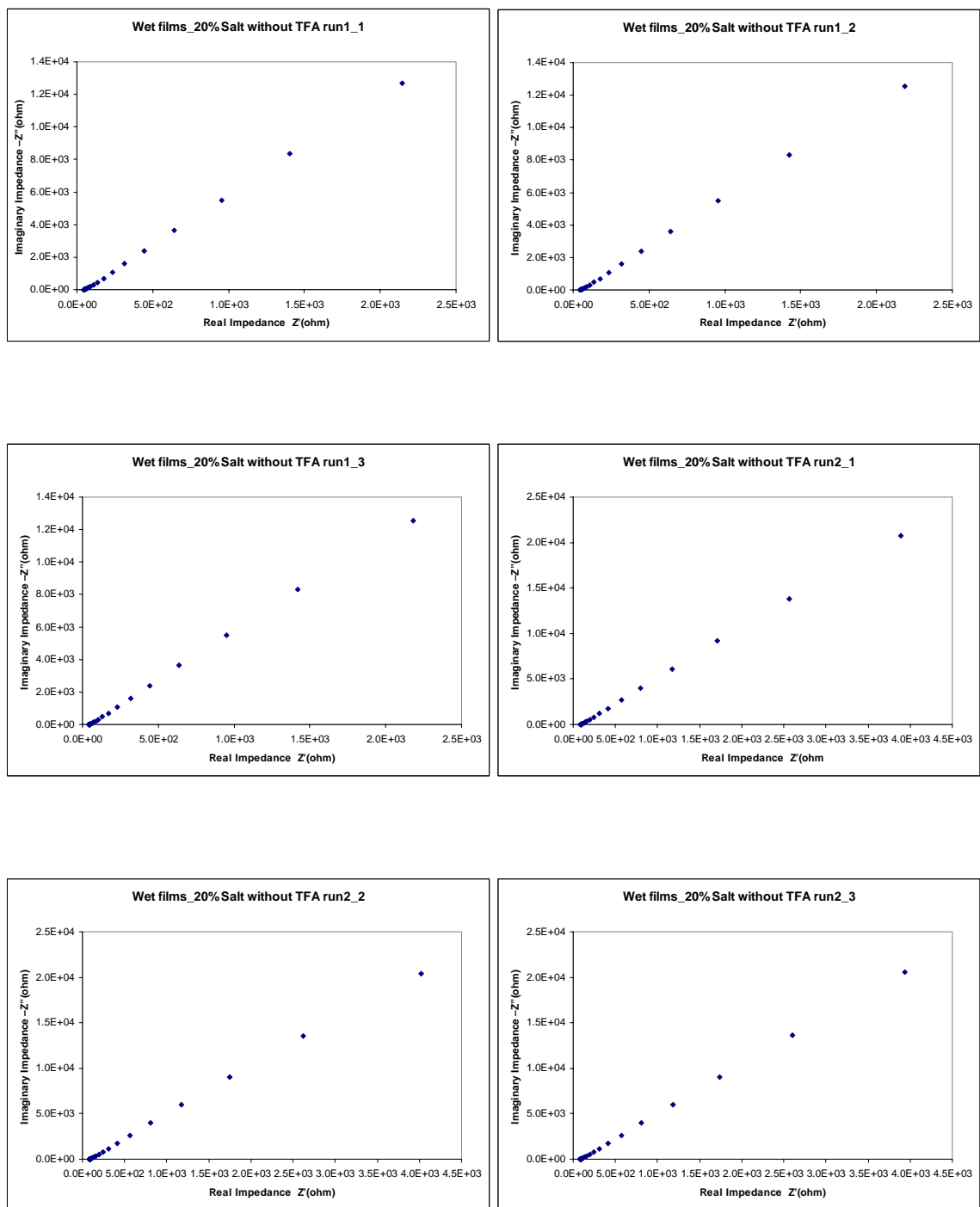


Figure 5.9 EIS of wet films of 20% Salt without TFA in THF, in PMMA.

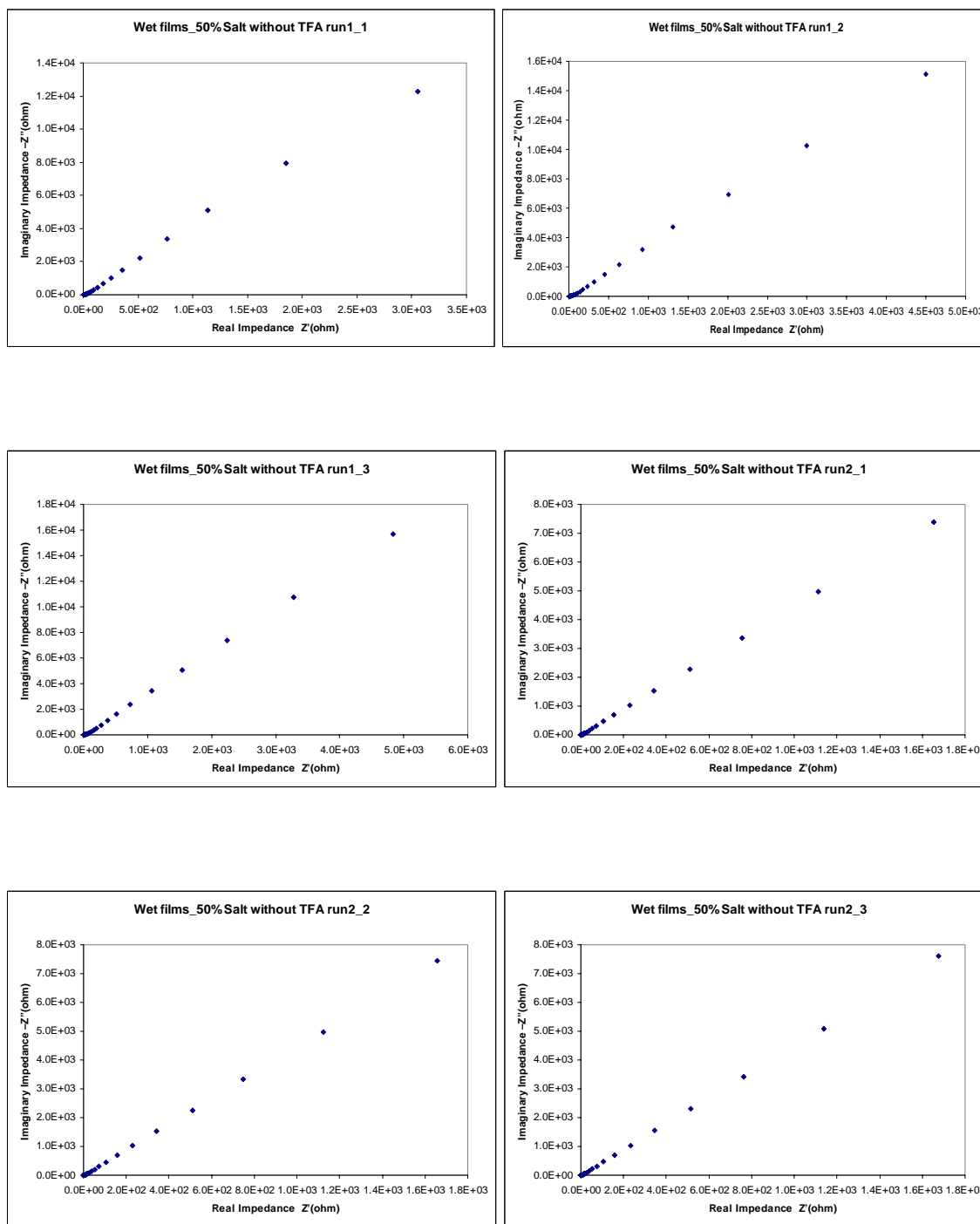


Figure 5.10 EIS of wet films of 50% Salt without TFA in THF, in PMMA.

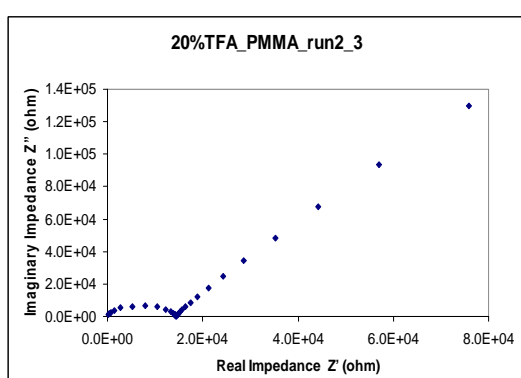
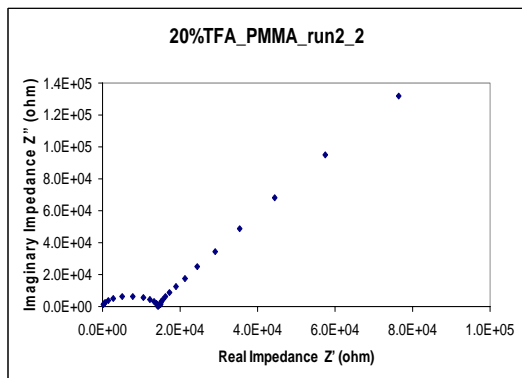
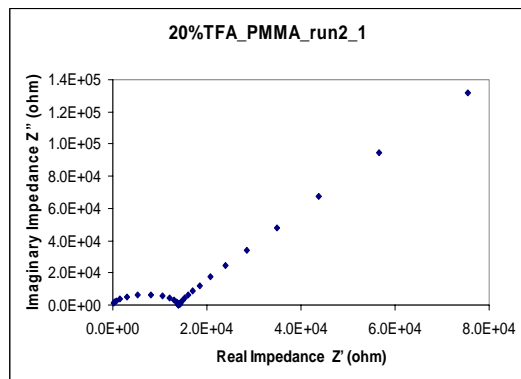
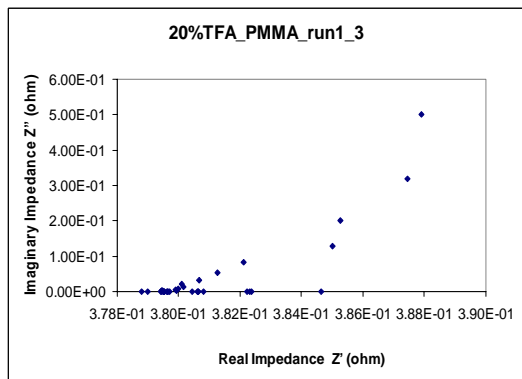
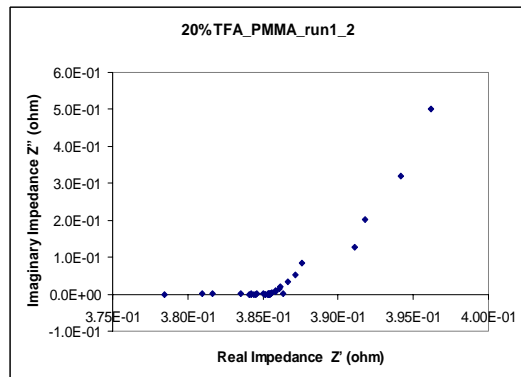
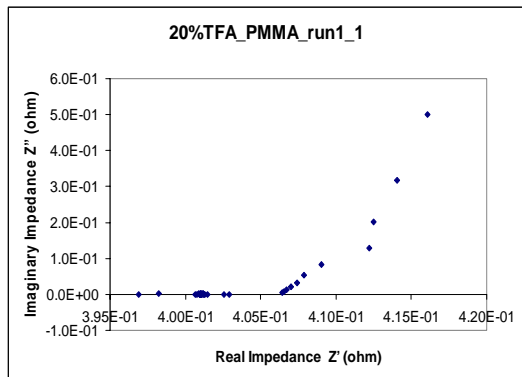


Figure 5.11 Nyquist plots for two samples of 20% TFA in PMMA

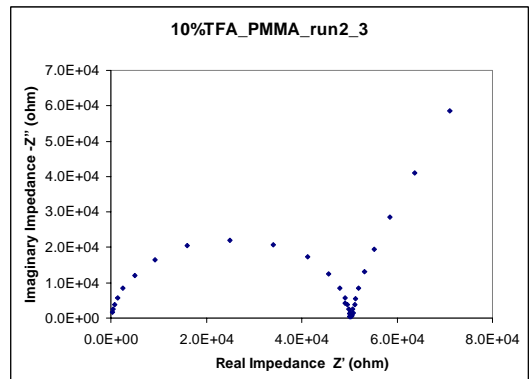
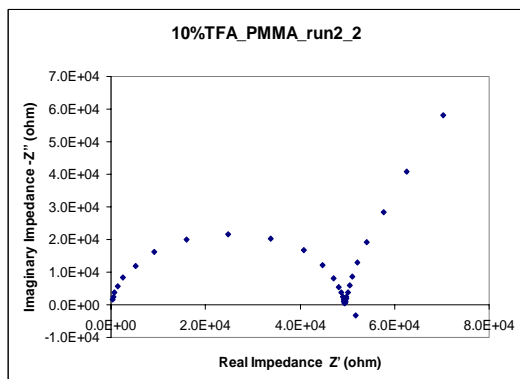
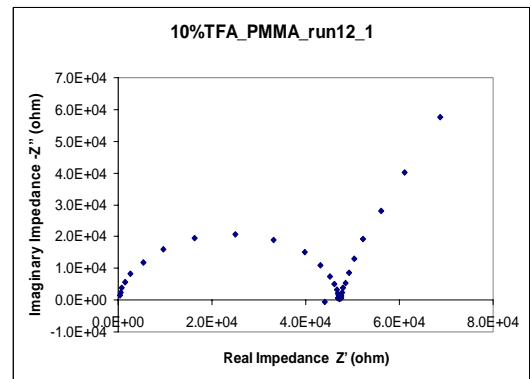
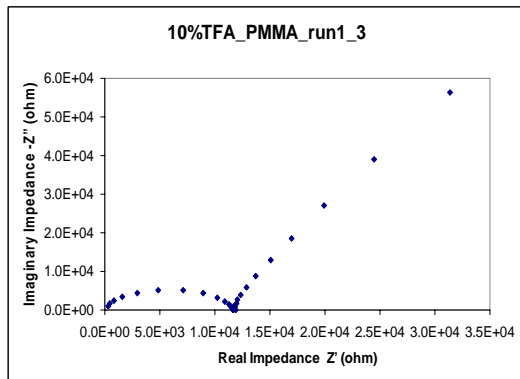
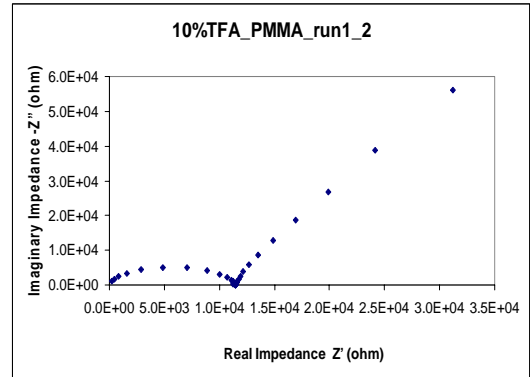
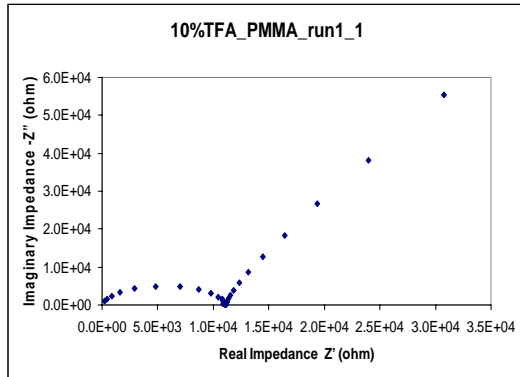


Figure 5.12 Nyquist plots for two samples of 10% TFA in PMMA

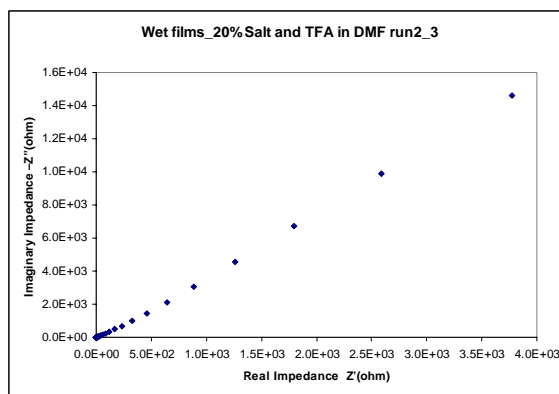
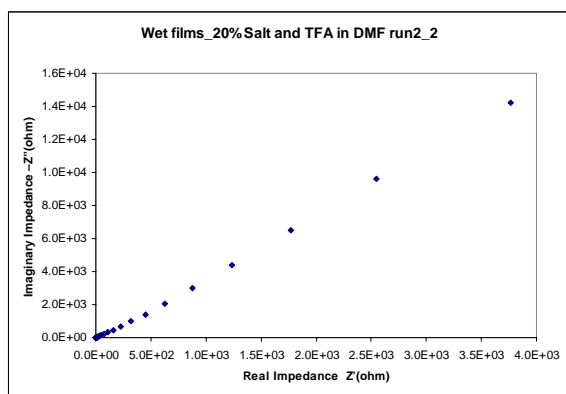
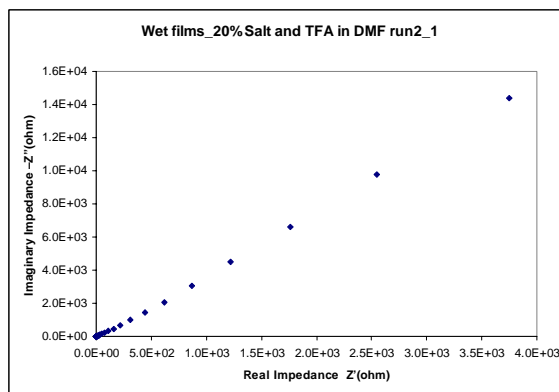
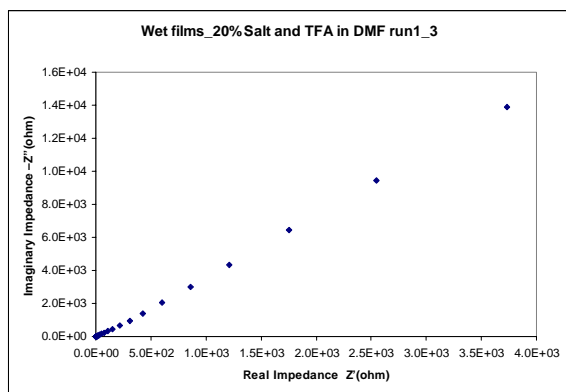
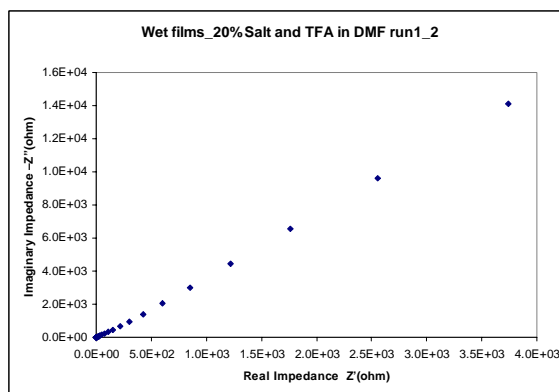
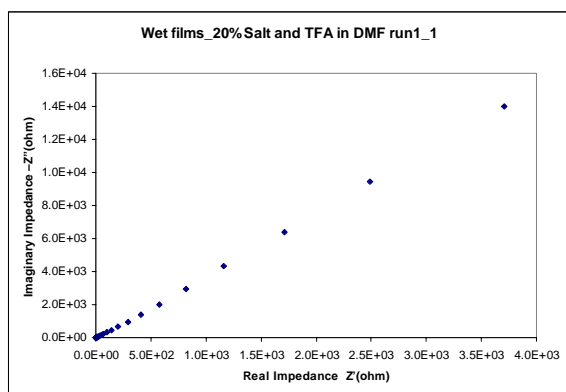


Figure 5.13 EIS of wet films of 20% Salt with 10vol% TFA in DMF as solvent, in PMMA.

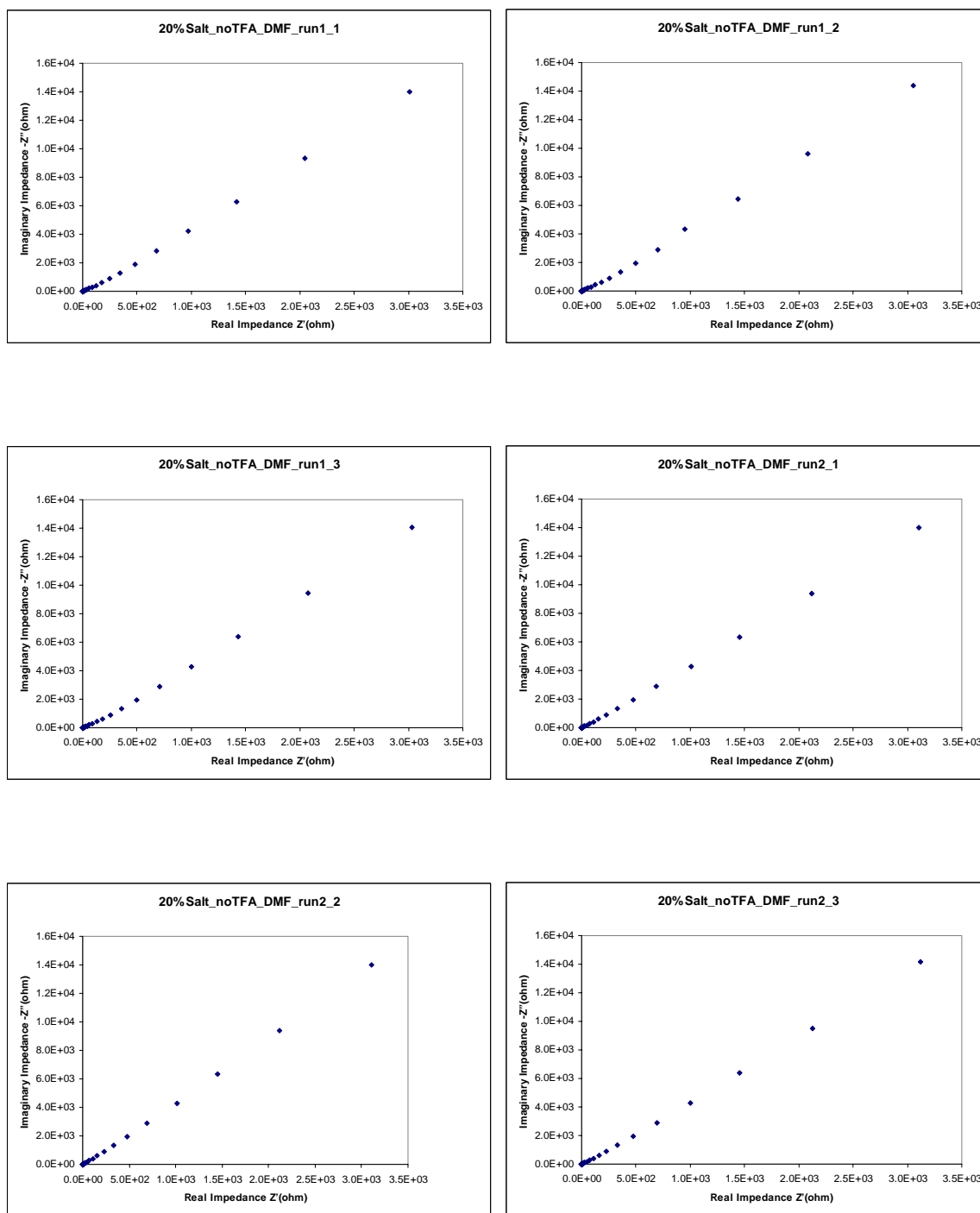


Figure 5.14 EIS of wet films of 20% Salt without TFA, in DMF as solvent, in PMMA.

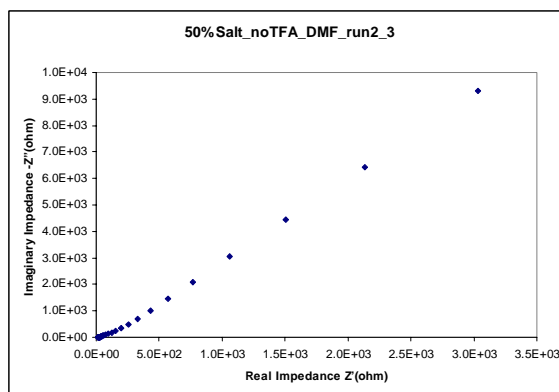
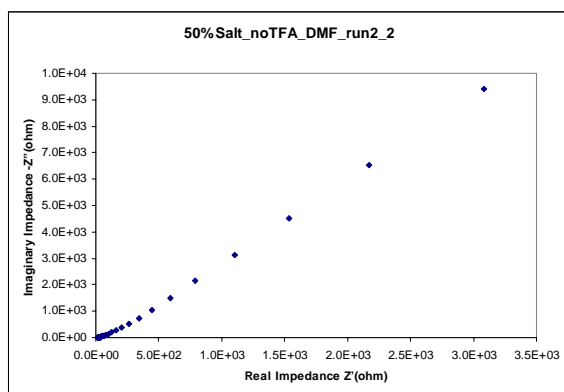
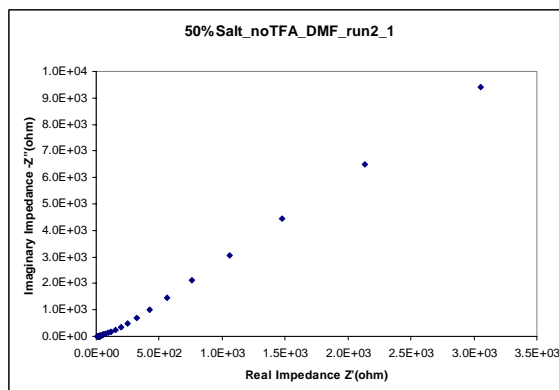
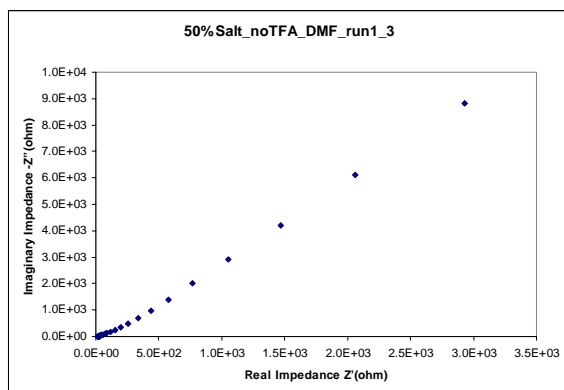
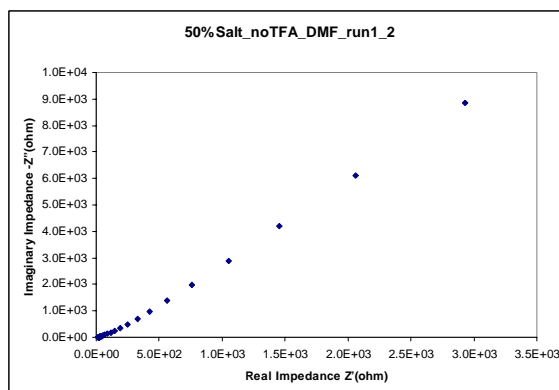
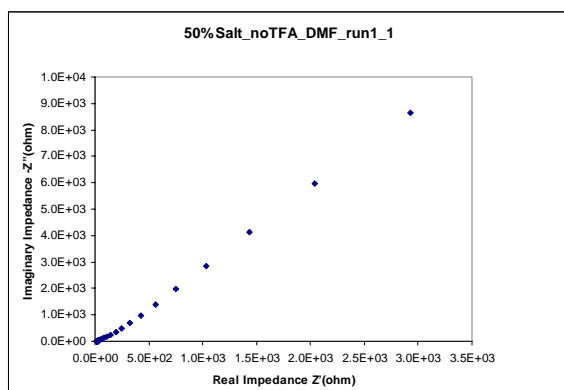


Figure 5.15 EIS of wet films of 50% Salt without TFA, in DMF as solvent, in PMMA.

The nyquist plots shown for all the polymer electrolyte systems show two basic shapes. In the first type, the curve follows an almost straight line path beginning from the high frequency side to the low frequency side. In these cases, the impedance of the interphase is not significant as compared to the resistance of the film for which the equivalent circuit model consists of a resistance R in series with a constant phase element which is shown in Fig 5.16a. In the second type of impedance curves, the curves first start as an arc of a semicircle from the high frequency side and then follow an almost straight line path at the low frequency side. In these cases the impedance of the interphase becomes significant and can be described by an equivalent circuit as shown in Fig 5.16b in which a parallel combination of interphase resistance R_2 and capacitance C is in series with a resistance R_1 and a constant phase element Q . At the interface between an electrode and electrolyte, a double layer is established which acts as a capacitor C in parallel with the interphase resistance R_2 . The ionically conducting electrolyte impedes the transfer of charge (ions) and, acts as a resistor, R_1 in series with the C and R_2 . A constant phase element is further introduced to model the response of the real world systems more accurately. The first real axis intercept at high frequencies represents the resistance of the PMMA/salt electrolyte and the second also includes the contribution of the interphase resistance.

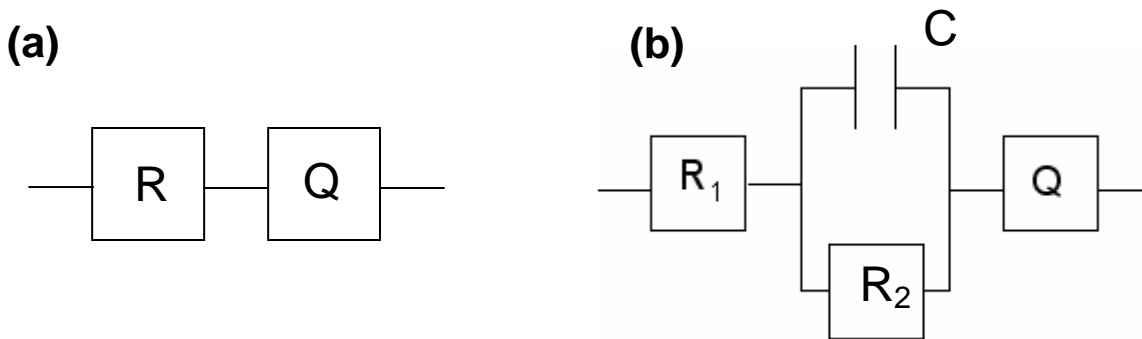


Figure 5.16 Equivalent circuit model for a) type one b) type two nyquist plots.

5.2.1.1.1 Conductivity of the Polymer Electrolyte Systems

The conductivity of the polymer electrolyte films was calculated from the equation

$$\sigma = L / (R \cdot A)$$

where R is the resistance found by curve fitting using the equivalent circuit models of the appropriate Nyquist plots obtained. 'A' is the area of polymer electrolyte film sandwiched between the electrodes and L is the thickness of the polymer films. All the geometrical measurements were done with a vernier caliper with a least count of 10 μm and the thickness measurements were reaffirmed with SEM imaging of the cross section. Representative images are shown in Fig 5.17.

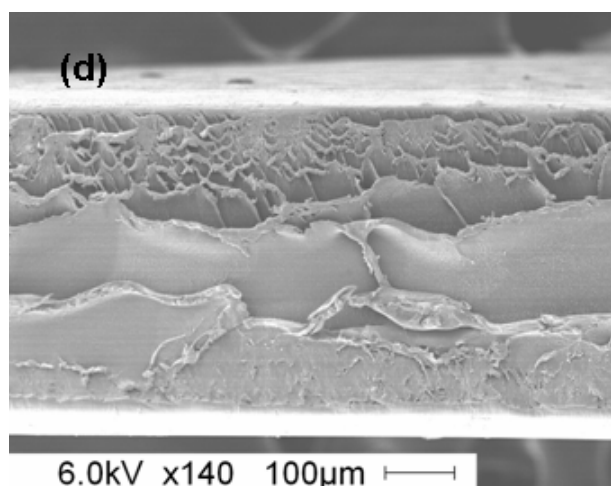
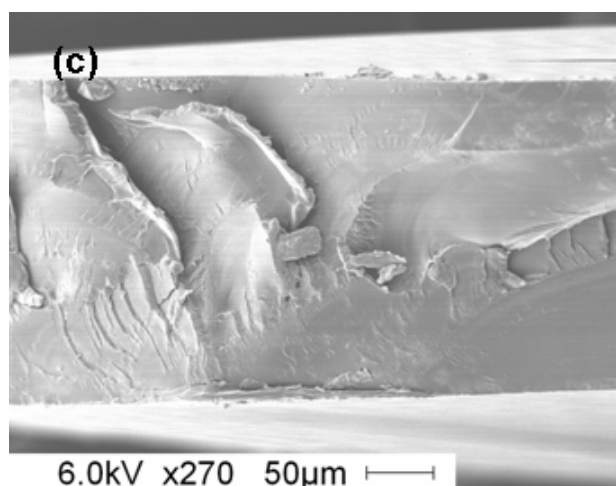
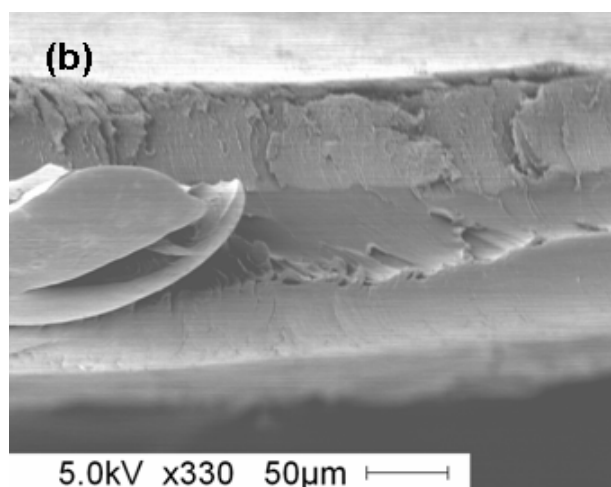
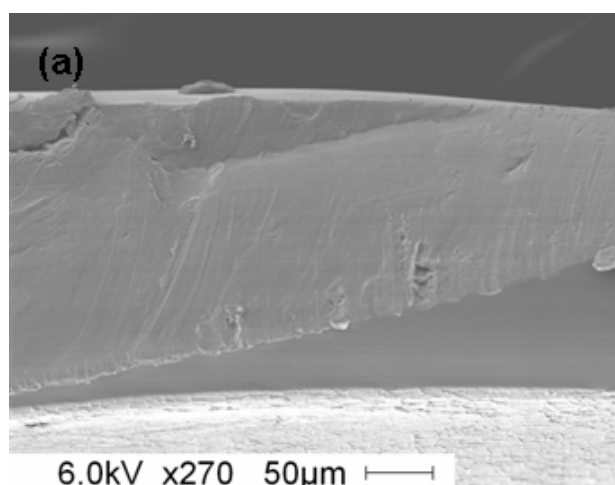


Figure 5.17 SEM images to measure the film thickness from the cross section of (a) 5wt% (b) 10wt% (c) 20wt% (d) 50wt% salt and 10vol%TFA in THF as solvent in PMMA. The films were vacuum dried for a week.

The conductivity values of the various polymer electrolyte systems were calculated and the results are shown in fig 5.18.

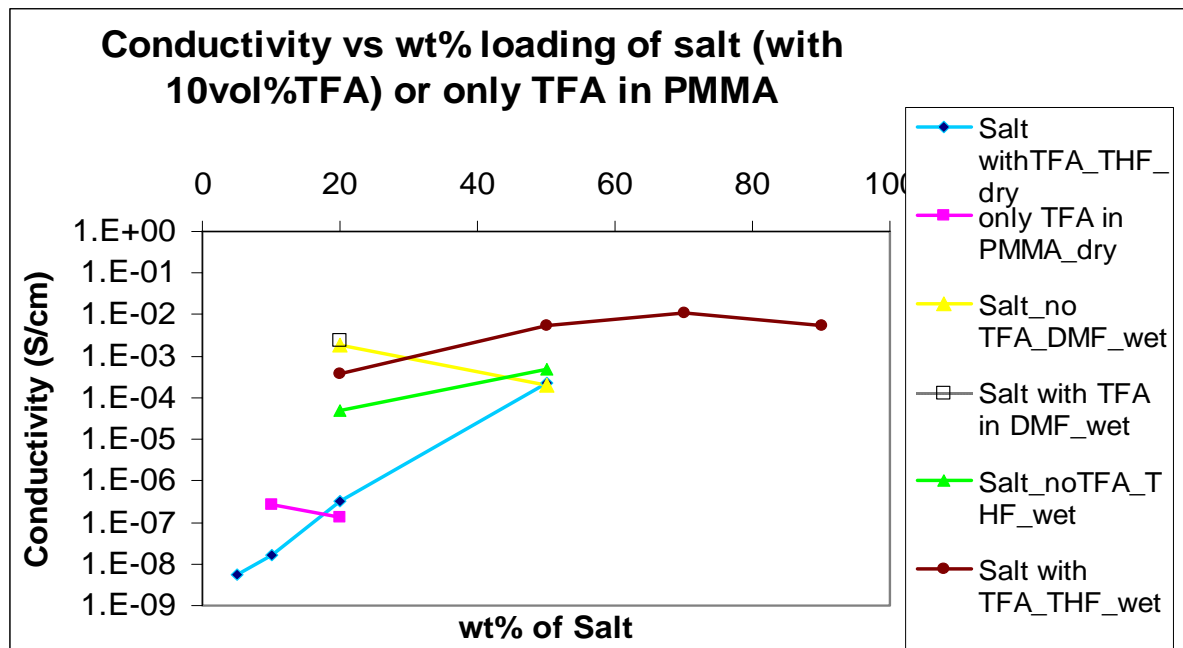


Figure 5.18 Conductivity of various polymer electrolyte systems obtained by varying the processing conditions and the amount of salt

The conductivity of the dry films of polymer electrolyte films processed with 10 vol%TFA in THF (blue curve) is seen to increase with the increase in the concentration of the lithium salt. But similar films under wet conditions (brown curve) shows atleast an order of magnitude increase in conductivity for similar loading ratios of the salt. This indicates that THF as a solvent might have a plasticizing effect on the polymer matrix resulting in an increase in conductivity of the polymer films. To study the effect of the solvent, polymer electrolyte films were prepared using DMF. The open square in the figure shows the conductivity of the film with 20 wt% salt and 10vol% TFA in DMF. Though the conductivity at the loading ratio of 20wt% salt was the highest, electrolyte system with a higher loading ratio of the salt could not be prepared due to the

precipitation of the salt and incompatibility of TFA with this particular system. The higher boiling point of DMF as compared to THF can be a factor contributing to the higher conductivity of the polymer films. Polymer electrolyte films were also prepared without the addition of TFA in the polymer/salt/DMF system (yellow curve). Though a loading of 50wt% salt could be achieved, a decrease in conductivity of the films was observed showing the increase in incompatibility with increase in the amount of salt in the system. In contrast, for the electrolyte system with TFA in THF as solvent (brown curve), a 90% salt loading could easily be achieved with the conductivity saturating at about 70wt% of the salt concentration. The conductivity obtained at this loading ratio is around 1.1×10^{-2} S/cm. To study the effect of TFA, wet films with THF as solvent without TFA were also prepared (green curve). These films have a conductivity that is almost an order of magnitude lower than films prepared using TFA as a cosolvent. TFA being a strong acid exists in ionic form and also has a plasticizing effect on the polymer electrolyte system giving rise to the higher conductivity. This effect is better appreciated when we notice the conductivity of the PMMA films prepared by using a solvent of 10 and 20vol% TFA in THF but without any salt loading (magenta curve). The dry film prepared using 10vol%TFA has a much higher conductivity when compared to the dry film prepared using 10wt% of the salt. But the effect of TFA becomes less significant at concentration greater than 10 vol% as observed by the almost similar conductivity of the 20vol% TFA films. It can be concluded that within the range of study, polymer electrolyte wet films prepared by using 10vol%TFA in THF showed the best performance in conductivity with the highest value reaching 1.1×10^{-2} S/cm at 70wt% of the salt concentration.

5.2.1.2 Cathode Material

The conductivity of the Li ions injected into the vanadium pentoxide host matrix were analysed by impedance spectroscopy. Fig 5.19 shows the nyquist plot of the vanadium oxide cathode material obtained by applying a DC potential of -0.25V. The insets show the nyquist diagram for the highest frequencies. The semicircular region at the high frequency side is associated with the bulk resistance and the geometrical capacitance of the films. The bulk resistance associated with the film is low at about $800 \Omega\text{cm}^2$ which is an indicator of a high conductivity at the negative potential of -0.25V. This can be described in terms of the electronic jump $V^{5+} \rightarrow V^{4+}$ creating an excess of V^{4+} sites over V^{5+} sites. Another feature to be noted from the nyquist plot is the straight line in the low frequency region which indicates the diffusion process of lithium ions into the V_2O_5 film[127].

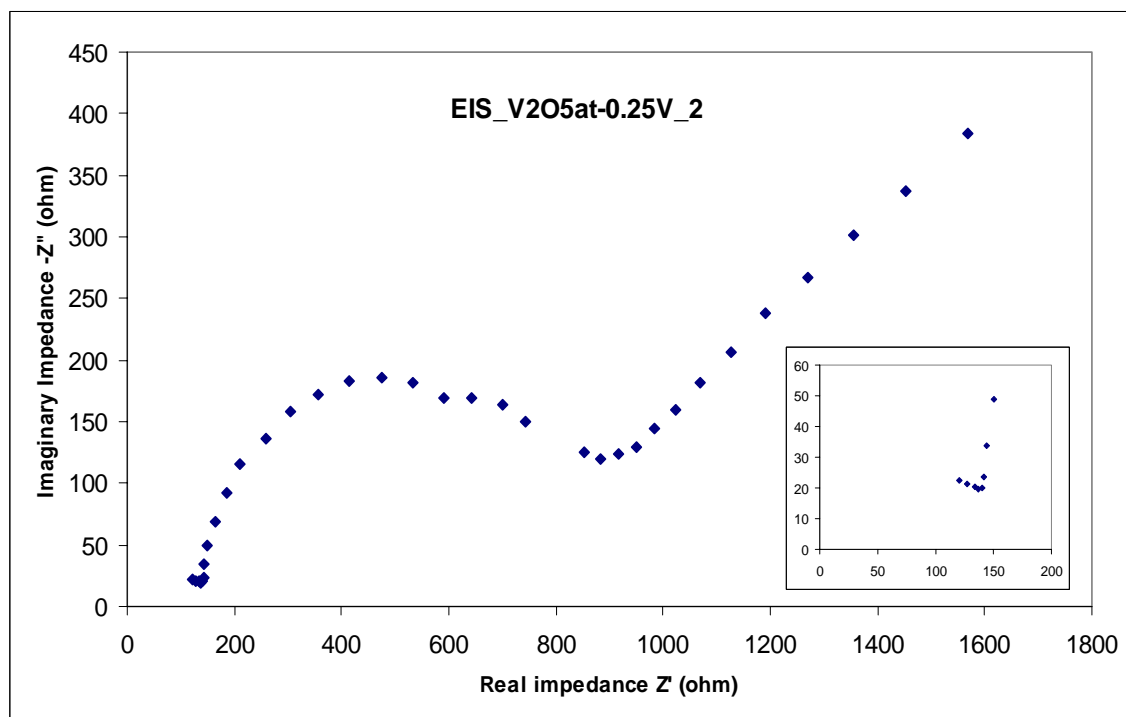
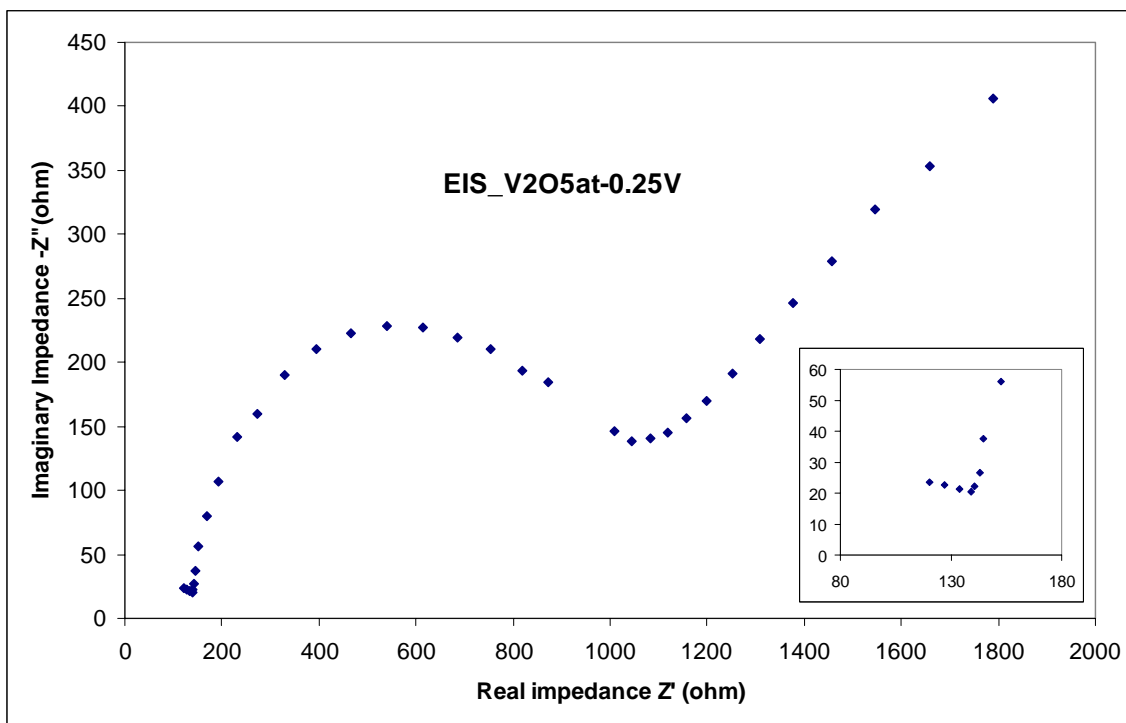


Figure 5.19 Nyquist Plots of the vanadium oxide cathode material by applying a DC potential of -0.25V.

5.2.1.3 Anode Material

Fig 5.20 shows the impedance spectrum of the carbon nanotube/ block copolymer composite at a DC potential of 0.3V. The impedance of the low frequency region is attributed to the diffusion process of Li ions in the composite layer and from its intercept on the real impedance axis, a low impedance of around $100 \Omega\text{cm}^2$ is clearly visible. This is an essential requirement for the application of composite as an anode material for lithium batteries.

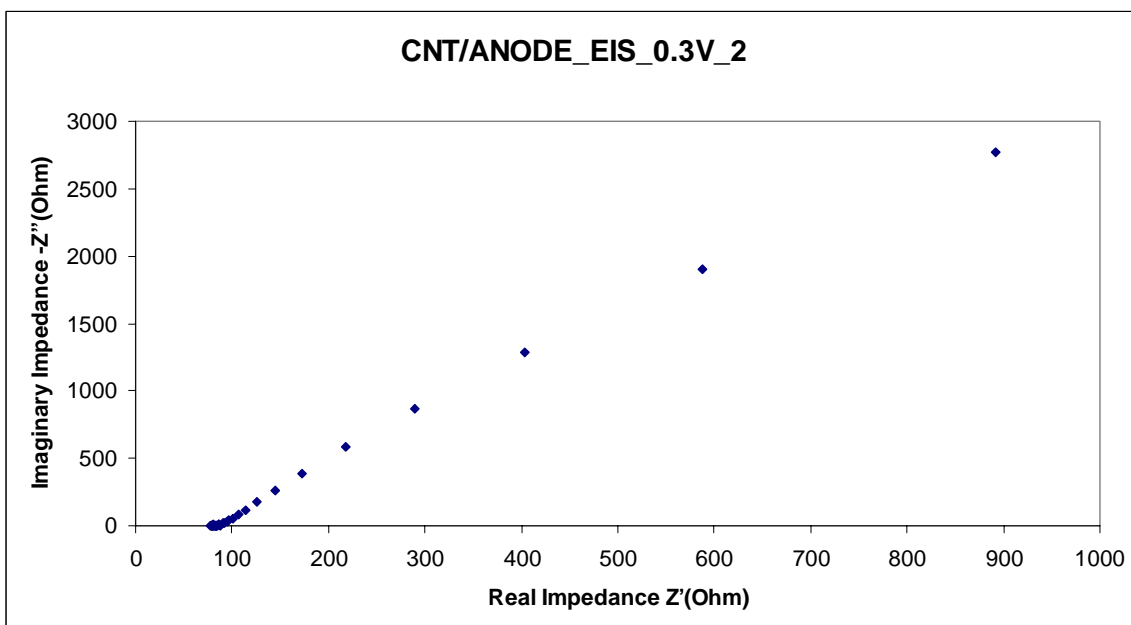
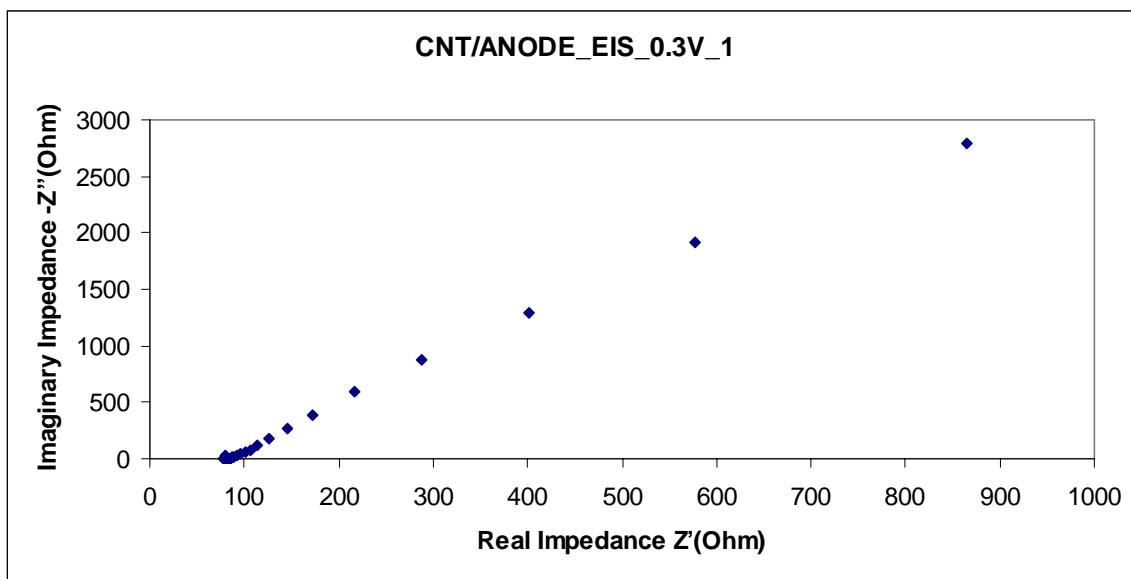


Figure 5.20 Nyquist Plots of the carbon nanotube composite material by applying a DC potential of 0.3V.

5.2.2 Fourier Transform Infrared (FTIR) Spectroscopy

Fourier Transform Infrared (FTIR) Spectroscopy was performed using a Perkin Elmer Spectrum 100 spectrometer. It was used to verify the lasting plasticizing effect of the TFA on polymer films. PMMA films were prepared with various percentages of TFA in THF as solvent. Fig 5.21 shows the FTIR spectrum of the films on the fourth and twelfth day after the films preparation. The $-\text{CH}_3$ and $-\text{CH}_2$ stretching of the polymer around 3000 cm^{-1} can be identified. The $-\text{CH}_2$ bending is around 1450 cm^{-1} . The carbonyl stretching of the polymer is around 1720 cm^{-1} . Apart from these, peaks originating from TFA can also be identified. The presence of electronegative atoms or groups adjacent to carboxylic acid groups have the effect of increasing the $\text{C}=\text{O}$ stretching vibration frequency, while hydrogen bonding tends to decrease it. The peak at 1779 cm^{-1} from the $\text{C}=\text{O}$ stretching vibration frequency of the acid can be identified. The C-F stretching modes can be assigned to the bands at 1212 cm^{-1} and 1168 cm^{-1} . The assignment of the bands in the region below 1000 cm^{-1} is difficult due to the nature of the vibrations expected. These include the out-of-plane OH deformation mode, the C-C stretching mode, the $-\text{COO}$ skeletal angle-bending mode and the $-\text{CF}_3$ group deformation modes. It can be concluded that TFA is not evaporated off completely and therefore helps keep the polymer system plasticized, improving its conductivity. Different experimental conditions were also used and similar results were obtained. Films were prepared and annealed at 75°C for 1 h. The prepared films were also subsequently dried under vacuum. Fig 5.22 shows the FTIR spectrum of the films. From the spectrum, groups originating from the TFA can still be identified.

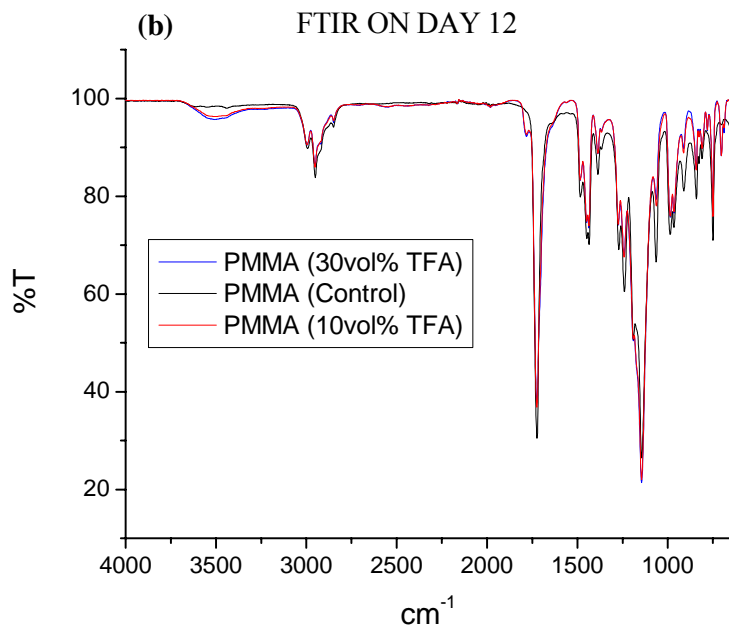
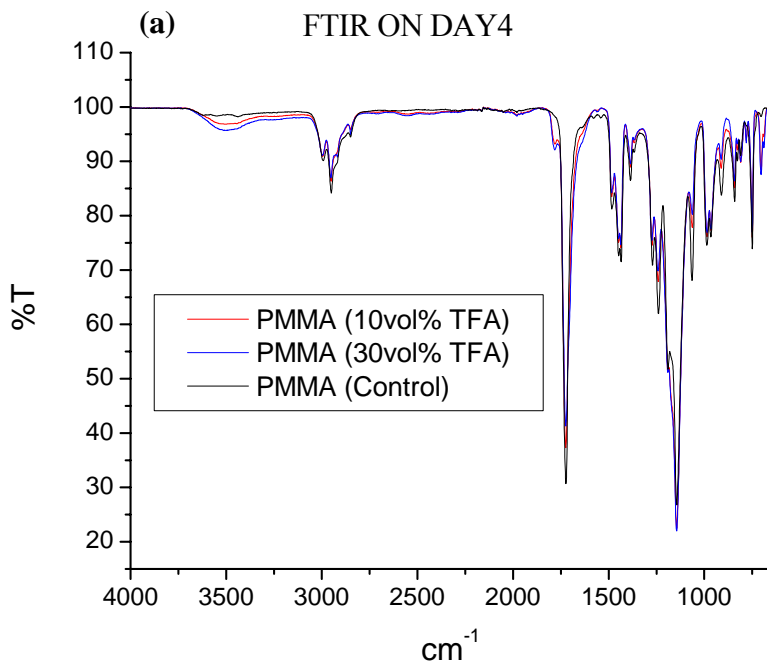


Figure 5.21 FTIR spectra of 30vol%TFA-PMMA (Blue curve), and 10 vol% TFA-PMMA (Red curve) and Pure PMMA (Black curve) film on a) day 4 b) day 12.

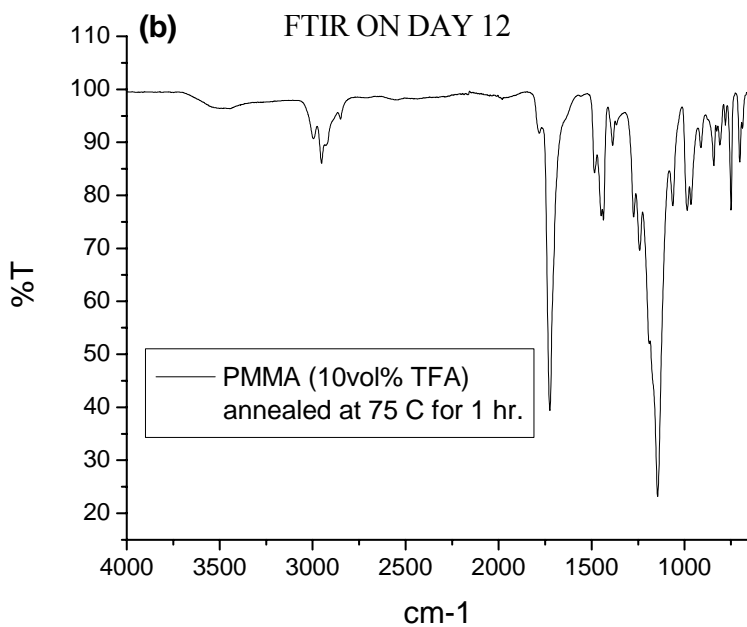
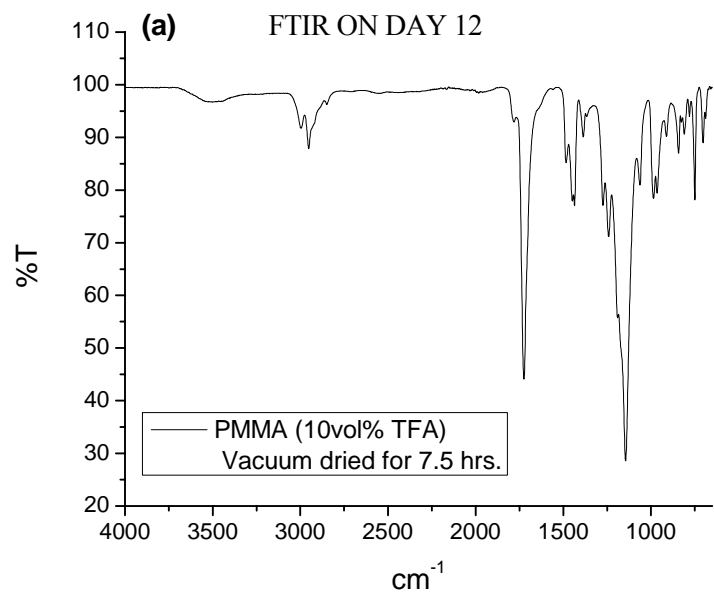


Figure 5.22 FTIR spectra of 10 vol% TFA-PMMA films a) vacuum-dried, on day 12 b) Oven-dried, on day 12.

Fig 5.23 shows the FTIR spectrum of the salt/acid/PMMA films. The IR spectra possess two pairs of highly characteristic absorption bands in the 1200 cm^{-1} region. These bands occur as partially resolved doublets with the first pair near 1270 cm^{-1} and 1240 cm^{-1} and the second pair near 1190 and 1150 cm^{-1} . This set of absorption bands has been assigned to the C-O-C stretching vibrations of the ester part. Peaks characteristic of the carboxylic group, as discussed previously can also be seen.

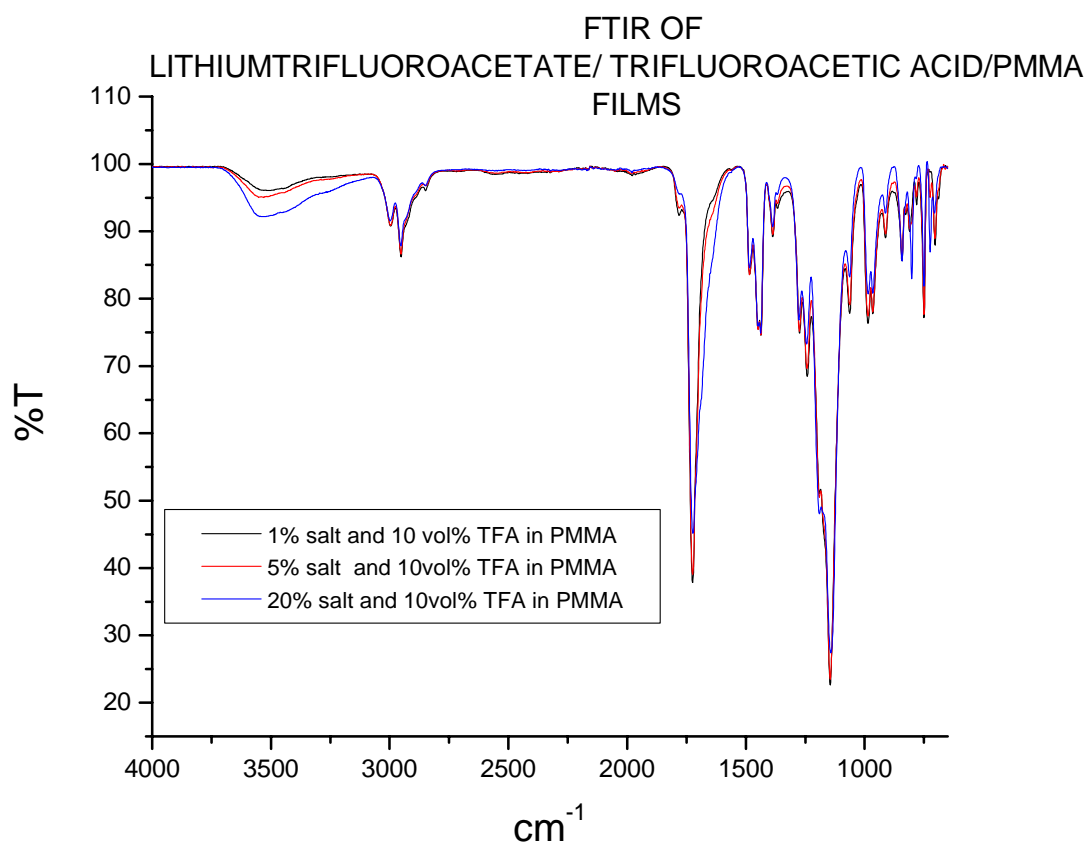


Figure 5.23 FTIR spectrum of Lithium trifluoroacetate/10vol%TFA/PMMA films.

5.2.3 Scanning Electron Microscopy (SEM).

5.2.3.1 TFA Processed PMMA Films

The effect of TFA on the PMMA films was studied by observing the surface morphology of the cross section of the dry polymer films. Fig 5.24 shows the SEM image of the polymer films prepared with various amounts of TFA in the solvent THF.

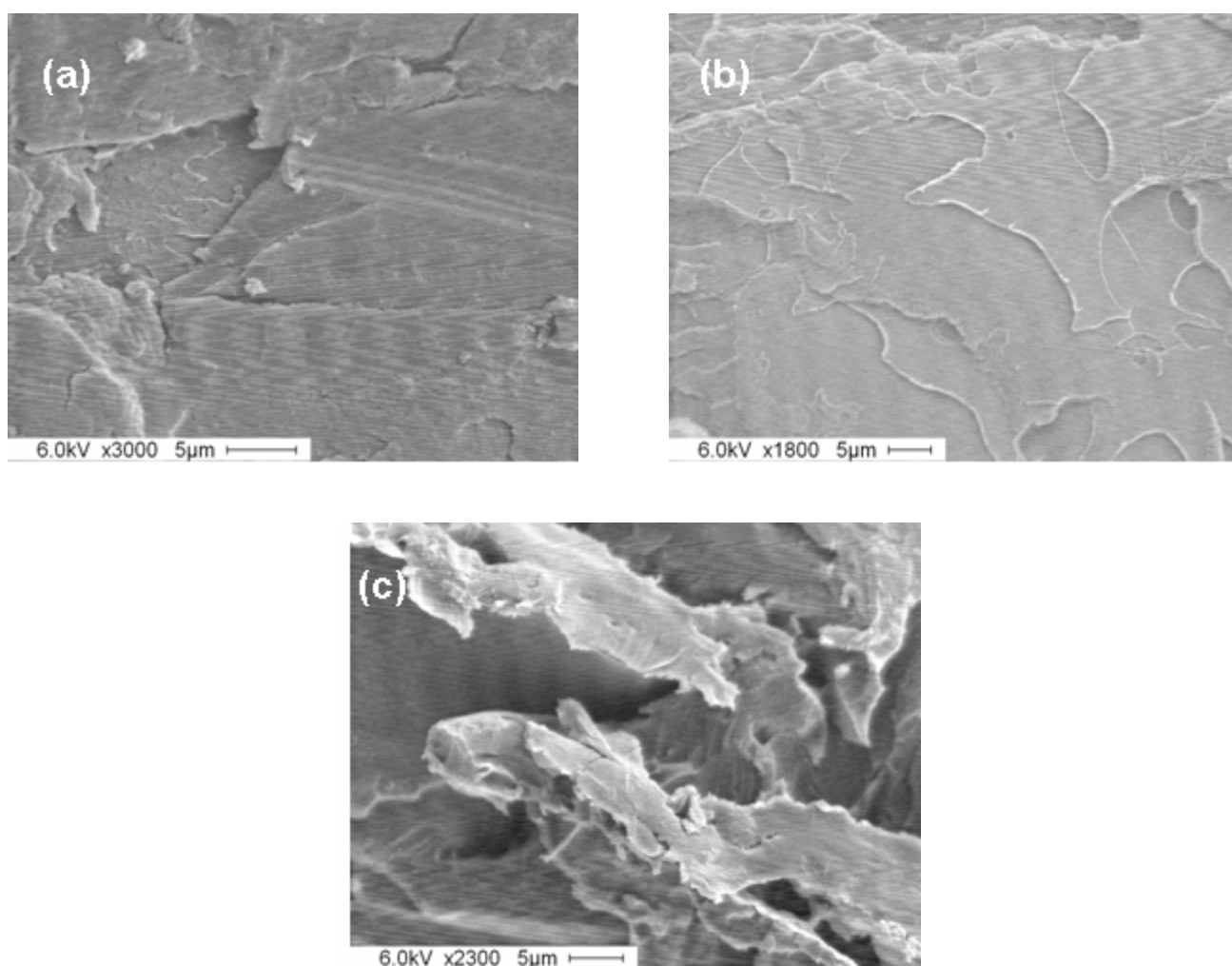


Figure 5.24 SEM image of a) 0vol%TFA b)10vol%TFA c) 30vol%TFA in PMMA films

It can be seen that as the percentage of TFA in the polymer increases the roughness of the cross section of the films increases which indicates the ductile nature of the broken films.

5.2.3.2 Polymer Electrolyte Films

The effect of increasing the salt concentration in the electrolyte films was also studied. Fig 5.25 shows the SEM images of cross section of the dry polymer electrolyte films prepared with 10vol%TFA in THF. The roughness of the films progressively increases with increasing concentration of the salt in the system.

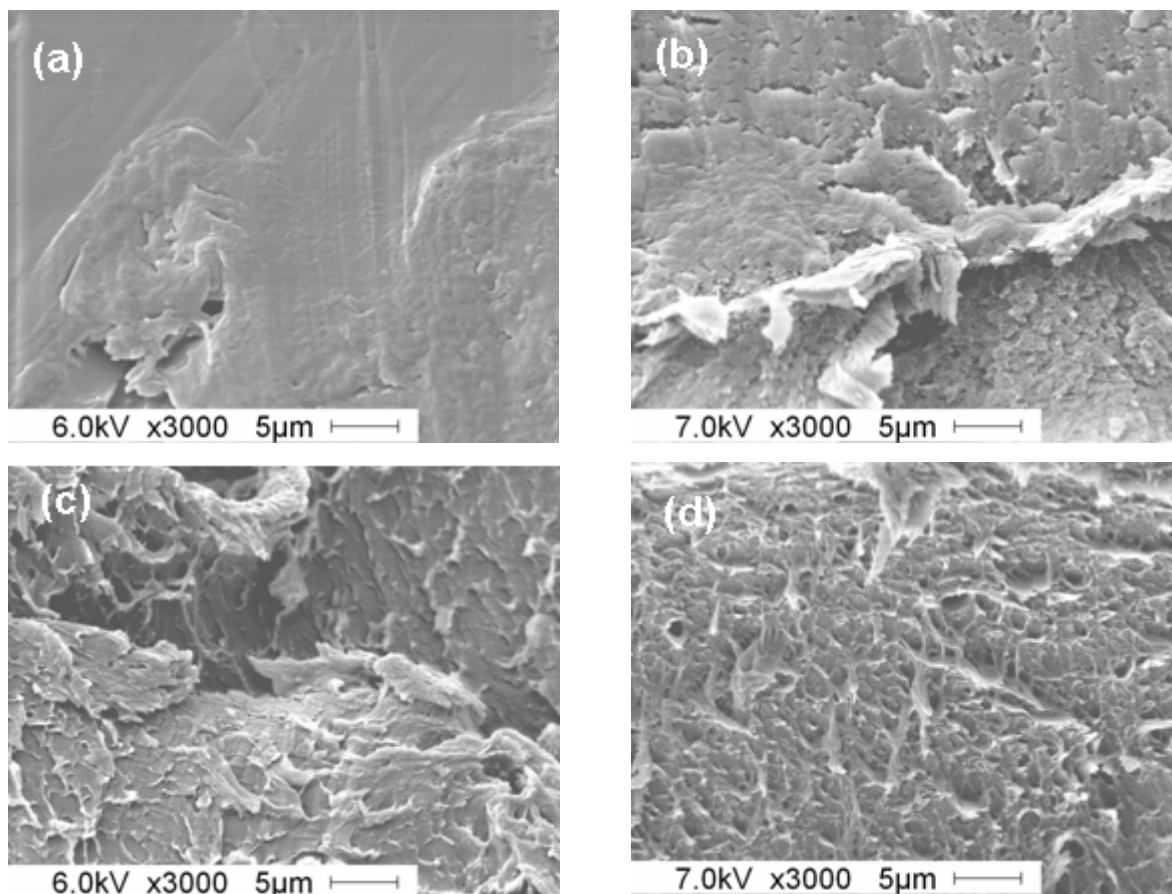


Figure 5.25 SEM images of the cross section of (a) 5wt% (b) 10wt% (c) 20wt% (d) 50wt% of salt in polymer electrolyte films.

5.2.3.3 Vanadium Oxide Films

Fig 5.26 shows the high magnification image of the vanadium oxide films. The presence of nano-scale morphology can be clearly seen. The scale of the figure indicates a possibility of the material being nanocrystalline.

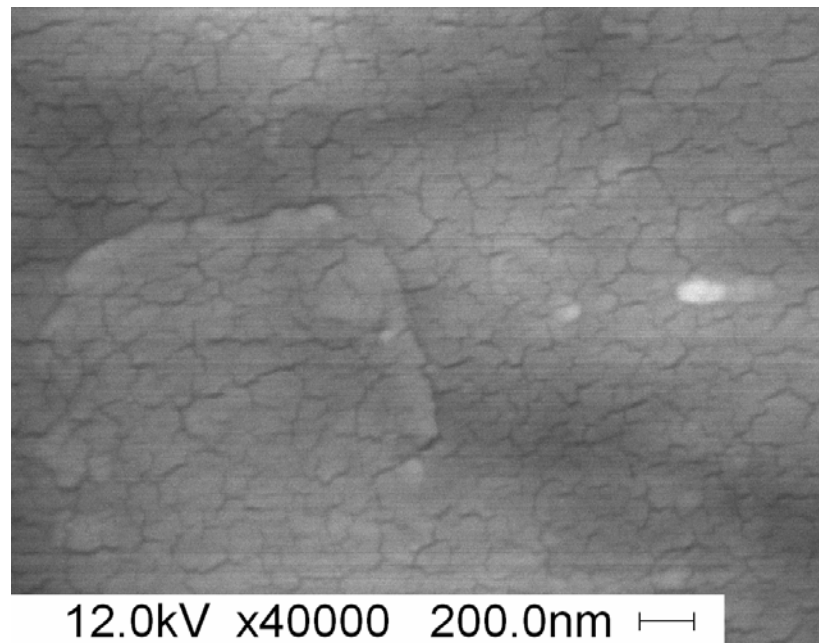


Figure 5.26 SEM image of the surface of the vanadium oxide films at high magnification.

CHAPTER 6 CONCLUSIONS AND FUTURE WORK

The whole thesis work can be divided into two parts. In the first part of the study we show that TFA can indeed be a multifunctional and versatile co-solvent for carbon nanotube dispersion and nanocomposite processing. This methodology opens a new frontier in addressing the issues of dispersion and purification of carbon nanotubes which have been a major challenge to date. TFA is completely miscible with a wide range of organic solvents and highly volatile, which means it can be used for processing of various types of polymers. After material processing, TFA can be evaporated or vacuum dried (for recycling) from the nanocomposites, leaving no or minimum additives in the composites. The optical images of the prepared composite films showed a uniform dispersion of the nanotubes in the matrix. Dynamic light scattering (DLS) experiments confirmed the improved dispersion of CNTs in the presence of TFA. TFA not only helps dispersing carbon nanotubes, it is also highly effective at purifying carbon nanotubes by eliminating carbonaceous particles and metal catalysts without oxidizing the nanotubes. The purification of the nanotubes was confirmed by SEM and TEM studies while the XPS analysis also confirmed that the walls of the nanotubes are not oxidized during the purification process. All the conventional purification techniques which use a strong acid also oxidize the walls of the nanotube which is detrimental to its properties. The electrical percolation threshold of carbon nanotube composite material is a good indicator of the state of dispersion of the nanotubes in the matrix. An enhanced dispersion leads to a lower percolation threshold of the composite. All the nanocomposite materials prepared from TFA-dispersed carbon nanotubes showed significantly lower percolation thresholds of electrical conductivity compared to nanocomposites using similar types of MWNTs, but processed with different methods. For many electronics and packaging

applications, it is very important to obtain a good conductivity with low nanofiller content. At about 0.12wt% of the CNT loading ratio, the conductivity of the prepared nanocomposite has already risen to 10^{-3} S/cm.

The thickness of the active layer of the organic solar cells is extremely small. This makes the fabrication of organic solar cells a delicate process as the chances of shorts or bad contacts are high. The substrates were first prepared and structured for the fabrication of solar cells. A layer of PEDOT:PSS was then deposited using spin coating. Another layer of the active material was then deposited, again by spin coating. The thicknesses of these layers were determined and the experimental parameters were altered to give the desired values of thickness for each of the layers. The back electrodes of the device were made by thermal evaporation of Al. All the fabrication steps were successful and the final device was free of the most frequent problems that occur in device fabrication such as shorts or bad contacts. This is visible from the IV characteristics of the device. The device shows a high dark current and low efficiency. One possible reason for this could be the significantly higher average length of the nanotubes used as compared to the thickness of the active layer. Future work can be carried out in resolving this issue. Also the active layer of the solar cell is sensitive to atmospheric oxygen and water, which significantly deteriorates the device efficiency. Efforts can be made in the future for the whole experiment to be set up in an argon filled glove box. The I-V characteristics measured for the solar cells do not use a standard light source. A solar spectrum simulator can be used in the future for standardization of the measurements and easy comparison of the results.

In the second part of the work electrode and electrolyte materials were developed for applications in Li-ion battery. A system of PMMA (as the polymer) and lithium trifluoroacetate (the salt) were used for the fabrication of polymer electrolyte material. The films were prepared

under different processing conditions and the influence of the processing parameters on the final electrical conductivity of the electrolyte films was studied. Electrochemical Impedance spectroscopy (EIS) was used to determine the conductivity of the electrolyte films. Of all the polymer electrolyte systems prepared under different processing conditions, wet films prepared by using 10vol% TFA in THF showed the most promising results. The conductivity reached 1.1×10^{-2} S/cm for a loading of 70wt% of the salt. Vanadium oxide and carbon nanotube/ block copolymer composite have immense potential as the cathode and anode material respectively, in a lithium ion battery. The purpose of the later part of the work was to synthesize and characterize these materials to evaluate their electrochemical performances. Both these materials showed a low resistance and favorable Li ion intercalation properties. Further work can be done in the future to test the cycle life and capacities of both the anode and cathode materials.

LIST OF REFERENCES

- [1] Iijima S. Helical microtubules of graphitic carbon.. *Nature*. 1991 Nov;354(6348):56-8.
- [2] Ajayan PM. Nanotubes from carbon. *Chemical Reviews*. 1999 Jul;99(7):1787-99.
- [3] Moniruzzaman M, Winey KI. Polymer nanocomposites containing carbon nanotubes. *Macromolecules*. 2006 Aug;39(16):5194-205.
- [4] Baughman RH, Zakhidov AA, de Heer WA. Carbon nanotubes - the route toward applications. *Science*. 2002 Aug;297(5582):787-92.
- [5] Iijima S, Ichihashi T. Single shell carbon nanotubes of 1 nm diameter. *Nature*. 1993 Jun;363(6430):603-5.
- [6] Wong EW, Sheehan PE, Lieber CM. Nanobeam mechanics: Elasticity, strength, and toughness of nanorods and nanotubes. *Science*. 1997 Sep;277(5334):1971-5.
- [7] Schadler LS, Giannaris SC, Ajayan PM. Load transfer in carbon nanotube epoxy composites. *Applied Physics Letters*. 1998 Dec;73(26):3842-4.
- [8] Frank S, Poncharal P, Wang ZL, de Heer WA. Carbon nanotube quantum resistors. *Science*. 1998 Jun;280(5370):1744-6.
- [9] Tans SJ, Verschueren ARM, Dekker C. Room-temperature transistor based on a single carbon nanotube. *Nature*. 1998 May;393(6680):49-52.
- [10] Dai HJ, Hafner JH, Rinzler AG, Colbert DT, Smalley RE. Nanotubes as nanoprobe in scanning probe microscopy. *Nature*. 1996 Nov;384(6605):147-50.
- [11] Deheer WA, Chatelain A, Ugarte D. A Carbon nanotube field emission electron source. *Science*. 1995 Nov;270(5239):1179-80.
- [12] Awasthi K, Srivastava A, Srivastava ON. Synthesis of carbon nanotubes. *Journal of Nanoscience and Nanotechnology*. 2005 Oct;5(10):1616-36.
- [13] Chen YC, Raravikar NR, Schadler LS, Ajayan PM, Zhao YP, Lu TM, et al. Ultrafast optical switching properties of single-wall carbon nanotube polymer composites at 1.55 μ m. *Applied Physics Letters*. 2002 Aug;81(6):975-7.
- [14] Kim HM, Kim K, Lee CY, Joo J, Cho SJ, Yoon HS, et al. Electrical conductivity and electromagnetic interference shielding of multiwalled carbon nanotube composites containing Fe catalyst. *Applied Physics Letters*. 2004 Jan;84(4):589-91.

- [15] Ago H, Petritsch K, Shaffer MSP, Windle AH, Friend RH. Composites of carbon nanotubes and conjugated polymers for photovoltaic devices. *Advanced Materials*. 1999 Oct;11(15):1281-+.
- [16] Kymakis E, Amaratunga GAJ. Single-wall carbon nanotube/conjugated polymer photovoltaic devices. *Applied Physics Letters*. 2002 Jan;80(1):112-4.
- [17] Rege K, Raravikar NR, Kim DY, Schadler LS, Ajayan PM, Dordick JS. Enzyme-polymer-single walled carbon nanotube composites as biocatalytic films. *Nano Letters*. 2003 Jun;3(6):829-32.
- [18] Lee SY, Kim BH, Park SK, Joo J, Beag YW, Koh SK. Low dielectric constant of MeV ion-implanted poly(vinylidene fluoride). *Macromolecular Research*. 2003 Feb;11(1):9-13.
- [19] Philip B, Abraham JK, Chandrasekhar A, Varadan VK. Carbon nanotube/PMMA composite thin films for gas-sensing applications. *Smart Materials & Structures*. 2003 Dec;12(6):935-9.
- [20] Biercuk MJ, Llaguno MC, Radosavljevic M, Hyun JK, Johnson AT, Fischer JE. Carbon nanotube composites for thermal management. *Applied Physics Letters*. 2002 Apr;80(15):2767-9.
- [21] Yang Z, Xu H, Li MK, Shi YL, Huang Y, Li HL. Preparation and properties of Ni/P/single-walled carbon nanotubes composite coatings by means of electroless plating. *Thin Solid Films*. 2004 Nov;466(1-2):86-91.
- [22] Carroll DL, Czerw R, Webster S. Polymer-nanotube composites for transparent, conducting thin films. *Synthetic Metals*. 2005 Dec;155(3):694-7.
- [23] Kelly A, Tyson WR. Tensile properties of fibre reinforced metals- copper/tungsten and copper/molybdenum. *Journal of the Mechanics and Physics of Solids*. 1965;13(6):329-&.
- [24] Dyke CA, Tour JM. Covalent functionalization of single-walled carbon nanotubes for materials applications. *Journal of Physical Chemistry A*. 2004 Dec;108(51):11151-9.
- [25] Munsonmcgee SH. Estimation of the critical concentration in an anisotropic percolation network. *Physical Review B*. 1991 Feb;43(4):3331-6.
- [26] Bai JB, Allaoui A. Effect of the length and the aggregate size of MWNTs on the improvement efficiency of the mechanical and electrical properties of nanocomposites - experimental investigation. *Composites Part a-Applied Science and Manufacturing*. 2003;34(8):689-94.
- [27] Israelachvili JN. *Intermolecular Surface Forces*. Academic Press, San Diego, ed.3, 2006.

- [28] Haggenueller R, Gommans HH, Rinzler AG, Fischer JE, Winey KI. Aligned single-wall carbon nanotubes in composites by melt processing methods. *Chemical Physics Letters*. 2000 Nov;330(3-4):219-25.
- [29] Xu JW, Florkowski W, Gerhardt R, Moon KS, Wong CP. Shear modulated percolation in carbon nanotube composites. *Journal of Physical Chemistry B*. 2006 Jun;110(25):12289-92.
- [30] Raravikar NR, Schadler LS, Vijayaraghavan A, Zhao YP, Wei BQ, Ajayan PM. Synthesis and characterization of thickness-aligned carbon nanotube-polymer composite films. *Chemistry of Materials*. 2005 Mar;17(5):974-83.
- [31] Du FM, Fischer JE, Winey KI. Effect of nanotube alignment on percolation conductivity in carbon nanotube/polymer composites. *Physical Review B*. 2005 Sep;72(12).
- [32] Dujardin E, Ebbesen TW, Krishnan A, Treacy MMJ. Purification of single-shell nanotubes. *Advanced Materials*. 1998 Jun;10(8):611-+.
- [33] Tohji K, Goto T, Takahashi H, Shinoda Y, Shimizu N, Jeyadevan B, et al. Purifying single-walled nanotubes. *Nature*. 1996 Oct;383(6602):679-.
- [34] Monthieux M, Smith BW, Burteaux B, Claye A, Fischer JE, Luzzi DE. Sensitivity of single-wall carbon nanotubes to chemical processing: an electron microscopy investigation. *Carbon*. 2001;39(8):1251-72.
- [35] Moon JM, An KH, Lee YH, Park YS, Bae DJ, Park GS. High-yield purification process of singlewalled carbon nanotubes. *Journal of Physical Chemistry B*. 2001 Jun;105(24):5677-81.
- [36] Bandow S, Rao AM, Williams KA, Thess A, Smalley RE, Eklund PC. Purification of single-wall carbon nanotubes by microfiltration. *Journal of Physical Chemistry B*. 1997 Oct;101(44):8839-42.
- [37] Duesberg GS, Burghard M, Muster J, Philipp G, Roth S. Separation of carbon nanotubes by size exclusion chromatography. *Chemical Communications*. 1998 Feb(3):435-6.
- [38] Georgakilas V, Voulgaris D, Vazquez E, Prato M, Guldi DM, Kukovec A, et al. Purification of HiPCO carbon nanotubes via organic functionalization. *Journal of the American Chemical Society*. 2002 Dec;124(48):14318-9.
- [39] Sandler JKW, Kirk JE, Kinloch IA, Shaffer MSP, Windle AH. Ultra-low electrical percolation threshold in carbon-nanotube-epoxy composites. *Polymer*. 2003 Sep;44(19):5893-9.
- [40] Qian D, Dickey EC, Andrews R, Rantell T. Load transfer and deformation mechanisms in carbon nanotube-polystyrene composites. *Applied Physics Letters*. 2000 May;76(20):2868-70.

- [41] Cadek M, Coleman JN, Barron V, Hedicke K, Blau WJ. Morphological and mechanical properties of carbon-nanotube-reinforced semicrystalline and amorphous polymer composites. *Applied Physics Letters*. 2002 Dec;81(27):5123-5.
- [42] Probst O, Moore EM, Resasco DE, Grady BP. Nucleation of polyvinyl alcohol crystallization by single-walled carbon nanotubes. *Polymer*. 2004 Jun;45(13):4437-43.
- [43] Ruan SL, Gao P, Yang XG, Yu TX. Toughening high performance ultrahigh molecular weight polyethylene using multiwalled carbon nanotubes. *Polymer*. 2003 Sep;44(19):5643-54.
- [44] Assouline E, Lustiger A, Barber AH, Cooper CA, Klein E, Wachtel E, et al. Nucleation ability of multiwall carbon nanotubes in polypropylene composites. *Journal of Polymer Science Part B-Polymer Physics*. 2003 Mar;41(5):520-7.
- [45] Potschke P, Bhattacharyya AR, Janke A, Goering H. Melt mixing of polycarbonate/multi-wall carbon nanotube composites. *Composite Interfaces*. 2003;10(4-5):389-404.
- [46] Andrews R, Jacques D, Qian DL, Rantell T. Multiwall carbon nanotubes: Synthesis and application. *Accounts of Chemical Research*. 2002 Dec;35(12):1008-17.
- [47] Bhattacharyya AR, Sreekumar TV, Liu T, Kumar S, Ericson LM, Hauge RH, et al. Crystallization and orientation studies in polypropylene/single wall carbon nanotube composite. *Polymer*. 2003 Apr;44(8):2373-7.
- [48] Siochi EJ, Working DC, Park C, Lillehei PT, Rouse JH, Topping CC, et al. Melt processing of SWCNT-polyimide nanocomposite fibers. *Composites Part B-Engineering*. 2004;35(5):439-46.
- [49] Liu TX, Phang IY, Shen L, Chow SY, Zhang WD. Morphology and mechanical properties of multiwalled carbon nanotubes reinforced nylon-6 composites. *Macromolecules*. 2004 Sep;37(19):7214-22.
- [50] Jia ZJ, Wang ZY, Xu CL, Liang J, Wei BQ, Wu DH, et al. Study on poly(methyl methacrylate)/carbon nanotube composites. *Materials Science and Engineering a-Structural Materials Properties Microstructure and Processing*. 1999 Nov;271(1-2):395-400.
- [51] Kumar S, Dang TD, Arnold FE, Bhattacharyya AR, Min BG, Zhang XF, et al. Synthesis, structure, and properties of PBO/SWNT composites. *Macromolecules*. 2002 Nov;35(24):9039-43.
- [52] Hamon MA, Hui H, Bhowmik P, Itkis HME, Haddon RC. Ester-functionalized soluble single-walled carbon nanotubes. *Applied Physics a-Materials Science & Processing*. 2002 Mar;74(3):333-8.

- [53] Sun YP, Huang WJ, Lin Y, Fu KF, Kitaygorodskiy A, Riddle LA, et al. Soluble dendron-functionalized carbon nanotubes: Preparation, characterization, and properties. *Chemistry of Materials*. 2001 Sep;13(9):2864-9.
- [54] Chattopadhyay D, Lastella S, Kim S, Papadimitrakopoulos F. Length separation of Zwitterion-functionalized single wall carbon nanotubes by GPC. *Journal of the American Chemical Society*. 2002 Feb;124(5):728-9.
- [55] Banerjee S, Wong SS. Synthesis and characterization of carbon nanotube-nanocrystal heterostructures. *Nano Letters*. 2002 Mar;2(3):195-200.
- [56] Azamian BR, Coleman KS, Davis JJ, Hanson N, Green MLH. Directly observed covalent coupling of quantum dots to single-wall carbon nanotubes. *Chemical Communications*. 2002(4):366-7.
- [57] Williams KA, Veenhuizen PTM, de la Torre BG, Eritja R, Dekker C. Nanotechnology - Carbon nanotubes with DNA recognition. *Nature*. 2002 Dec;420(6917):761-.
- [58] Ravindran S, Chaudhary S, Colburn B, Ozkan M, Ozkan CS. Covalent coupling of quantum dots to multiwalled carbon nanotubes for electronic device applications. *Nano Letters*. 2003 Apr;3(4):447-53.
- [59] Banerjee S, Wong SS. Structural characterization, optical properties, and improved solubility of carbon nanotubes functionalized with Wilkinson's catalyst. *Journal of the American Chemical Society*. 2002 Jul;124(30):8940-8.
- [60] Haddon RC. π -electrons in 3 dimensions. *Accounts of Chemical Research*. 1988 Jun;21(6):243-9.
- [61] Chen ZF, Thiel W, Hirsch A. Reactivity of the convex and concave surfaces of single-walled carbon nanotubes (SWCNTs) towards addition reactions: Dependence on the carbon-atom pyramidalization. *Chemphyschem*. 2003 Jan;4(1):93-+.
- [62] Kamaras K, Itkis ME, Hu H, Zhao B, Haddon RC. Covalent bond formation to a carbon nanotube metal. *Science*. 2003 Sep;301(5639):1501-.
- [63] Garg A, Sinnott SB. Effect of chemical functionalization on the mechanical properties of carbon nanotubes. *Chemical Physics Letters*. 1998 Oct;295(4):273-8.
- [64] Mickelson ET, Chiang IW, Zimmerman JL, Boul PJ, Lozano J, Liu J, et al. Solvation of fluorinated single-wall carbon nanotubes in alcohol solvents. *Journal of Physical Chemistry B*. 1999 May;103(21):4318-22.

- [65] Khabashesku VN, Billups WE, Margrave JL. Fluorination of single-wall carbon nanotubes and subsequent derivatization reactions. *Accounts of Chemical Research*. 2002 Dec;35(12):1087-95.
- [66] Banerjee S, Wong SS. Rational sidewall functionalization and purification of single-walled carbon nanotubes by solution-phase ozonolysis. *Journal of Physical Chemistry B*. 2002 Nov;106(47):12144-51.
- [67] Bahr JL, Yang JP, Kosynkin DV, Bronikowski MJ, Smalley RE, Tour JM. Functionalization of carbon nanotubes by electrochemical reduction of aryl diazonium salts: A bucky paper electrode. *Journal of the American Chemical Society*. 2001 Jul;123(27):6536-42.
- [68] Dyke CA, Tour JM. Unbundled and highly functionalized carbon nanotubes from aqueous reactions. *Nano Letters*. 2003 Sep;3(9):1215-8.
- [69] Georgakilas V, Kordatos K, Prato M, Guldi DM, Holzinger M, Hirsch A. Organic functionalization of carbon nanotubes. *Journal of the American Chemical Society*. 2002 Feb;124(5):760-1.
- [70] Qin SH, Qin DQ, Ford WT, Herrera JE, Resasco DE, Bachilo SM, et al. Solubilization and purification of single-wall carbon nanotubes in water by in situ radical polymerization of sodium 4-styrenesulfonate. *Macromolecules*. 2004 Jun;37(11):3965-7.
- [71] Viswanathan G, Chakrapani N, Yang HC, Wei BQ, Chung HS, Cho KW, et al. Single-step in situ synthesis of polymer-grafted single-wall nanotube composites. *Journal of the American Chemical Society*. 2003 Aug;125(31):9258-9.
- [72] Xin T, Chang L, Cheng HM, Zhao HC, Feng Y, Zhang XQ. Surface modification of single-walled carbon nanotubes with polyethylene via in situ Ziegler-Natta polymerization. *Journal of Applied Polymer Science*. 2004 Jun;92(6):3697-700.
- [73] Xia HS, Wang Q, Qiu GH. Polymer-encapsulated carbon nanotubes prepared through ultrasonically initiated in situ emulsion polymerization. *Chemistry of Materials*. 2003 Oct;15(20):3879-86.
- [74] Fu KF, Huang WJ, Lin Y, Riddle LA, Carroll DL, Sun YP. Defunctionalization of functionalized carbon nanotubes. *Nano Letters*. 2001 Aug;1(8):439-41.
- [75] Blake R, Gun'ko YK, Coleman J, Cadek M, Fonseca A, Nagy JB, et al. A generic organometallic approach toward ultra-strong carbon nanotube polymer composites. *Journal of the American Chemical Society*. 2004 Aug;126(33):10226-7.
- [76] Bhattacharyya S, Sinturel C, Salvétat JP, Saboungi ML. Protein-functionalized carbon nanotube-polymer composites. *Applied Physics Letters*. 2005 Mar;86(11).

- [77] McCarthy B, Coleman JN, Czerw R, Dalton AB, Panhuis MIH, Maiti A, et al. A microscopic and spectroscopic study of interactions between carbon nanotubes and a conjugated polymer. *Journal of Physical Chemistry B*. 2002 Mar;106(9):2210-6.
- [78] Chen J, Liu HY, Weimer WA, Halls MD, Waldeck DH, Walker GC. Noncovalent engineering of carbon nanotube surfaces by rigid, functional conjugated polymers. *Journal of the American Chemical Society*. 2002 Aug;124(31):9034-5.
- [79] Coleman JN, Dalton AB, Curran S, Rubio A, Davey AP, Drury A, et al. Phase separation of carbon nanotubes and turbostratic graphite using a functional organic polymer. *Advanced Materials*. 2000 Feb;12(3):213-+.
- [80] Baibarac M, Baltog I, Lefrant S, Mevellec JY, Chauvet O. Polyaniline and carbon nanotubes based composites containing whole units and fragments of nanotubes. *Chemistry of Materials*. 2003 Oct;15(21):4149-56.
- [81] Coleman JN, Curran S, Dalton AB, Davey AP, McCarthy B, Blau W, et al. Percolation-dominated conductivity in a conjugated-polymer-carbon-nanotube composite. *Physical Review B*. 1998 Sep;58(12):R7492-R5.
- [82] Barraza HJ, Pompeo F, O'Rear EA, Resasco DE. SWNT-filled thermoplastic and elastomeric composites prepared by miniemulsion polymerization. *Nano Letters*. 2002 Aug;2(8):797-802.
- [83] Regev O, ElKati PNB, Loos J, Koning CE. Preparation of conductive nanotube-polymer composites using latex technology. *Advanced Materials*. 2004 Feb;16(3):248-+.
- [84] Ramasubramaniam R, Chen J, Liu HY. Homogeneous carbon nanotube/polymer composites for electrical applications. *Applied Physics Letters*. 2003 Oct;83(14):2928-30.
- [85] Dispersion of carbon nanotubes and polymer nanocomposite fabrication using trifluoroacetic acid as a co-solvent.
- [86] Bandyopadhyaya R, Nativ-Roth E, Regev O, Yerushalmi-Rozen R. Stabilization of individual carbon nanotubes in aqueous solutions. *Nano Letters*. 2002 Jan;2(1):25-8.
- [87] Shvartzman-Cohen R, Levi-Kalisman Y, Nativ-Roth E, Yerushalmi-Rozen R. Generic approach for dispersing single-walled carbon nanotubes: The strength of a weak interaction. *Langmuir*. 2004 Jul;20(15):6085-8.
- [88] Nepal D, Geckeler KE. Proteins and carbon nanotubes: Close encounter in water. *Small*. 2007 Jul;3(7):1259-65.
- [89] Zheng M, Jagota A, Semke ED, Diner BA, McLean RS, Lustig SR, et al. DNA-assisted dispersion and separation of carbon nanotubes. *Nature Materials*. 2003 May;2(5):338-42.

- [90] Coleman JN, Blau WJ, Dalton AB, Munoz E, Collins S, Kim BG, et al. Improving the mechanical properties of single-walled carbon nanotube sheets by intercalation of polymeric adhesives. *Applied Physics Letters*. 2003 Mar;82(11):1682-4.
- [91] Vigolo B, Penicaud A, Coulon C, Sauder C, Pailler R, Journet C, et al. Macroscopic fibers and ribbons of oriented carbon nanotubes. *Science*. 2000 Nov;290(5495):1331-4.
- [92] Mamedov AA, Kotov NA, Prato M, Guldi DM, Wickstedt JP, Hirsch A. Molecular design of strong single-wall carbon nanotube/polyelectrolyte multilayer composites. *Nature Materials*. 2002 Nov;1(3):190-4.
- [93] Gregg BA. Excitonic solar cells. *Journal of Physical Chemistry B*. 2003 May;107(20):4688-98.
- [94] Haugeneder A, Neges M, Kallinger C, Spirkl W, Lemmer U, Feldmann J, et al. Exciton diffusion and dissociation in conjugated polymer fullerene blends and heterostructures. *Physical Review B*. 1999 Jun;59(23):15346-51.
- [95] Eidman K F and Nichols P J 2004 *Encyclopedia of Reagents for Organic Synthesis* (New York: Wiley)
- [96] Hennrich F, Wellmann R, Malik S, Lebedkin S, Kappes MM. Reversible modification of the absorption properties of single-walled carbon nanotube thin films via nitric acid exposure. *Physical Chemistry Chemical Physics*. 2003;5(1):178-83.
- [97] Murphy H, Papakonstantinou P, Okpalugo TIT. Raman study of multiwalled carbon nanotubes functionalized with oxygen groups. *Journal of Vacuum Science & Technology B*. 2006 Mar-Apr;24(2):715-20.
- [98] Lee WH, Kim SJ, Lee WJ, Lee JG, Haddon RC, Reucroft PJ. X-ray photoelectron spectroscopic studies of surface modified single-walled carbon nanotube material. *Applied Surface Science*. 2001 Sep;181(1-2):121-7.
- [99] Kovtyukhova NI, Mallouk TE, Pan L, Dickey EC. Individual single-walled nanotubes and hydrogels made by oxidative exfoliation of carbon nanotube ropes. *Journal of the American Chemical Society*. 2003 Aug;125(32):9761-9.
- [100] Potschke P, Dudkin SM, Alig I. Dielectric spectroscopy on melt processed polycarbonate - multiwalled carbon nanotube composites. *Polymer*. 2003 Aug;44(17):5023-30.
- [101] Dufresne A, Paillet M, Putaux JL, Canet R, Carmona F, Delhaes P, et al. Processing and characterization of carbon nanotube/poly(styrene-co-butyl acrylate) nanocomposites. *Journal of Materials Science*. 2002 Sep;37(18):3915-23.

- [102] McNally T, Potschke P, Halley P, Murphy M, Martin D, Bell SEJ, et al. Polyethylene multiwalled carbon nanotube composites. *Polymer*. 2005 Sep;46(19):8222-32.
- [103] Rao BML, Francis RW, Christopher HA. Lithium aluminum electrode. *Journal of the Electrochemical Society*. 1977;124(10):1490-2.
- [104] Armand MB, Chabagno SM, Duclot M. Proceedings of the second International meeting on solid electrolytes. St Andrews, Scotland. Sept 20-22, 1978.
- [105] Gray FM. *Solid Polymer Electrolytes*. VCH New York (1991). Chapter 2.
- [106] Leveque M, Lenest JF, Gandini A, Cheradame H. Cationic transport numbers in polyether-based networks containing lithium salts. *Journal of Power Sources*. 1985;14(1-3):27-30.
- [107] Armand MB, Gorecki W, Andreani R. Second International Meeting on Polymer Electrolytes. (Ed. Scrosati, B.) 91-96 (Elsevier, London, 1989).
- [108] Kita F, Kawakami A, Nie J, Sonoda T, Kobayashi H. On the characteristics of electrolytes with new lithium imide salts. *Journal of Power Sources*. 1997 Oct;68(2):307-10.
- [109] Appetecchi GB, Henderson W, Villano P, Berrettoni M, Passerini S. PEO-LiN(SO₂CF₂CF₃)(2) polymer electrolytes - I. XRD, DSC, and ionic conductivity characterization. *Journal of the Electrochemical Society*. 2001 Oct;148(10):A1171-A8.
- [110] Benrabah D, Sanchez JY, Deroo D, Armand M. Synthesis and electrochemical characterization of new bulky lithium salts. *Solid State Ionics*. 1994 May-Jun;70:157-62.
- [111] Alloin F, Bayoud S, Azimipour B, Reibel L, Sanchez JY. Electrochemical investigation of lithium aromatic sulfonyl imide salts. *Electrochimica Acta*. 2000;45(8-9):1193-201.
- [112] Stallworth PE, Fontanella JJ, Wintersgill MC, Scheidler CD, Immel JJ, Greenbaum SG, et al. NMR, DSC and high pressure electrical conductivity studies of liquid and hybrid electrolytes. *Journal of Power Sources*. 1999 Sep;82:739-47.
- [113] Sakurai Y, Okada S, Yamaki J, Okada T. Electrochemical behavior of amorphous V₂O₅(-P₂O₅) cathodes for lithium secondary batteries. *Journal of Power Sources*. 1987 Jul;20(3-4):173-7.
- [114] Sakurai Y, Yamaki J. Correlation between microstructure and electrochemical behavior of amorphous V₂O₅-P₂O₅ in lithium cells. *Journal of the Electrochemical Society*. 1988 Apr;135(4):791-6.
- [115] Baddour R, Pereiramos JP, Messina R, Perichon J. A thermodynamic, structural and kinetic study of the electrochemical lithium intercalation Thermodynamic, structural and kinetic

study of the electrochemical lithium intercalation into the xerogel $V_2O_5 \cdot 1.6H_2O$ in a propylene carbonate solution. *Journal of Electroanalytical Chemistry*. 1991 Sep;314(1-2):81-101.

[116] Salloux K, Chaput F, Wong HP, Dunn B, Breiter MW. Lithium intercalation in vanadium pentoxide aerogels. *Journal of the Electrochemical Society*. 1995 Oct;142(10):L191-L2.

[117] Dong W, Rolison DR, Dunn B. Electrochemical properties of high surface area vanadium oxide aerogels. *Electrochemical and Solid State Letters*. 2000 Oct;3(10):457-9.

[118] Liu P, Wu HQ. Diffusion of lithium in carbon. *Solid State Ionics*. 1996 Nov;92(1-2):91-7.

[119] Levi MD, Aurbach D. Simultaneous measurements and modeling of the electrochemical impedance and the cyclic voltammetric characteristics of graphite electrodes doped with lithium. *Journal of Physical Chemistry B*. 1997 Jun;101(23):4630-40.

[120] Funabiki A, Inaba M, Ogumi Z, Yuasa S, Otsuji J, Tasaka A. Impedance study on the electrochemical lithium intercalation into natural graphite powder. *Journal of the Electrochemical Society*. 1998 Jan;145(1):172-8.

[121] Levi MD, Aurbach D. Diffusion coefficients of lithium ions during intercalation into graphite derived from the simultaneous measurements and modeling of electrochemical impedance and potentiostatic intermittent titration characteristics of thin graphite electrodes. *Journal of Physical Chemistry B*. 1997 Jun;101(23):4641-7.

[122] Funabiki A, Inaba M, Ogumi Z. Ac impedance analysis of electrochemical lithium intercalation into highly oriented pyrolytic graphite. *Journal of Power Sources*. 1997 Oct;68(2):227-31.

[123] Zaghbi K, Tatsumi K, Abe H, Ohsaki T, Sawada Y, Higuchi S. Optimization of the dimensions of vapor-grown carbon fiber for use as negative electrodes in lithium-ion rechargeable cells. *Journal of the Electrochemical Society*. 1998 Jan;145(1):210-5.

[124] Jeffries-El M, Sauve G, McCullough RD. In-situ end-group functionalization of regioregular poly(3-alkylthiophene) using the Grignard metathesis polymerization method. *Advanced Materials*. 2004 Jun;16(12):1017-+.

[125] Iovu MC, Jeffries-El M, Sheina EE, Cooper JR, McCullough RD. Regioregular poly(3-alkylthiophene) conducting block copolymers. *Polymer*. 2005 Sep;46(19):8582-6.

[126] Wang ZC, Chen JF, Hu XF. Electrochromic properties of aqueous sol-gel derived vanadium oxide films with different thickness. *Thin Solid Films*. 2000 Oct;375(1-2):238-41.

[127] Huguenin F, dos Santos DS, Bassi A, Nart FC, Oliveira ON. Charge storage capability in nanoarchitectures of V₂O₅/chitosan/poly (ethylene oxide) produced using the layer-by-layer technique. *Advanced Functional Materials*. 2004 Oct;14(10):985-91.